DISSERTATION

RESILIENCE-BASED SEISMIC DESIGN BASED ON TIME-TO-FUNCTIONALITY FOR TALL MASS TIMBER BUILDINGS

Submitted by

Jace Furley

Department of Civil and Environmental Engineering

In partial fulfillment of the requirements

For the Degree of Doctor of Philosophy

Colorado State University

Fort Collins, Colorado

Spring 2023

Doctoral Committee:

Advisor: John van de Lindt

Erin Arneson
Yanlin Guo
Hussam Mahmoud

ABSTRACT

RESILIENCE-BASED SEISMIC DESIGN BASED ON TIME-TO-FUNCTIONALITY FOR TALL MASS TIMBER BUILDINGS

Mass timber has existed for years as a structural material; however, only in the last decade or so has progress been made in North America on the adoption of mass timber for moderate to high seismic regions. During this time, there has been significant research effort and resources allocated to demonstrating various mass timber products as suitable for seismic applications, in particular as seismic force resisting systems (SFRS). However, during the research process, the potential suitability of mass timber for mid-rise or tall buildings was identified, and research efforts into the applicability of mass timber for taller buildings in seismic regions have been increasing in the past several years. Along with the growing interest in mass timber for tall buildings, a larger more general push for resilient buildings and communities has also been prevalent, providing the opportunity to design mass timber SFRS for tall buildings that not only meet current performance standards, but also have the potential to contribute to resilience-based design and ultimately community resilience. This research presented in this dissertation develops and applies the time-to-functionality fragility (TTF) methodology to provide resilience-based design guidance for tall mass timber buildings. The new TTF methodology incorporates many of the considerations of previous performance-based methodologies (such as FEMA P-58) and resilience methods (such as the REDi rating system) into a multi-layer direct Monte Carlo

simulation to estimate various recovery levels. This method was then applied to a two-story test specimen utilizing a new mass timber SFRS (a cross laminated timber [CLT] rocking wall), developed as a part of the Natural Hazards Equipment Research Infrastructure (NHERI) TallWood project, to demonstrate the resilience capabilities of the system. While the CLT rocking wall SFRS demonstrated excellent resilience capabilities, a dearth of data in mass timber (in terms of resilience considerations) were identified both as a part of the TTF methodology development and as a part of NHERI TallWood. To address some this lack of data, nail laminated timber (NLT) and dowel laminated timber (DLT) diaphragms were tested using quasi-static reversed cyclic loading, determining the lateral capacity of these systems as well as identifying damage states to better incorporate them into the TTF methodology. With the resilience of the CLT rocking wall system demonstrated, and several of the identified research data gaps addressed, the TTF methodology was applied to the two-story, six-story, and ten-story archetypes utilizing the CLT rocking wall system and varying the different structural components to create a database of TTF performance. A total of 243 SFRS designs were considered, and this database was leveraged using the developed resilience-based design guidance to estimate the TTF performance of two ten-story design examples. The research presented here demonstrates that it is possible to design tall mass timber buildings with resilience considerations, and that there are mass timber SFRS suitable for resilient design. While the findings focus on mass timber, the methodology itself is not limited to mass timber. The design guidance presented herein represents the first step towards a more prescriptive solution for TTF performance, with the potential for the incorporation of other structural systems and materials beyond the CLT rocking wall. In addition, there is a significant push

to codify functionality, often termed “functional recovery”, into U.S. design codes in the next 10 years. The TTF methodology directly considers functionality as a part of the method and this research and research like it will provide the foundation for the codification effort.

ACKNOWLEDGEMENTS

The process of researching and writing this dissertation was a long journey, and I would like to take a moment to thank the many people that have helped me along the way.

First I would like to thank my advisor and Chair Dr. John van de Lindt, without his guidance, advice, and support throughout both my Master's degree and the writing of this dissertation, I would not have made it. I also would like to thank my remaining committee members. The input and advice given by Dr. Hussam Mahmoud, Dr. Yanlin Guo, and Dr. Erin Arneson throughout the research planning and writing processes have been essential to the completion of this project. I would also like to thank the NHERI TallWood team and all of the professional and academic collaborators, particularly Dr. Shiling Pei, Dr. Keri Ryan, Dr. Jeffrey Berman, and Dr. Andre Barbosa. The research conducted by this team provides the foundation for this dissertation and their cooperation has been essential.

To my family and friends, I appreciate the patience and the support throughout this long journey, we've finally made it! And a special thanks to my parents, who have been my emotional rock throughout my life and particularly through my college career. Thank you for always believing in me and supporting my efforts through many trials and tribulations.

TABLE OF CONTENTS

ABSTRACT ii
ACKNOWLEDGEMENTS iv
LIST OF TABLES vi
LIST OF FIGURES vii
CHAPTER 1 – An Introduction 1
Introduction to CLT 1
European Developments 2
Early Research 3
SOFIE Project 6
Other European Efforts 12
North American Developments 12
Current State of the CLT industry in North America 16
Mass Timber, PBSD, and Growing Resilience Trends 17
Performance-Based Design 17
Resilience Considerations 19
Resilient Mass Timber 21
CHAPTER 2 – Time to Functionality Methodology 23
Overview 23
Building Performance Model and Ground Motion Requirements 25
Loss Analysis 26
Repair Sequencing using REDi Methodology 28
Time-to-Functionality Fragility Curves 32
CHAPTER 3 – Illustrative Example: Two-story CLT Building with Rocking Walls 34
Building Overview 34
Building Performance Model and IDA 35
Loss Analysis 37
Structural Fragility Selection 37
Non-Structural Fragility Selection 40
Repair Sequencing 43
Synthesis of Time-to-Functionality Fragility Curves 44
Closing 49
CHAPTER 4 – Nail Laminated and Dowel Laminated Diaphragm Test Setup 51
Introduction 51
Specimen Information and Testing Methodology 54
Testbed and Loading Protocol 61
Instrumentation 67
CHAPTER 5 – Nail Laminated and Dowel Laminated Diaphragm Test Results 70
Fixed-Beam Assumption 70
Force-Displacement Hystereses 71
Diaphragm Displacement and Time Series Profile 76
Diaphragm Deformation 81
Panel Deformation 85

Infill Joint and OSB Joint Displacement....88
Damage States and Fragility Curves....91
Closing....95
CHAPTER 6 – Application and Evaluation of TTF to Archetypes for Design Guidance....97
Introduction....97
Design Selection....98
Time-to-Functionality Method Application....100
Fragility Curve Selection....100
Building Performance Model and Ground Motion Selection....100
Repair Sequencing....101
Time-to-Functionality Curves....101
Evaluation of the TTF Results....104
Incremental Dynamic Analysis....104
Time-to-Functionality Curves....107
Panel Width in Relation to TTF Performance....107
Number of Plys in Relation to TTF Performance....112
Number of UFPs in Relation to TTF Performance....116
Post-Tensioning Rod Diameter in Relation to TTF Performance....120
Closing....124
CHAPTER 7 – Resilience-Based Seismic Design Guidance using the TTF Database....126
Introduction to Design Guidance....126
Step 1: Selection Location, Initial Design, and TTF Requirements....127
Step 2: Designs that meet TTF Requirements....128
Step 3: Geometric and Viability Check....129
Step 4: Cost Analysis....130
Step 5: Performance Evaluation using Alternative Methods in ASCE 7....130
Illustrative Design Guidance Examples....131
10-story Re-occupancy at MCE_R....132
10-story Functional Recovery at MCE_R....141
Closing....148
CHAPTER 8 – Conclusions, Contributions, and Future Work....149
REFERENCES....154
APPENDIX....161

LIST OF TABLES

Table 1..... 29
Table 2.....30
Table 3.....38
Table 4.....40
Table 5.....41
Table 6.....43
Table 7.....64
Table 8.....65
Table 9.....72
Table 10.....75
Table 11.....77
Table 12.....80
Table 13.....82
Table 14.....86
Table 15.....88
Table 16.....93
Table 17.....98
Table 18.....134
Table 19.....136
Table 20.....143
Table 21.....146
Table 22.....147
Table 23.....161
Table 24.....163
Table 25.....165

LIST OF FIGURES

Figure 1..... 24
Figure 2..... 27
Figure 3..... 34
Figure 4..... 35
Figure 5..... 37
Figure 6..... 39
Figure 7..... 45
Figure 8..... 45
Figure 9..... 47
Figure 10.....47
Figure 11.....56
Figure 12.....57
Figure 13.....58
Figure 14.....59
Figure 15.....61
Figure 16.....62
Figure 17.....63
Figure 18.....65
Figure 19.....67
Figure 20.....68
Figure 21.....69
Figure 22.....70
Figure 23.....72
Figure 24.....73
Figure 25.....74
Figure 26.....75
Figure 27.....79
Figure 28.....81
Figure 29.....83
Figure 30.....84
Figure 31.....85
Figure 32.....86
Figure 33.....87
Figure 34.....92
Figure 35.....95
Figure 36.....102
Figure 37.....103
Figure 38.....104
Figure 39.....105
Figure 40.....106
Figure 41.....108
Figure 42.....109
Figure 43.....110
Figure 44.....113
Figure 45.....114
Figure 46.....115
Figure 47.....118

Figure 48.....119
Figure 49.....120
Figure 50.....122
Figure 51.....123
Figure 52.....124
Figure 53.....127
Figure 54.....128
Figure 55.....133
Figure 56.....136
Figure 57.....142
Figure 58.....146

CHAPTER 1– AN INTRODUCTION

Introduction to CLT

Timber as a construction material is as old as civilization itself, with a well-established market; in the United States (U.S.) this mostly consists of low rise, light frame timber construction. In recent decades however timber has experienced significant growth in potential applications, with the development of mass timber leading the way. Mass timber is a general term that includes both new methods of producing and implementing highly engineered timber products in high performance situations on various scales. Cross Laminated Timber (CLT) is a mass timber product first developed in Central Europe several decades ago. CLT is a prefabricated, engineered, solid wood panel that is produced by utilizing kiln-dried dimension lumber (1x or 2x are typical) and glue lamination to create lamination layers that are then stacked with long wood grains in alternating, orthogonal, directions to create panels, resulting in a non-homogenous, anisotropic material [50]. The number of layers in a panel is variable and depends on the application and required properties, but it is typical to have an odd number of layers (3 to 7 is common but 9 recently possible), creating major and minor flexural and shear axes. The dimensions of a CLT panel are normally rectangular (with the major axes typically in the long direction), with the width limited by the size of the press, and the length by the mode of transport to the project site. In addition, using precision routers, it is possible to cut holes in the panels in a variety of shapes and sizes for such things as doors, windows, etc. as well as alter the rectangular shape of the panel to fit various architectural and design constraints. CLT manufacturing methods lend themselves well to panelization, allowing for the building segments to be prefabricated at the manufacturer, transported, and assembled on site. This, combined with its high strength to weight ratio, low

environmental impact, and other performance characteristics were the incentives for investigations into CLT as an alternative to conventional materials (concrete, steel, etc.) for several building applications. Specifically, mid-rise buildings were identified as an ideal area for CLT to be competitive, but quickly implementation challenges presented themselves. Panelized CLT buildings perform well resisting gravity loads due to the panel's rigid properties, however, it was discovered that the behavior of CLT panels under lateral load was not well understood. While the ridged properties of the panels were an asset in bearing, they didn't allow for CLT wall systems to deflect laterally as well as its light frame counterparts, limiting applications of CLT in moderate to high seismic regions. More ductility or an energy dissipating mechanism was needed in the design to reduce the high acceleration amplitudes and overturning moments experienced by rigid CLT wall systems. A review of notable applicable research with CLT as a seismic force resisting system (SRFS) is presented in herein, with more conventional SFRS presented first, by region and chronologically, then followed up with an introduction into newer, more resilient designs.

European Developments

The history of heavy timber construction in Central Europe created an economy in which mass timber companies could expand. By the early 2000s, little over a decade since its inception, several mass timber companies were producing CLT panels, and even complete panelized CLT buildings. However, most of these applications were limited to single family homes and low-rise buildings, due to the gaps in contemporary research demonstrating CLT as an effective lateral force resisting system, with wind specifically limiting mid-rise applications in non-seismic regions. Furthermore, in some regions of Central Europe (Italy, Slovenia, etc.) as well as Southern Europe (Portugal, Greece, Turkey), high seismicity was an obstacle, providing additional incentive to use CLT as

not just a lateral force resisting system for wind loading, but for seismic resistance as well.

Early Research

Slovenia was situated at the crux of the limitations of CLT in the early 2000s, part of Central Europe and the heavy timber traditions, and several mass timber companies producing panelized CLT buildings existed in the country, however seismicity in the region limited the market to Northern Europe. Demand to incorporate the local market as well as expand the use of CLT to mid-rise applications provided motivation for further research. Published in 2004, Dujic et. al (2004) [20] was one of the first studies conducted with the intent of demonstrating CLT as a lateral force resisting system. The testing took place at the University of Ljubljana in Slovenia, financed in part by the Slovenian Ministry of Education, Science, and Technology, RIKO HISE Ltd. (a local panelized CLT building company), and KLH Massivholz GmbH (an Austrian CLT Manufacturer). RIKO HISE Ltd. Produced mostly single-family panelized CLT homes and desired to expand into the local market, preferably utilizing mostly existing designs. The building designs were connected to the foundation using steel anchorages, and as mentioned previously, even prior to this study, it was identified that connectors and anchorages were the most advantageous component of a CLT wall system to introduce ductility or energy dissipation. Therefore, the study focused on testing the existing anchorage design for several modifications with the goal of determining their mechanical properties. To do this, a CLT panel cantilever test set-up was designed, in which a CLT panel was connected to a steel frame along the top of the panel, and to a horizontally displaceable mechanism controlled by an actuator along the base. A constant vertical load was then applied to the panel, and displacement-controlled horizontal loading was applied to rack the panel. Three different vertical load magnitudes were used along with three

different horizontal loading protocols, utilizing a combination of monotonic and cycling loading, a first for CLT panel testing. Three anchorage configurations were tested, leading to a total of 15 tests. The test results revealed that the anchorage strength and local wood failures were the controlling factors in the capacity of a CLT lateral force resisting system. This was already suspected due to the rigid nature of the CLT panels and their limited ability to deflect laterally, forcing the anchorages and connectors to be the main means of energy dissipation. In addition, similar to lateral force resisting systems using other materials, CLT wall systems see improved lateral performance when the panels are simultaneously engaged in bearing, especially in cases when the anchorages were weak. This study took the first initial steps towards building the necessary knowledge to incorporate CLT wall systems as lateral force resisting systems, resulting in further studies, and laying the groundwork for a variety of studies in Europe and beyond.

While designing and conduction the testing in Dujic et. al (2004) [20], several deficiencies in the application of contemporary European testing protocol to CLT became apparent. The testing protocol EN594, which was the most current at the time, was only designed to estimate the racking strength of timer frame walls with sheathing (such has plywood) and fully restrained frame studs as well as only accounting for monotonic racking loads [19]. In the case of partially anchored studs and minimal vertical load as well as high seismic regions, the aforementioned testing protocol overestimates the bearing capacity of the wall. To address the need for updated testing protocols for realistic boundary conditions and seismic prone regions, an investigation was launched by Dujic et. al (2006) [19] with the objective of demonstrating a variety of testing possibilities using adaptable boundary conditions and various loading protocols. Three boundary cases were identified as most likely to occur in reality, and were designated Case A, B, and C

respectively. Case A included a shear cantilever mechanism, where the base of one edge of the CLT panel is fixed, and the other is free to rotate and translate. This is most commonly seen with flexible roof systems, or narrow, slender CLT panels. Case B, featured a restricted rocking mechanism, where one edge of the panel is fixed, and the other can translate and rotate, but only as much as a ballast restricted to vertical translation, typical for walls carrying floor load, allows. The final boundary condition, Case C, is a shear wall mechanism, where one edge of the panel is fixed, and the other is only allowed to translate parallel to the fixed edge. This case usually occurs with the infill of a stiff surrounding frame. Case A and B had a constant vertical load throughout the testing, while Case C had a variable vertical load due to the need to increase the load during testing, preventing panel uplift. The testing incorporated both timber-framed walls and CLT wall panels subjected to both monotonic and cyclic loading, using the aforementioned boundary condition cases, as well as three levels of vertical loads. The results showed that boundary conditions can significantly impact the measured load bearing capacity of a sample. For the CLT panels, Case C had a capacity of almost double that of Case A, leading the authors to concluded that additional loading protocols needed to be developed, and that designing a CLT shear wall using Case C alone was not recommended. This study quantified the suspected deficiencies in contemporary loading protocol for timber structures and particularly CLT panels. It also emphasized the need for additional development of loading protocols using cyclic loading for CLT shear walls located in seismic regions.

The culmination of the multi-year project funded by the Slovenian government and various commercial partners was shake table tests conducted at the Dynamic Testing Laboratory of the Institute of Earthquake and Engineering Seismology (IZIIS) in Skopje, Macedonia [21]. The

primary objective of these tests was to correlate the shake table results with the quasi-static test results from the earlier study, ultimately providing the necessary information to design and construct seismically resistant CLT buildings. The test specimens were single story boxes that consisted of parallel CLT wall panels with perpendicular panels used for support only. During the testing, both single and double panel configurations were tested, and subjected to earthquake motion records with frequencies ranging from 5 Hz-7.5 Hz. The tests showed that the wall configurations exhibited a non-linear behavior with the connectors deforming and dissipating energy, while the CLT panels acted as a rigid, linear elastic body. These tests were the first shake table tests performed on CLT lateral force resisting systems, and provided valuable insight into the behavior of the systems under seismic loading, as well as identifying needs for future research. The authors of the study specifically described the need for new protocols and design limits (inter-story drift, base shear, etc.) to be developed for CLT structures located in seismic areas, as well as the need for further testing to develop a behavior factor "q" for CLT for use in Eurocode. The "q" factor is similar to the R factor used in U.S. seismic design.

SOFIE Project

Other seismic regions of Europe were also extremely interested in the potential application of CLT as a lateral force resisting system. Specifically, beginning in 2005, a comprehensive, landmark study investigating all components of a prefabricated CLT building's behavior, including mechanical properties, building physics, acoustics, fire, durability, and seismic performance [38]. The project was funded by the Trento Province in Northern Italy, and its components were coordinated and conducted by the Italian National Research Council – Trees and Timber Institute (CNR-IVALSA). The generalized approach of the study was to start with smaller scale quasi-static experiments on connectors and wall panels, eventually leading to multiple full-scale shake

table tests.

The first stage of the project began in the mid-2000s with Ceccotti (2008) [14]. The study conducted monotonic and cyclic tests performed on four different CLT wall panel configurations, and also a one-story pseudo-dynamic test. The wall panel configurations tested different connectors, configurations, and inter-story connections. Configuration A was based on a real first story CLT wall system with commercial connectors and hold-downs, and a constant vertical load. There were three steel angle brackets spaced across the bottom edge of the panel, and a hold-down on either end, with the number and strength of nails variable by tests. These configurations were tested a total of seven times using a combination of monotonic and cyclic loading. The tests were performed to document different failure types (i.e., hold-down vs connector). Specifically, the number of nails used to secure the hold-down to the CLT wall panel was changed to influence the failure mode. Configuration B, similar to Configuration A, was based on a real CLT wall system, in this case a typical second floor shear wall. The configuration consists of the same basic components of A, however there are only two shear connectors across the base of the panel instead of three. Configuration B was tested in a similar way to Configuration A with both monotonic and cyclic test being conducted, however the number of nails securing the shear connector to the panels was varied instead to achieve different failure modes. Configuration C was also a first story CLT wall system, however there were no shear connectors and only hold-downs located at each of the four corners of the panel. The testing of this configuration consisted of only one monotonic and one cyclic test with no variation in the configuration. Configuration D was unique among the four configurations due to the presences of an opening in the form of a doorway, otherwise the connectors and hold-downs were similar to Configuration B. The testing program was similar to

that of Configuration C; however, the size of the opening was increased between the monotonic and cyclic test. The tests provided more evidence that the connectors were the ductile part of the CLT wall system, with the panels themselves exhibiting rigid behavior. This localized displacement and force concentration was discovered to potentially cause material failure in the CLT panel itself if defects (such as an error in the lamination) were present. The tests also produced an average viscous damping of 14%, demonstrating the suitability of CLT wall systems for seismic regions. After the individual CLT wall systems were tested, a larger scale one-story CLT wall assembly with three different configurations was tested. A pseudo-dynamic testing approach was taken where the forces on the structure are calculated using the weight of the structure and the acceleration values of a real ground motion record. This method is limited in its ability to accurately simulate the velocity of an earthquake and is usually considered as a precursor or proof of concept test before a full scale shake table test. The first test configuration was a symmetric layout with external openings, and one smaller internal opening, with the goal of simulating a real structure. The second configuration was identical to the first except the internal opening was increased to the same size as the external openings. The final configuration was an asymmetric layout with one external opening being approximately 1.8 times larger than the other openings. It should be noted that cyclic tests were carried out in between the pseudo-dynamic tests to establish the stiffness of the structure. In general, it was observed that the configurations were very stiff, but still have sufficient ductility (mostly provided by the connections). This was observed in other testing, and this result reinforces the observations of earlier tests. What was a surprising and consequential discovery was the similarity in performance and stiffness of the second and third configurations. The third configuration featured a much larger opening than the second configuration, and the results imply that the lateral stiffness is determined by the

connections, not the wall panels, for low magnitude shear forces. In general, this test further reinforced the importance of the connections in determining seismic behavior (and capacity) and in particular demonstrated that connector strength can be increased to a point approaching the material without compromising ductility. This revealed the clear potential of CLT wall systems as a SFRS and provided the necessary data and proof of concept needed for larger scale tests.

The next step in the SOFIE project was to progress from pseudo-dynamic testing to full scale shake table testing, in order to determine an over strength factor for Eurocode design. This was done in two phases, with the first phase consisting of testing a three-story CLT building on the National Institute for Earth Science and Disaster Prevention's (NIED) Tsukuba Shake Table in Japan [14]. The building was a full scale 7m x 7m (23 ft x 23 ft) three-story CLT building with a total height of 10 m (33ft). The panels were made of spruce imported from Italy, and the building was constructed on a steel frame connected directly to the shake table. The building itself was connected to the steel frame using commercial connectors and anchors, and consisted of four outer walls, one inner wall, floor diaphragms, and roof panels, all composed of CLT panels. Three different configurations were tested, following a similar pattern to the one-story test with each configuration using a different sized opening on the ground floor of the structure. Additional weight was added on each floor of the building to account for the insulation and finishing to the building as well as a percentage of the design live load as stipulated by the European and Italian seismic code. The building itself was designed assuming all of the ductility was provided by the connectors. The connecters were then designed to ensure that energy dissipation (deformation and pull out) occurred first in the inter-panel joints between panels, then the shear connectors between the walls and the floors, and finally the hold-downs resisting overturning moment. This approach

was taken to maximize energy dissipation and was based on results from the panel and connection tests previously discussed. Instrumentation including accelerometers and displacement transducers were placed on each story of the structure to measure acceleration, relative displacements, inter-story drift, and uplift. Load cells were also used to measure the force in the hold-down rods at the base of the structure. The three story CLT building then was subjected to a total of 15 shake table tests with peak ground accelerations (PGA) ranging from 0.5 g to 1.2 g. Between tests, only minor repairs were made to the structure, and the building performed well and did not sustain any damage that was not felt to be repairable. There was however, a significant amount of damage observed in the connections that would need to be repaired, but which was expected since the connections had been established by this point to provide the energy dissipation. In conjunction with the seismic tests, a numerical model was developed to model the behavior of the building. The numerical model used a nonlinear time history approach that modeled CLT panels as rigid braced frames interconnected with nonlinear connector springs. The purpose of the model was to incorporate previous test findings and shake table tests to produce a model capable of accurately predicting the response of CLT buildings for seismic loads. The developed numerical model incorporated the over strength factor calculated from the responses of the three story CLT building, attempting to recreate the test numerically. The results of the efforts were in good agreement with the experimental results. The testing was not only the first shake table test on a realistically sized full-scale CLT building, it also provided information necessary to suggest an over strength factor necessary for design using Eurocode, as well as to calibrate a powerful numerical model.

The SOFIE project culminated in a seven-story full scale shake table test conducted in 2007 at

NIED's shake table in Miki, Japan (the largest shake table in the world). The test was the largest 3D shake table test ever conducted up to that point on a full-scale structure composed of any material. The structure itself was designed using the simplified lateral force method in Eurocode 8, using knowledge from other parts of the project such as the over strength factor from the three-story tests. The test is documented in Ceccotti et al. (2013) [15], and similar to the three-story tests, the structure was constructed using CLT from trees in Northern Italian forests. The building consisted of a 7.5 m x 13.5 m (24.5 ft x 44ft) floor plan with seven stories, resulting in a total height of 23.5 m (77ft) with the thickness of the wall varying per story due to decreasing structural demand on the higher floors. The connections were designed according to the shear demand for each floor and consisted of the same commercial connectors tested in the earlier phases of the project. The structure was heavily instrumented with over 260 sensors, and accelerations, uplift, relative displacements, inter-story drifts, and slip between floor and wall panels were measured. The structure was subjected to more than 10 shakes with a maximum PGA of 0.82 g. After the tests, no residual displacement was observed in the structure, but damage was observed on the hold-downs on the first floor, confirming that the combination of the stiff behavior seen in previous tests with a slender profile would produce large overturning moments. Large accelerations were also observed (over 4 g) at the upper levels of the building. Additionally, it was determined that uplift, slip, and inter-story drift were not critical. The test emphasized the need to introduce more ductility in the system for mid-rise buildings during large earthquakes, as well as to expect large overturning moments. Overall, the test and the SOFIE project as a whole demonstrated the suitability of CLT for used in low and mid-rise structures in seismic areas in a very thorough and highly visible way that could be used to convince government agencies as well as the general public. In addition, the project also left a clear path forward for research, improvements in the

contemporary design philosophy were still very much possible.

Other European Efforts

In a follow up of sorts to the SOFIE project, Gavric et al. (2011) [29] summarizes a multipart project investigating the some of the areas identified as in need of further research during the course of the SOFIE project. In particular, the study focused on the performance of connections in CLT wall panels, with the ultimate objective of developing analytical models to predict strength and stiffness properties of connectors, allowing for the development of over strength factors. Gavric et al. (2011) [29] was the third and final phase of the investigation with the previous two parts testing hold-down connections and angle bracket connection tests [35]. The final phase of the investigation tested over 20 different configurations of panel connectors with screws as fasteners. Monotonic and cyclic loading were used in all three components of the testing, and the results of the project provided valuable information on the design of CLT connections where limited damage under seismic load is desired. The study proposed over strength factors for design ranging from 1.2 to 1.9, depending on design and applications.

North American Developments

These early CLT studies, along with its growing popularity in Europe, demonstrated the properties and applications of CLT to both the research and practicing engineering communities, as well as demonstrated its competitiveness with concrete and steel in certain applications, leading to its spread to other places around the world. In North America, Canada with its large timber industry has long had significant economic incentives to make timber as versatile as possible. It is no surprise then that they should take the leading role for introducing CLT into the North American market. Similar to Europe however, moderate seismicity in British Columbia limited its

application there, and in response, FPInnovations commenced a series of studies on the seismic design of CLT systems. Popovski et al. (2010) [57] conducted 32 monotonic and cyclic tests using CLT panels imported from KLH Massivholz in Austria. Twelve different wall configurations were tested with a wide variety of aspect ratios, connector types, connector configurations, boundary conditions, and openings. In addition to the wall configurations, a two-story panel test was conducted. These relatively comprehensive tests provided valuable information on a wide variety of wall configurations, with the results agreeing well with previous European studies. The inter-panel joints and shear connectors were the main source of ductility in the tested CLT seismic systems, and while this was expected, the tests began a large and extensive research effort in North America to further research CLT for use in seismic design. In a follow up study, Popovski et al. (2012) [55] attempted to build on previous European studies quantifying the behavioral factor of CLT for Eurocode 8. This included estimating the seismic modification factors (R-factors) for CLT wall systems for the National Building Code of Canada (NBCC). The effort consisted of three distinct methods: comparison to existing timber systems in NBCC, using a similar methodology to previously conducted European studies, and following the equivalency approach that is recommended by the International Code Council 2013. The recommended AC130 approach was conducted using the test results from Popovski et al. (2010) [57]. The final recommended factors for R_0 and R_d were 1.5 and 2.0 respectively. This study represented a first attempt to estimate these factors and would provide a basis for further studies.

A summary of contemporary knowledge of CLT systems in North America was presented in Popovski et al. (2011) [56], which was then incorporated into FPInnovations' CLT Design Handbook, Canadian edition. Similarly in the U.S., through a collaborative effort including:

FPInnovations, the American Wood Council, APA- The Engineered Wood Association, Woodworks U.S., and the U.S. Forest Products Laboratory a corresponding US edition of the CLT Handbook was developed [34]. Both editions present a wide collection of information on CLT including manufacturing techniques, design methodology, connection design, lateral performance of CLT wall systems, fire performance, etc. The handbooks provided a comprehensive compilation of contemporary CLT research for use in the design and construction of CLT buildings in North America.

Previous European studies had demonstrated the capability of CLT for use in performance based seismic design. However, a system for quantifying damage levels for CLT had not yet been developed. Schneider et al. (2012) [65] attempted to fill this gap using test data from previous North American studies. The approach attempted to quantify damage using an energy-based index first developed by Kratzig et al. (1989) [35]. The different failure modes for the connectors were identified, and five damage categories were developed: None, Minor, Moderate, Severe, and Collapse. The energy-based damage method was compared with a visual damage assessment over the course of the testing. The correlation between the calculated and observed damage was good and represented the wall behavior satisfactorily. The establishment of these damage categories were an essential component of the implementation of CLT into performance-based design and laid the groundwork for further development.

With a satisfactory number of preliminary 2-D investigations conducted in North America, Popovski et al. (2012) [55] investigated the 3-D performance of a CLT structure subjected to lateral loading. Documenting the global behavior of the structure, its deformation capacity, and the

frequency response of the structure before and after each test were the primary objectives. A 6.0 m x 4.8 m (19.75 ft x 15.75 ft) house was subjected to five quasi-static tests (one push-over and four cyclic), with each direction being tested sequentially. During the different tests, the connector's configurations as well as the loading was varied and included the direction of loading, quantity of hold-downs, and connections between the CLT panels. This test demonstrated that sliding and rocking are caused by bracket failures and represent the majority of the ductility of the CLT panel. The testing also demonstrated the ability of CLT panels to exhibit rigid body motion (i.e., rocking). In addition, the study particularly stressed the need for further research into the effect of different aspect ratios on the behavior of the panels. One of the objectives of the larger research was to determine the effects of various aspect ratios on the performance and behavior of CLT shear wall systems.

An effort to estimate suitable seismic design factors (R-factors) for CLT buildings in the U.S. was undertaken by Pei et al. (2013) [48] because the R-factors are a necessary component of force-based seismic codes in the U.S. To that end, a nonlinear, load-resistance model was developed for CLT shear walls based on previous reverse cyclic test data. Possible R-factors were estimated by re-designing a 6-story CLT apartment building that was originally part of the NEESWood Project (van de Lindt et al, 2010 [75]), then using peak inter-story drifts as the performance requirement and selecting R-factors that achieve the desired performance. An R-factor of 4.5 was suggested thereby providing a probability of non-exceedance of 80% for a 4% inter-story drift. This study was one of the earlier attempts to estimate an R factor, however it was limited by scope and methodology. This estimate only used one building configuration, so to be more rigorous, a number of archetypes should be developed and used instead.

To develop more rigorous estimates of R factors for CLT shear walls, a team of researchers undertook a multi-year project funded by the Forest Products Laboratory to identify seismic performance factors for CLT using the procedure laid out in FEMA P695 (2009) [24], with the goal of incorporating CLT into US seismic design codes and standards. The project was divided into several sub levels: (1) Component and assembly level testing, (2) Design methodology development and calibration based on test data, (3) Developing and calibrating numerical model, (4) Representing the design space with the development of archetypes, and (5) Extensive nonlinear analysis to identify seismic performance factors. The details of this testing can be found in Amini et al. (2018) [6]. The ultimate result of the project was the recommendation of an R factor equal to three for panels with an aspect ratio of 2:1 or mixed 4:1 and 2:1 and an R factor value of four for use in high aspect ratio panels only (van de Lindt et al. 2022 [74]).

Current State of the CLT industry in North America and CLT code in the U.S.

Since its introduction, CLT has seen steady growth in North America, with numerous manufacturers such as Structurlam and Nordic Structures in Canada, and Smartlam (located in Montana) in the U.S. appearing since 2010 [50]. Another region seeing a growing interest in CLT is the Pacific Northwest in the U.S. The region has high interest in CLT due to the regional timber industry. DR Johnson Lumber Co. was the first to begin CLT production in 2015. Sterling Lumber Company is another example of the growing presence of CLT and began production in the spring of 2016 outside of Chicago. Several research efforts funded by various private and government agencies have been conducted to identify local wood species ideal for CLT production, as well as to develop the most economical production chain for CLT. The general idea is to create an efficient industry capable of using low grade hardwoods and other low-value sources to produce CLT with

satisfactory strength and other material properties. One of the first steps to introduce a new engineering product is to develop product standards. In North America, the first standard was developed by a collaboration of APA-The Engineered Wood Association and FPInnovations [50]. The PRG 320 standard was then published and recognized by the American National Standards Institute (ANSI). This standard, along with a dedicated chapter for CLT design was added into the 2015 version of the National Design Specification® (NDS®) [45]. The International Building Code (IBC) then adopted CLT construction by referencing the NDS®. CLT was also recognized as a heavy timber material, and thereby permitted in Type IV construction. This was due in most part to the efforts of the American Wood Council (AWC) and their sponsorship of an ASTM E119 fire endurance test. CLT is slowly gaining acceptance in seismic building codes as a result of work like van de Lindt et al. (2022) [74], but prescriptive life-safety focused code-based design is not the only design methodology; specifically supplementary design methodologies based on the performance of the building (among others) may also have applications for CLT and other mass timber products.

Mass timber, PBSD, and Growing Resilience Trends

Performance-Based Design

Seismic risk mitigation has garnered significant attention from academic and professional engineering over the last several decades, primarily in the form of performance-based seismic design (PBSD). In more recent years resilience has gained increasing attention as initiatives such as the United States Resiliency Council (USRC) [72] and the Seismic Resilience Initiative (SRI) (Sahabi et al., 2018) [62]. For earthquake engineering specifically, this has manifested as a result of shifting design objectives. Traditionally, in the U.S. as well as across most of the world, seismic design focused on life-safety objectives, with the majority of current seismic design codes

worldwide defining adequate seismic performance during a major event as “life-safety”; meaning occupants should survive unharmed during a “design level” or even larger event. Life-safety is and will remain the fundamental objective of any seismic design philosophy; however, with increasing knowledge in the field of seismic design, additional impacts of a seismic event such as financial losses (both direct and indirect losses), societal disruptions, and adverse effects (population migration, community degradation, etc.) can now more readily and directly be considered through modeling. This translates into a more comprehensive consideration of the resilience of a building system and the broader interconnected community network, by including the ability to recover after an earthquake.

Any second-generation PBSD approach requires a robust loss assessment methodology, as well as any attempt to incorporate resilience into a design. As a consequence of this, over the past decade research has focused on financial loss models of individual buildings when subjected to a seismic event. The Federal Emergency Management Agency (FEMA) headed these efforts in the US and culminated in a new approach to PBSD in FEMA P-58 (FEMA 2018) [23]. FEMA P-58 details the assessment of the seismic performance of a building through a five-step process. This process includes assembling a building performance model, defining earthquake hazards, analyzing building response, developing a building collapse fragility, and then determining performance. The tangible consequences of building performance are predicted using the structural response as well as developed fragility curves and consequence functions. The probability of collapse as a function of ground motion intensity (also known as an overall collapse fragility) is utilized to help predict casualties as well as other considerations (such as component level damage). The purpose of the consequence functions is to relate damage to other quantifiable measures such as repair time,

potential repair and replacement costs, casualties, unsafe placarding, and other potential impacts. Each damage state has its own set of independently defined consequences (FEMA P-58 2018 [23]). As an adjacent project, the Performance Assessment Calculation Tool (PACT) (FEMA 2012) [26] was developed to utilize the principles of FEMA P-58 and incorporate them into a Monte Carlo procedure based on Yang et al. (2009) [79]. This led to other efforts to incorporate FEMA P-58 and PACT into other models, such as in Terzic et al. (2016) [71], where a repair model was designed to specifically integrate with PACT utilizing the critical path method (CPM) to estimate the repair time. The model additionally was designed to be an applicable repair model in a larger effort to determine the resiliency index of a building as defined in Cimellaro et al. (2010) [16].

Resilience Considerations

With the rapid development of building level loss estimation, it was now possible to integrate them into regional loss estimates such as the "ShakeOut Scenario". The "ShakeOut Scenario" was a collaborative effort involving both academic and government institutions to estimate the financial losses of a 7.8 magnitude earthquake on the southernmost 200 miles of the San Andreas Fault (Sahabi et al., 2018) [62]. Outside the US in New Zealand, the devastating losses suffered during the 2011 Christchurch, NZ earthquakes prompted studies such as Mayes et al. (2013) [41] and Terzic et al. (2012) [70] to implement PACT to estimate financial losses of buildings designed to the contemporary prescriptive building codes. Mayes et al. (2013) [41] calculated that the losses could be in excess of 20% of replacement value, which further motivated exploration of design alternatives to reduce financial losses. Studies at the individual and regional level illustrated a distinct problem. There is a substantial disconnect between prescriptive design code performance requirements (i.e., life-safety) and societal expectations of design (i.e., earthquake "proof") (Mayes

et al., 2013) [41]. Terzic et al. (2014) [69] performed a life cycle cost analysis on five different designs, ranging in cost and performance, of a hypothetical three-story steel office building located in Oakland, CA. the study found that a middle ground between performance and cost produced the best return on investment for the stakeholders. Yamin et al. (2017) [77] developed an economic loss estimation model that considers repair and commercial costs, incorporates both structural and non-structural components, and assesses business interruption costs. This model was applied to a suite of archetypes and vulnerability curves were constructed and compared to existing methods from HAZUS.

With the demand for more resilient building design established and growing, and robust tools such as PACT available, government and academic institutions began to push and develop evaluation systems for the resilience of buildings. The Resilience-based Earthquake Design Initiative (REDi) Rating System was introduced in 2013. The system is a comprehensive rating that considers building resilience, organizational resilience, and ambient resilience of a facility (Almufti and Willford, 2013) [4]. The system includes a three-level rating (silver, gold, and platinum) as well as a guide to the criteria to achieve each rating, from the design of the structural system, to the utility operations after a seismic event (Almufti and Willford, 2013) [4]. The USRC (2015) [72] used REDi along with numerous other supporting materials to develop their own building rating system for earthquake hazards. Despite the existing framework for RBSD using tools such as PACT or REDi, the process is still computationally intensive, reducing its applicability and economic feasibility in many cases.

Resilient Mass Timber

Resilient mass timber seismic research began in New Zealand in the mid-2000s with the adaptation of a rocking wall concept originally used in concrete walls, applying the concept to laminated veneer lumber (LVL), and investigating different moment connections and post-tensioning configurations (Palermo, et al. 2006) [47]. This early research laid the groundwork for further development of a post-tensioned lateral force resisting rocking wall system capable of utilizing a variety of mass timber products (Buchanan, et al. 2008) [10]. Post-tensioned rocking walls made from LVL were eventually incorporated into a number of commercial projects including the 3-story Arts & Media Building in Nelson, NZ (Holden, et al. 2012) [32]. The success of the system inspired component tests implementing CLT instead of LVL, with the specific intention of improving the ductility of contemporary lateral force resisting systems in CLT buildings (Ganey, et al. 2017) [28]. Akbas, et al. (2017) [3] derived model parameters from the experimental test data of Ganey, et al (2017) [28]. These results were then used to design a full-scale shake table test of a two story CLT building with post-tensioned rocking walls. The experiment demonstrated the resilience capabilities of the system; the building re-centered without unintended structural damage after each of a series of 14 earthquakes and sustained inter-story drift ratios far beyond design level, i.e., up to 5% (Pei, et al. 2019) [52]. CLT resilient design has been making strides in recent years, and a resilient CLT structural system suitable for mid-rise buildings was demonstrated to be effective in small- and large-scale testing. However, current resilient design for CLT only considers the structural system itself, thereby underscoring the need to incorporate other non-structural systems into the design.

To address the current research deficit incorporating both resilient mass timber structural design and non-structural components, a large multi-institutional study was commenced to test a full scale 10-story mass timber building incorporating both the rocking wall system in Pei, et al. (2019) [52] and non-structural components typical of a mixed-use building (NHERI TallWood). Much of the research presented in this dissertation was developed for the express purpose of evaluating and understanding the design of this 10-story structure with resilient-focused techniques, however, this does not mean the presented research is limited only to this specific case. In fact, general applicability beyond the NHERI TallWood project and mass timber were important considerations throughout the research process. Chapter 2 focuses primarily on a stochastic methodology developed to evaluate and estimate the downtime of the structure under various seismic loads. This general methodology was then specifically applied to the two-story structure in Chapter 3, with information intended to lead to the ten-story project designs. Chapter 4 presents the testing that was performed on mass timber diaphragms in preparation for incorporation into the larger 10-story design. This testing provided an additional opportunity to identify damage states of the various diaphragms, and to develop basic fragility curve estimates. The results of these efforts are presented in Chapter 5. Chapter 6 further expands upon the framework developed in Chapters 1 and 2 by developing OpenSees models for various archetypes of building implementing the rocking wall system and by evaluating their downtime performance. A total of 243 different designs across two-, six-, and ten-story archetypes were evaluated, and Chapter 6 presents the compilation of the downtime of the various designs. Chapter 7 presents the full resilience-based seismic design guidance for tall mass timber structures, incorporating the database in Chapter 6.

CHAPTER 2 – TIME TO FUNCTIONALITY METHODOLOGY

Overview

The objective of the presented methodology is to develop fragility curves for the time it takes a building to become fully functional following a simulated earthquake (e.g., 60 days, 90 days, etc.). The time-to-functionality (TTF) fragility curves are developed by evaluating the performance of structural and non-structural components of the system subjected to a variety of ground motions at different intensities and integrating time and resource demands for repair and replacements. The evaluation of a full structure (particularly damage and corresponding repair process) introduces uncertainty into the model, with quantification of this uncertainty occurring later in the Chapter, for the evaluation, a multi-layer Direct Monte Carlo approach is used.

Figure 1 represents a flow chart of the methodology consisting of four major sections: (a) *Building Performance Model and Response Data (Steps 1-4)*, (b) *Loss Analysis (Steps 5-8)* (c) *Repair Sequencing (Step 9)*, and (d) *TTF Fragility Curves (Steps 10-11)*.

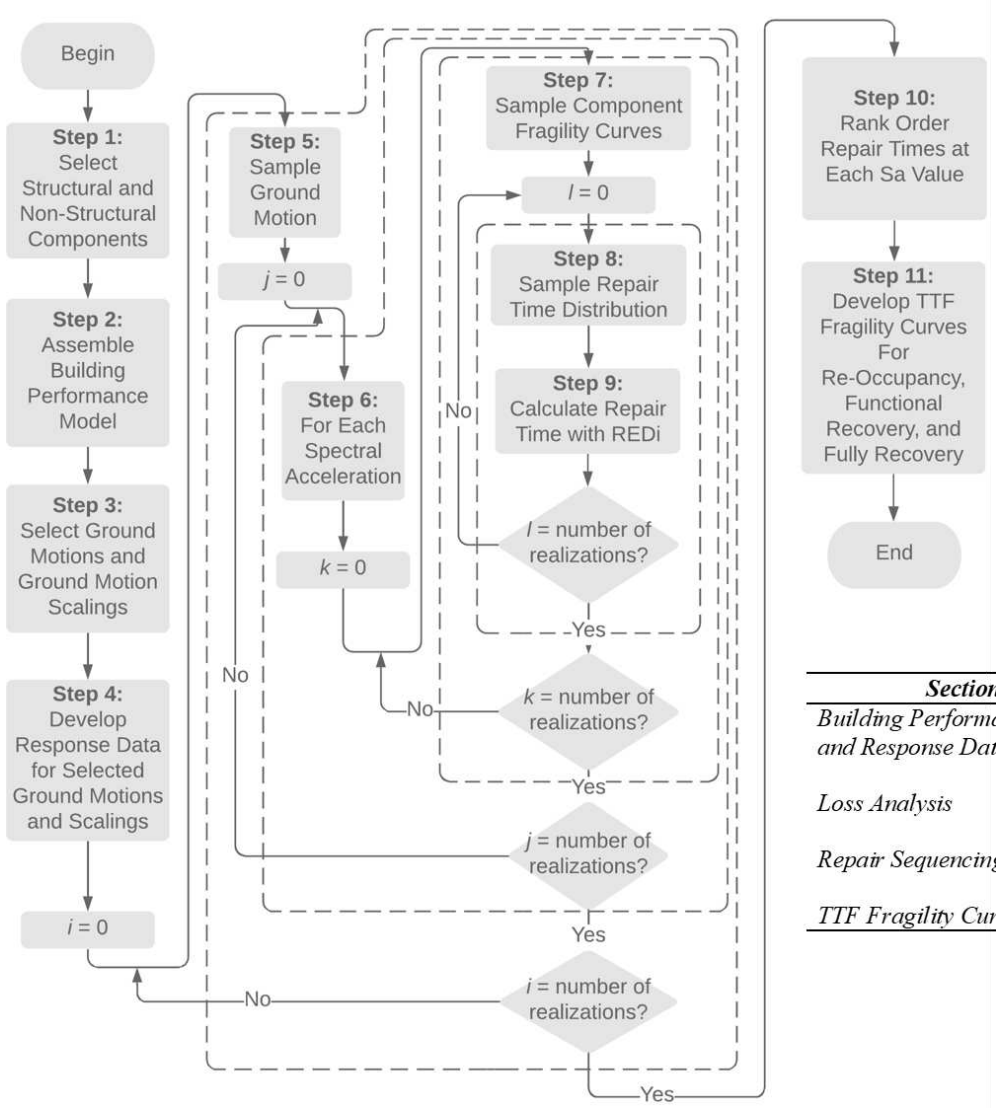

Section	*Steps*
Building Performance Model and Response Data	1-4
Loss Analysis	5-8
Repair Sequencing	9
TTF Fragility Curves	10-11

Figure 1: Procedure for repair fragility generation

The *Building Performance Model and Response Data* section consists of determining basic system characteristics such as structural and non-structural components, quantities, and ground motion selection and scaling. It also incorporates the selection of the Building Performance Model, which will determine the response of the structure to the scaled ground motions. The *Loss Analysis* determines the damage sustained by individual components using fragility and consequence functions from FEMA P-58 [23]. The *Repair Sequencing* section determines the order in which components will be repaired and determines the TTF for the structure for a given realization. The

REDi Downtime Assessment Methodology is utilized in the *Repair Sequencing* section to construct and evaluate a repair model for the structure and produce estimates of the system level TTF. The *TTF Fragility Curves* represent the probability of a TTF being exceeded as a function of spectral acceleration (S_a), and they are developed by iterating the *Loss Analysis* and *Repair Sequencing* sections over a number of realizations, each representing a different ground motion and scaling. The different levels of the Monte Carlo simulation are represented by the dotted lines, and correspond to realizations *i*, *j*, *k*, and *l* in Figure 1.

Building Performance Model and Ground Motion Requirements

As previously mentioned, the first section of the methodology (Figure 1: Steps 1-4) includes identifying the structural and non-structural characteristics of the system and the building performance model, which is typically a structural model to estimate engineering demand parameters (EDP) and for selecting desired ground motions. Once the system, model, and motions have been selected, an analysis of the system excited by a suite of ground motions is performed with the response of the system determined by the selected building performance model. The remainder of the method operates on the EDP results, thus the proposed procedure does not dictate the building dynamic modeling approach to be used, as long as it provides reasonably accurate EDP predictions. Similar to the model selection, the ground motion selection and model analysis procedures are also quite flexible with either a typical incremental dynamic analysis (IDA) Vamvatsikos, et al (2002) [73] or multi-stripe analysis Baker (2015) [8] being viable. In general, the model analysis needs to produce vectors containing the EDPs for all spectral scalings at each story of the structure (specifically peak acceleration and inter-story drift ratio), as associated with various scale factors for each of the selected ground motions.

Loss Analysis

The Loss Analysis of the system (Figure 1: Steps 5-8) incorporates fragility and consequence functions for the nonstructural components that were developed for FEMA P-58 [23]. FEMA background documents provide documentation of the development of fragilities for individual components (e.g., Mosqueda 2016; Porter 2009a; Porter 2009b; Porter, 2009c) [43, 58, 59, 60]. In general, the fragilities have been developed through a combination of laboratory testing, collection of historic earthquake data, structural analysis, and engineering judgement (FEMA 2012) [26]. To support the methodology proposed here, repair time consequence functions were utilized. Specifically, each damage state includes a time-related consequence function indicating the number of labor hours associated with a specific repair. The actual time that a building will be unusable for re-occupancy following an earthquake is affected by many factors that make the reliable estimation of interruption time difficult (Mitrani-Reiser 2008) [44]. Thus, the consequence function method introduced in FEMA P-58 considers not only repair time, but also the time to procure needed resources, the probability that a building will be posted with an unsafe placard, and the influence of the overall occupancy interruption.

The fundamental parameter for developing repair time is the number of workers who can work in the building at the same time. The number of workers per square foot that may effectively occupy an area is limited, and FEMA P-58 provides an upper bound on this value. The repair time for each damage state is described using five parameters: lower quantity LQ (a quantity below which there is no reduction in efficiency), maximum repair time associated with the lower quantity RT_L, upper quantity UQ (the quantity above which there is no further gain in efficiency), minimum repair time associated with the upper quantity RT_U, and dispersion (uncertainty). Each point on the repair time

vs. quantity curve follows a lognormal or normal distribution (determined by experimental data), characterized by the lower and upper quantities (median values) and the dispersion (β). Figure 2 represents a conceptual repair time consequence function featuring all the necessary parameters.

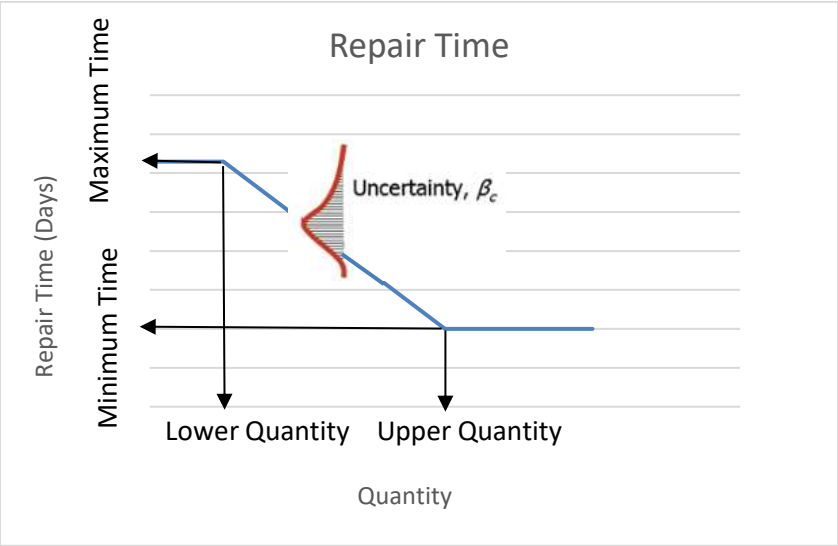

Figure 2: Sample repair time function per FEMA P-58

The repair time for all components and a single realization is represented by array $R_{i,j,k,l}$ where i, j, k, l are the repair sample identification indices for ground motion, spectral acceleration, repair fragility curve, and time consequence function, respectively. To determine each repair time realization, a ground motion and scale factor is first randomly sampled (Figure 1: Step 5-6), with the distribution of ground motions represented by $g\left(\theta_{i,j}\middle|M\right)$ where $\theta_{i,j}$ is the demand parameter result array (interstory drift ratios or acceleration) determined by the building performance model for given motions *M*. The component level fragility curves are then sampled to determine damage states for each component (Figure 1: Step 7). These fragilities are randomly sampled from $P_{i,j,k} \sim U(0,1)$, where $P_{i,j,k}$ is the probability of occurrence array given probability sample k, spectral acceleration j, and ground motion sample i. Then using $P_{i,j,k}$ and $\theta_{i,j}$, damage states for each component are determined using their associated fragility curves. Damage states are represented by $D\left(DS_{i,j,k}\middle|\theta_{i,j}, P_{i,j,k}, \pi\right)$ where $DS_{i,j,k}$ is the damage state array; $\theta_{i,j}$ is the demand

(peak inter-story drift ratio or floor acceleration); $P_{i,j,k}$ is the probability of occurrence; and π are the fragility curves. The final step in the *Loss Analysis* is to sample the repair time probability density functions (pdf) for the components given the determined damage state (Figure 1: Step 8). The pdf of a component is either lognormal or normal depending on the experimental data fit, and the mean of the distribution is determined using the quantity of the component and the sample repair time consequence function. The component pdf is then sampled to determine the time realization array $R_{i,j,k,l}$. This can be represented as $RD\left(R_{i,j,k,l}\middle|DS_{i,j,k},\Pi\right)$ where $R_{i,j,k,l}$ is the repair time realization array given damage state $DS_{i,j,k}$ and component pdfs Π. This deviates from FEMA P-58 in that it considers all repair time samples, while FEMA P-58 methodology uses the 90th percentile of the repair time samples in its calculations.

Repair Sequencing using REDi Methodology

Once the repair times for all of the individual components are estimated for a realization (Figure 1: Steps 1-8), the system level TTF is calculated (Figure 1: Step 9). There are a variety of considerations to accomplish this objective. Firstly, the component importance needs to be considered. For example, using typical best practice and engineering judgement, certain elements such as structural components are the primary concern and typically repaired first, with other non-structural components such as partition walls and suspended ceiling tiles being of secondary or tertiary concern. The REDi Downtime Assessment Methodology provides a relatively comprehensive database of repair priorities corresponding to the fragility data in PACT. This data was compiled using various methods including testing results and expert opinions of engineering and architectural professionals (Almufti and Willford 2013) [4]. This methodology categorizes the components of the structure into three distinct classes corresponding to a system recovery or

operation as can be seen in Table 1.

Table 1: REDi repair classes and system recovery levels (after Almufti and Willford, 2013) [4].

Repair Class	Repair Description
3	Heavily damaged non-structural or structural components that pose a life-safety risk and must be repaired for Re-occupancy
2	Damaged non-structural components that inhibit the functionality of the structure, but do not pose a life safety risk; Required for Functional Recovery
1	Minimal or minor cosmetic damage to structural or non-structural components that inhibit the return of the structure to its pre-hazard state; Required for Full Recovery

The system recovery levels, namely re-occupancy, functional recovery, and full recovery, are each defined by the amount of time to repair the components in their repair class (3, 2, and 1 respectively) to regain a certain level of functionality to the structure. Re-occupancy is defined as the minimum amount of time required for the structure to safely be used as shelter. For functional recovery, re-occupancy demands must be met in addition to the time required for the structure to regain its primary function. Finally, to achieve full recovery, the building must be repaired to its pre-earthquake condition (Almufti and Willford 2013) [4].

Once the priority of component repair is determined, a repair schedule is developed. The repair schedule is dependent on factors such as worker availability, component lead times, and inter-component dependencies. This includes parallelization, allocation, and number of workers per floor using a grouping system for components where similar components are assigned to a single group and workers are allocated to each group as an entity. Every group or repair sequence can be in parallel except for the structural component group, and it is assumed that structural

components are completely repaired prior to any non-structural repair (Almufti and Willford 2013) [4]. A limitation of this method that is shared with many other methods including the FEMA's National Disaster Recovery Framework (2011) [25] is the assumption of an unlimited worker pool. This is a best case assumption and is rarely the case, and in fact in markets such as the US west coast there has been a steady decrease in construction labor force, not only limiting the number of workers, but potentially raising the cost of the labor. In addition, impeding factors such as inspection, engineering mobilization, financing, contractor mobilization, and permitting are estimated using normal distributions. The estimated distributions vary by the facility type, story number, mitigation measure, maximum structural/non-structural damage, and financing source as seen in Table 2. β and θ represent the mean and dispersion for a normal distribution.

Table 2: REDi impeding factors distribution (per Almufti and Willford 2013) [4]

Impeding Factor	Building	Mitigation Measure	Other Conditions	β	θ
Inspection	All Facilities	BORP Equivalent	-	1 day	0.54
	Essential Facility	-	-	2 days	0.54
	Non-Essential Facility	-	-	5 days	0.54
Engineering Mobilization and Review/Re-Design	All Facilities	Engineer on Contract	Max Structural RC=1	2 weeks	0.32
			Max Structural RC=3	4 weeks	0.54
			Complete Redesign	42 weeks	0.45
		-	Max Structural RC=1	6 weeks	0.40
			Max Structural RC=3	12 weeks	0.40
			Complete Redesign	50 weeks	0.32
Financing	All Facilities	Pre-arranged Credit Line	-	1 week	0.54
		-	Insurance	6 weeks	1.11

		-	Private Loans	15 weeks	0.68
		-	SBA-backed Loans	48 weeks	0.57
Contractor Mobilization	Essential Facility < 20 Stories	GC on Contract	Max RC=1	3 weeks	0.66
			Max RC=3	7 weeks	0.35
		-	Max RC=1	7 weeks	0.60
			Max RC=3	19 weeks	0.38
	Non-Essential Facility < 20 Stories	GC on Contract	Max RC=1	3 weeks	0.66
			Max RC=3	7 weeks	0.35
		-	Max RC=1	11 weeks	0.43
			Max RC=3	23 weeks	0.41
	≥ 20 Stories	GC on Contract	Max RC=1	3 weeks	0.66
			Max RC=3	7 weeks	0.35
		-	Max RC=1	28 weeks	0.30
			Max RC=3	40 weeks	0.31
Permitting	All Facilities	-	Max Structural RC=1	1 week	0.86
		-	Max Structural RC=3	8 weeks	0.32

The resulting repair schedule is then constructed for a time corresponding to each recovery level (re-occupancy, functional recovery, full recovery). A universal total TTF for the structure for one realization can be represented by:

$$[RO_{i,j,k,l}, FR_{i,j,k,l}, FuR_{i,j,k,l}] = r(R_{i,j,k,l}) \quad (1)$$

where $R_{i,j,k,l}$ is the repair time realization array from the *Loss Analysis* procedure (Figure 1: Steps 5-8); $r(R_{i,j,k,l})$ is the repair sequencing function (Figure 1: Step 9); and $RO_{i,j,k,l}$, $FR_{i,j,k,l}$, and

$FuR_{i,j,k,l}$ are the TTF values corresponding to realization i, j, k, l for re-occupancy, functional recovery, and full recovery respectively.

Time-to-Functionality Fragility Curves

With the process and equations developed for determining re-occupancy, functional recovery, and full recovery for an iteration, equations are developed to represent the multi-layered Direct Monte Carlo, as follows:

$$\widehat{H}_K = \frac{1}{K}\sum_{i=1}^{K} g(\xi_i) \qquad (2)$$

where $\widehat{H}_K$ is the estimator, K is the number of samples, and $g(\xi_i)$ is the model evaluated at a sample point. The multi-layer Direct Monte Carlo can therefore be represented by:

$$\widehat{H}_{K\,i,j} = \frac{1}{K}\sum_{k=k}^{K}\frac{1}{L}\sum_{l=l}^{L} r(R_{i,j,k,l}) \qquad (3)$$

where $\widehat{H}_{K\,i,j}$ is the estimator array for re-occupancy, functional recovery, and full recovery for motion i and spectral acceleration j . Equation $r(R_{i,j,k,l})$is the repair sequencing function with repair time realization array $R_{i,j,k,l}$ given samples ξ_k, ξ_l and demand parameter array $\theta_{i,j}$.

Utilizing estimator $\widehat{H}_{K\,i,j}$, repair fragility scatter plots can be developed for re-occupancy, functional recovery, and full recovery, respectively (Figure 1: Step 10). This is accomplished by rank ordering the total times at each spectral acceleration (Sa) as

$$P_{E\,i,j} = \frac{m_{i,j}}{n_j} \qquad (4)$$

where m is the rank order of estimator $\widehat{H}_{K\,i,j}$ for ground motion i at Sa j, n is the total number of

realizations at Sa j, and $P_{E_{i,j}}$ is the probability of exceedance for the TTF for motion i at Sa j. The interval at which repair fragility scatter plots can be developed is limited by the resolution of repair data provided by PACT, i.e., person-days. Once plots have been developed, individual TTF data is fit using a lognormal cumulative distribution function (CDF) of the form:

$$F_X(x) = \phi\left(\frac{\ln x - \mu}{\beta}\right) \quad (5)$$

where μ is the mean and β is the dispersion of the logarithmized samples for each of the TTF fragility scatter plots (Figure 1: Step 11). The resulting family of fragility curves present information on the probability of exceedance for a variety of TTF values for the structure over a large range of demand parameters, representing a concise summary of the structure's performance. In contrast to REDi methodology which only does one simulation for a given design, the TTF methodology expands this to a stochastic methodology that incorporates many simulations into the development of the TTF curves. This was possible due to the development of a repair schedule algorithm capable of constructing repair schedules for each individual simulation. This information can then be used to set performance objectives for the structure and can fit into a larger decision framework on the selection of structural and non-structural components to reduce TTF. Further, the effect of cost to improve certain classes of building type could be weighed against the change in community-level recovery or resilience (Ellingwood et al, 2016) [22] in order to modify current building code.

CHAPTER 3 – ILLUSTRATIVE EXAMPLE: TWO-STORY CLT BUILDING WITH ROCKING WALLS

Building Overview

The TTF fragilities methodology described is applied herein to a two-story mass timber building with post-tensioned CLT rocking walls as the seismic force resisting system. The previously mentioned two-story CLT building with post-tensioned CLT rocking walls was tested at the University of California, San Diego's shake table (NHERI@UCSD) in 2017 as part of the NHERI Tallwood Project. The building floor diaphragms were 6.10 m x 17.68 m (20 ft x 58 ft) in plan and the story heights were 3.66 m (12 ft) and 3.05 m (10 ft), respectively (Pei, et al. 2019) [52]. The main force resisting structural system consisted of two sets of post-tensioned CLT rocking walls coupled using U-shaped flexural steel plates (UFP), as well as CLT diaphragms. The gravity framing consisted of glulam columns and beams. The test structure including the lateral and gravity systems can be seen in Figure 3.

Figure 3: Two-story CLT building with post-tensioned rocking walls

Building Performance Model and IDA

Numerical modeling of the post-tensioned CLT rocking walls was performed using OpenSees (Mazzoni, et al. 2009) [42]. The *Building Performance Model* consisted of six main components: (1) Elastic Timoshenko beam-column wall elements, (2) multi-spring contact elements, (3) post-tensioned (PT) bar truss elements, (4) UFP spring elements, (5) rigid diaphragm elements, and (6) a P-Delta column. This model utilized modeling concepts originally developed by Ganey, et al (2015) [27] and can be seen in Figure 4.

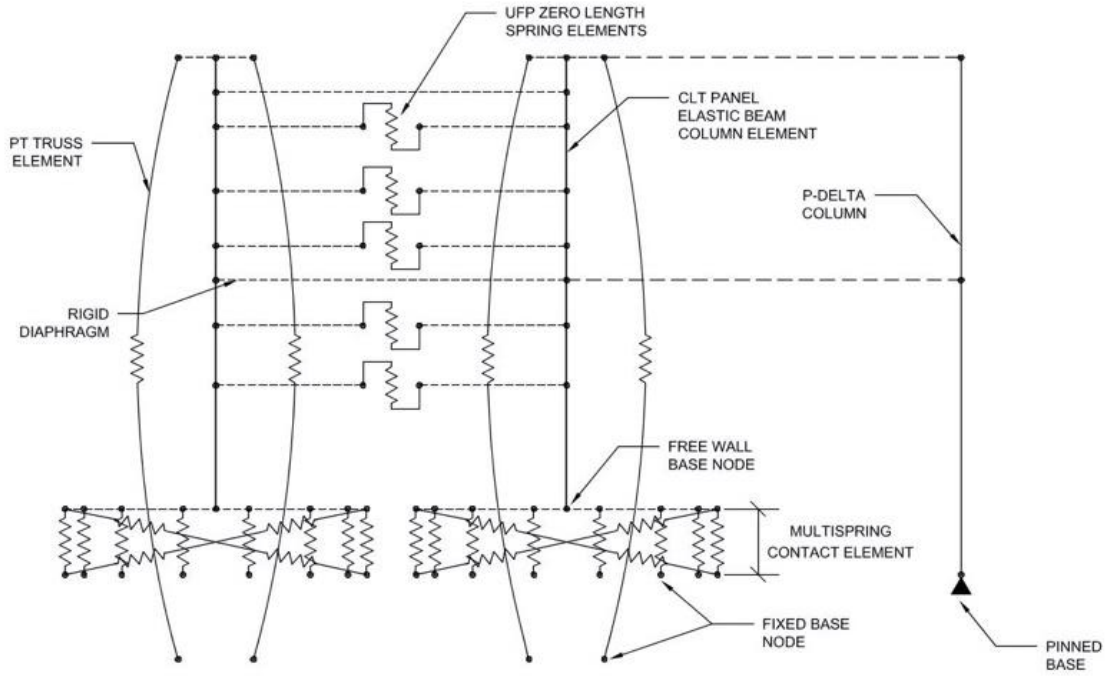

Figure 4. OpenSees numerical model schematic for the coupled CLT rocking walls used in analysis [76]

The elastic portion of the walls were modeled using a series of elastic Timoshenko beam-column elements. The first element spanned from the free wall base node to the location of the first UFP, the subsequent elements spanned between the UFP locations and the diaphragm locations on the panels, and the last element spanned from the roof diaphragm connection to the top of the wall. The non-linear rocking behavior of the panels and the compressive deformation of the CLT was

modeled using a multi-spring contact element at the base of each panel, initially developed by Spieth et al. (2004) [66]. The multi-spring contact element consisted of a set of parallel zero-length springs spaced along the length of the base of the panel in accordance with a Gauss-Labatto distribution. The top of each spring was linked by a rigid element to the free wall base node while the bottom of each spring was fixed. Each spring was only allowed to deform axially and was defined with an elastic-perfectly plastic, compression only material model to model the CLT compression behavior and the gap opening at the base of the panel. The overall compression stiffness of each panel was calculated using basic mechanics and each spring stiffness was a fraction of the total stiffness weighted according to the Gauss-Labatto distribution. Similarly, the yield strength of each spring was calculated by taking the weighted portion of the CLT panel yield stress and the panel cross section. Finally, a diagonal shear spring, connecting the corners of each multi-spring contact element, was used to transfer shear at the base of the panels. The full description of the model and its application can be found in Wichman et al (2022) [76]

The post-tensioned bars were modeled using tension only corotational truss elements. In tension, a bi-linear hysteretic material model was used. These elements were fixed at the base and connected to a rigid element spanning from the location of the PT bar to the top center of the panel. An initial strain was applied to the bars to model the initial post-tensioning [76]. Each UFP was modeled with a zero-length spring incorporating a uniaxial Giuffrè-Menegotto-Pinto steel material model with isotropic strain hardening. A rigid element connected each elastic beam-column element at the center of the wall panel to the zero length UFP spring located between the two wall panels. At the diaphragm levels, rigid truss elements were used to link the two wall panels. Gravity loads and associated inertial forces were represented using the leaning column approach, whereby

an additional pinned-pinned P-Delta column representing the tributary gravity framing was connected to the wall system [76].

Next, a suite of 22 ground motions from FEMA P695 (FEMA 2009) was selected, and IDA was performed (Figure 5). In IDA, each motion is incrementally scaled to different Sa values until the IDA curve flattened and collapse was identified. The flatting of the curve is significant because the IDA curve herein is plotted as inter-story drift ratios versus Sa so would indicate very large drift increases with minimal Sa increases i.e., collapse. This produced vectors of peak inter-story drift ratios and peak floor acceleration for each story of the structure which are a function of both spectral acceleration and ground motion that are used in the loss and repair analysis of the building.

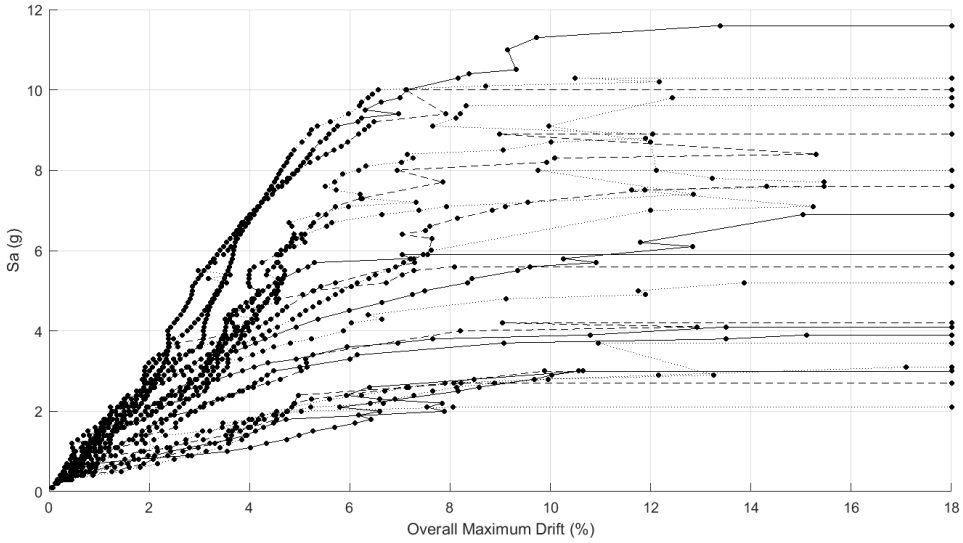

Figure 5: FEMA P695 suite IDA curves for two-story CLT test structure

Loss Analysis

Structural Fragility Selection

While the FEMA P-58 database contains a large collection of fragility information for a variety of structural components such as reinforced concrete, and steel, there is a lack of information on mass timber components. In this study, results from existing experimental and analytical studies on an isolated post-tensioned CLT rocking wall (Akbas, et al 2017; Ganey, et al 2017) [3, 29] were used

to approximate the various damage states (Table 3) of the rocking wall system. Note that it would also be possible to characterize the fragility of the rocking wall system by its constituent parts (e.g., wall itself, UFPs and PT Bars) separately, and will likely be done in future analyses.

Table 3: CLT rocking wall damage states (per Akbas, et al 2017; Ganey, et al 2017) [3, 29]

Damage State	**ELL**	**EDP**	**YCLT**	**SCLT**	**CCLT**	**LLP**
Inter-story Drift Limit (%)	0.4	1.6	1.7	4.6	7.3	4.2

ELL = Effective Linear Limit
EDP= Yielding of UFPs
YCLT= Yielding of CLT
SCLT = Splitting of the CLT (exceedance of the splitting strain at compression edge of wall)
CCLT= Crushing of CLT (exceedance of the compression strain at compression edge of wall)
LLP = Yielding of PT Bars

Several of the damage states would be difficult to detect with typical inspection techniques, and would be interpreted as no damage, thus they are not included in the repair activity (i.e., down-time). As a result, the ELL and YCLT damage states were not considered in this example due to their detection difficulty, and the remaining damage states were considered in the analysis. To develop the fragility curves from these deterministic drift damage state limits, several assumptions were made. Primarily, the drift limit was assumed to represent the mean value in a lognormal fragility curve, and a dispersion value of $\beta = 0.3$ was selected to represent the expected variation in the drift limit states. The basis of this assumption was incorporation of the median value of dispersion values for fragility curves presented in FEMA P695 [12], where 0.2 dispersion

represents the lower bound and 0.4 represents the upper bound of dispersion. These assumptions resulted in the rocking wall fragility curves shown in Figure 6.

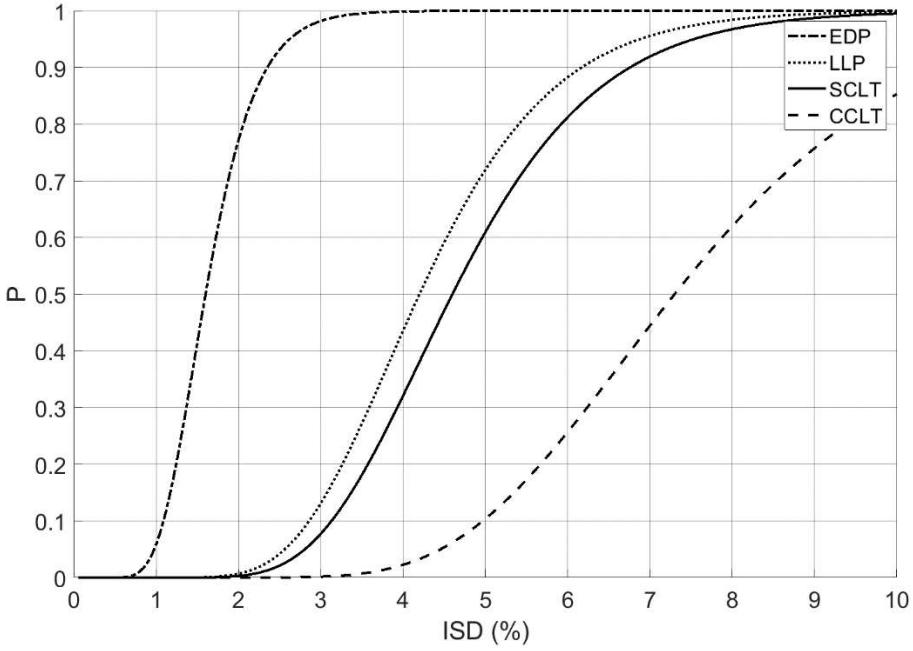

Figure 6: CLT Post-tensioned rocking wall fragility curves

While fragility curves for the glulam beam and column gravity system and CLT diaphragms are technically also required for a complete structural characterization, these components were designed to and remained undamaged during the test (Pei et al. 2019). Therefore, fragility curves for these components have been neglected from this work.

There is believed to be no research on repair time consequence functions for a CLT rocking wall at the time of writing. Thus, repair time consequence functions were determined using engineering judgement and the CLT experience of the authors, see Table 4. In addition, a normal distribution was assumed to represent the variation in repair times (similar to PACT) with the mean being the interpolated repair time based on the quantity, and an assumed dispersion of $\beta = 0.3$ for all damage states. While the lack of information on CLT rocking walls and diaphragms is not ideal, it should be noted that similar to the gravity frame and diaphragm, the rocking wall would remain mostly

undamaged at practical intensities. Thus, minor variations in the rocking wall repair time consequence functions should not translate into a significant change in global time to functionality.

Table 4: Summary of repair times of CLT rocking wall

				Repair Time (person-days)			
Category	**EDP**	**Damage State Description**	**Q**	**LQ**	**RT$_L$**	**UQ**	**RT$_U$**
CLT Rocking Wall – Lateral force resisting system including PT bars, two CLT walls, and UFP connectors	SDR	Yielding of UFPs	SF 240	2	2	10	1
		Yielding of PT bars			2		1
		Crushing of CLT			23		23
		Splitting of the Composite Material			23		23

EDP = Engineering Demand Parameter
SDR= Story Drift Ratio
Q= Quantity
LQ = Lower Quantity
UQ = Upper Quantity
SF = Square Foot

Non-Structural Fragility Selection

Note that the CLT structure was tested in 2017 without non-structural systems, and the non-structural component data was added for this illustrative example. Fragility and consequence functions for the most damageable nonstructural components were incorporated, based on a review of previous loss estimation studies (Zeng, et al. 2016; Cutfield, et al. 2016) [80, 17]. Selected components include partition walls, glazing, suspended ceilings, cooling towers, chillers, compressors, HVAC systems, and sprinkler-piping systems. For each component for which multiple fragility functions have been developed to represent detailing variations, the most modern and resilient detailing was selected to meet the resilient design objectives of a timber building with a post-tensioned rocking wall. For example, for partition walls slip-track detailing was selected over fully fixed connections for its ability to absorb drift by sliding of the top track (Hasani, et al. 2018) [31]. Table 5 summarizes the components utilized in this study based on FEMA P-58

classifications, EDP upon which damage is assessed, potential damage states associated with the components, basic quantity unit Q, and lower and upper quantities and repair times.

Table 5: Summary of repair time of nonstructural components in a two-story building example

				Repair Time (person-days)			
Category	**EDP**	**Damage State Description**	**Q**	**LQ**	**RT_L**	**UQ**	**RT_U**
C1011.001c - Partition wall - Gypsum with metal studs - Fixed Below, Slip Track Above	SDR	Minor damage that can be repaired without replacement of wallboard	SF 1300	1	1.36	10	0.366
		Severe damage such that replacement of wallboards is necessary			2.85		0.863
		Damage to wallboard and framing (replacement of wall is necessary)			5.46		1.64
B2022.011 – Glazing - Midrise stick-built curtain wall, Config: Asymmetric insulating glass units, Laminated, Annealed,	SDR	Gasket seal failure.	SF 30	20	0.905	100	0.482
		Glass cracking.			1.3		0.696
		Glass falls out.			1.04		0.74
C3032.003a – Ceiling - Suspended Ceiling, SDC D, E (Ip=1.0), Area (A): A < 250, Vert & Lat support	PFA	5 % of ceiling grid and tiles damaged.	SF 250	1	0.697	10	0.211
		30% of ceiling grid and tiles damaged.			5.41		1.62
		50% of ceiling grid and tiles damaged.			11.2		3.34
D3031.023b - Cooling Tower - Capacity: < 100 Ton - Equipment that is either hard anchored or is vibration isolated with seismic snubbers/restraints - Equipment fragility only	PFA	Damage to equipment and attached piping but anchorage is OK.	EA 1	1	8.36	5	2.79
D3031.013b - Chiller - Capacity: < 100 Ton - Equipment that is either hard anchored or is vibration isolated with seismic snubbers/restraints - Equipment fragility only	PFA	Damaged, inoperative but anchorage is OK.	EA 1	1	14.3	5	4.76
D3032.013b Compressor	PFA	Equipment does not function	EA 1	1	0.97	5	0.794

- Capacity: Small non-medical air supply - Equipment that is either hard anchored or is vibration isolated with seismic snubbers/restraints - Equipment fragility only		but anchorage is OK. Motor is damaged.			1		
		Equipment does not function but anchorage is OK. Equipment damaged beyond repair.			0.635		0.159
D3041.002c HVAC Fan In Line Fan, Fan independently supported but not on vibration isolators, SDC D, E, F	PFA	Bellows fail at fans	EA 10	1	9.06	5	7.41
D3041.011c HVAC Galvanized Sheet Metal Ducting less than 6 sq. ft in cross sectional area, SDC D, E, or F	PFA	Individual supports fail and duct sags - 1 failed support per 1000 feet of ducting	LF 1000	1	0.841	5	0.688
		Several adjacent supports fail and sections of ducting fall - 60 feet of ducting fall per 1000 foot of ducting			2.99		1.49
D3041.103b HVAC Fan - Capacity: all - Equipment that is either hard anchored or is vibration isolated with seismic snubbers/restraints - Equipment fragility only	PFA	Damaged, inoperative but anchorage is OK.	EA 1	1	3.43	5	2.81
D4011.023a Fire Sprinkler Water Piping - Horizontal Mains and Branches - Old Style Victaulic - Thin Wall Steel - Poorly designed bracing, SDC D, E, or F, PIPING FRAGILITY	PFA	Spraying and dripping leakage at joints - 0.02 leaks per 20 ft section of pipe	LF 1000	3	0.451	10	0.369
		Joints break and major leakage - 0.02 breaks per 20 ft section of pipe			0.937		0.313
D4011.053a Fire Sprinkler Drop Standard Threaded Steel - Dropping into braced lay-in tile SOFT ceiling - 6 ft. long drop maximum, SDC D, E, or F	PFA	Spraying & Dripping Leakage at drop joints - 0.01 leaks per drop	EA 100	2	0.649	5	0.531
		Drop joints break and major leakage - 0.01 breaks per drop			0.179		0.0612

EDP = Engineering Demand Parameter
SDR = Story Drift Ratio
Q = Quantity
LQ = Lower Quantity
UQ = Upper Quantity
PFA = Peak Floor Acceleration

LF = Linear Foot
SF = Square Foot
TN = Ton
EA = Each

Repair Sequencing

The *Repair Sequencing* for the two-story structure consisted of interpreting the components (CLT seismic force resisting system and non-structural) for use in the REDi Downtime Assessment methodology (Almufti and Willford 2013) [4]. Repair classes were selected for each of the components. As previously mentioned, repair classes determine the priority of repair for the component. For the majority of the components, repair classes have been pre-defined as part of the development of the methodology. The CLT rocking wall however, has not been considered in REDi, so repair classes needed to be defined. After minor damage i.e., damage state 1, the CLT rocking wall system is believed to have enough remaining lateral capacity to be considered safe for occupation. However, because of potential yielding of the UFP's, it was conservatively assumed that the structure would be tagged with a yellow placard (restricted use) by inspection after a minor event in accordance with FEMA P-58. This is interpreted as repair class 3 as defined in Table 1 for all damage states considered. It would also be possible to store extra UFPs on site to reduce lead time for fabrication. Descriptions and selected repair class priority for all considered components are summarized in Table 6. It should be noted that the average damage state for a component across a floor is used for the repair class determination. This is primarily done as a simplification as well as an indicator for the damage of the component across an entire floor.

Table 6: REDi repair classes for two-story components

Component	**Average Damage States ($\overline{DS}$)**		
	$0 < \overline{DS} \leq 1$	$1 < \overline{DS} \leq 2$	$\overline{DS} > 2$
CLT Rocking Wall – Lateral force resisting system including PT	3	3	3

bars, two CLT walls, and UFP connectors			
Partition walls - Gypsum with metal studs - Fixed Below, Slip Track Above Ceiling – Suspended Ceiling	1	1	3
Glazing - Midrise stick-built curtain wall.	1	3	3
Cooling Tower - Capacity: < 100 Ton	2	3	3
Chiller - Capacity: < 100 Ton	2		
Compressor - Capacity: Small non-medical air supply	2		
Fire Sprinkler Drop Standard	2	3	
HVAC Fan in Line Fan	2		
HVAC Galvanized Sheet Metal Ducting	3	3	
Fire Sprinkler Water Piping - Horizontal Mains and Branches	2	3	

Synthesis of Time-to-Functionality Fragility Curves

TTF fragility curves were developed using the previously described rank ordering method with a density of one day; 5,000 ground motion realizations were considered, resulting in the equivalent amount of individual time samples for each of the recovery levels (re-occupancy, functional recovery, and full recovery). The data for each day was assumed to correspond to a lognormal distribution of the previously described form, and with this assumption, fragility curves were fit to the data. Figure 7 shows the Re-occupancy TTF scatter plot as well as fitted Re-occupancy fragility curves, while Figure 8 presents only the fitted Re-occupancy fragility curves and the corresponding fit data for 86 days, 95 days, 120 days, 140 days, and 182 days respectively. The TTFs were chose

to represent the behavior of the TTF family of curves, apart from the 182 day TTF. This was chosen to represent approximately 6 months and a 3-star resilience rating as defined by the United States Resiliency Council (USRC) [72]. The other four ratings (5 days, 4 weeks, 1 year, and more than 1year) were not included do the TTF behavior of the structure. The impeding factors discussed in detail previously prevent 5 days and 4 weeks being feasible for any damage beyond no damage. 1 year and greater than 1 year are near or exceed the maximum TTF determined from the simulation, and therefore are not realistic to consider for this structure.

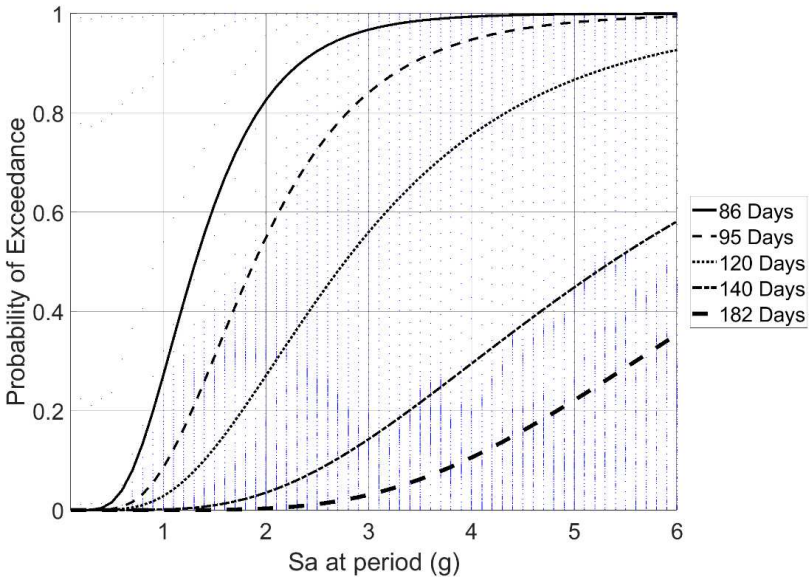

Figure 7: Re-occupancy scatter plot and lognormal fits

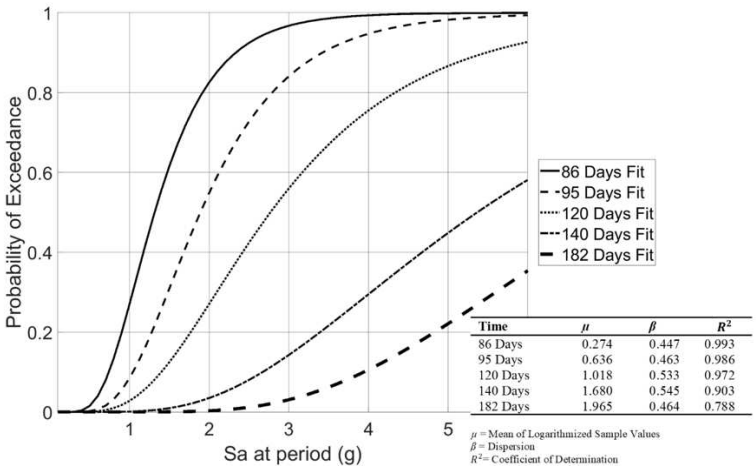

Figure 8: Re-occupancy TTF fragility curves

Observing the scatter plot in Figure 7, two phenomena become apparent. First, there is a relatively low density of points for lesser TTF values (such as 86 days). This can be explained by the stochastic nature of the simulation. Data in this region represents moderate to minor damage to the structure which represents a lower probability of occurrence. There also seems to be a correlation between increasing number of repair days and a noticeable reduction in the R^2 value of the lognormal curve fits. This correlation can be attributed to the flattening of the curves as time increases. In other words, the probability of exceedance increases with increasing spectral acceleration slower for larger TTF times than in lesser TTF values, which is expected. It also demonstrates the applicability of the lognormal fit, with lesser TTF values (in terms of the structure) adhering well, and larger values deviating fairly significantly.

The lognormal curve fits in Figure 8 directly represents the probability that a Re-occupancy time (i.e., 86 days, 95 days, etc.) is exceeded at a given spectral acceleration. For example, at a spectral acceleration of 2g, the two-story CLT structure has approximately a 0.83 (83%) probability of exceeding 86 days for Re-occupancy, while simultaneously having a 0.26 (26%) chance of

exceeding 120 days. This can be further applied to estimate TTF performance for specific events, using the approximated event spectral acceleration at the structure's period. Figure 9 and Figure 10 show the corresponding fragility curves for Functional recovery and Full recovery, respectively.

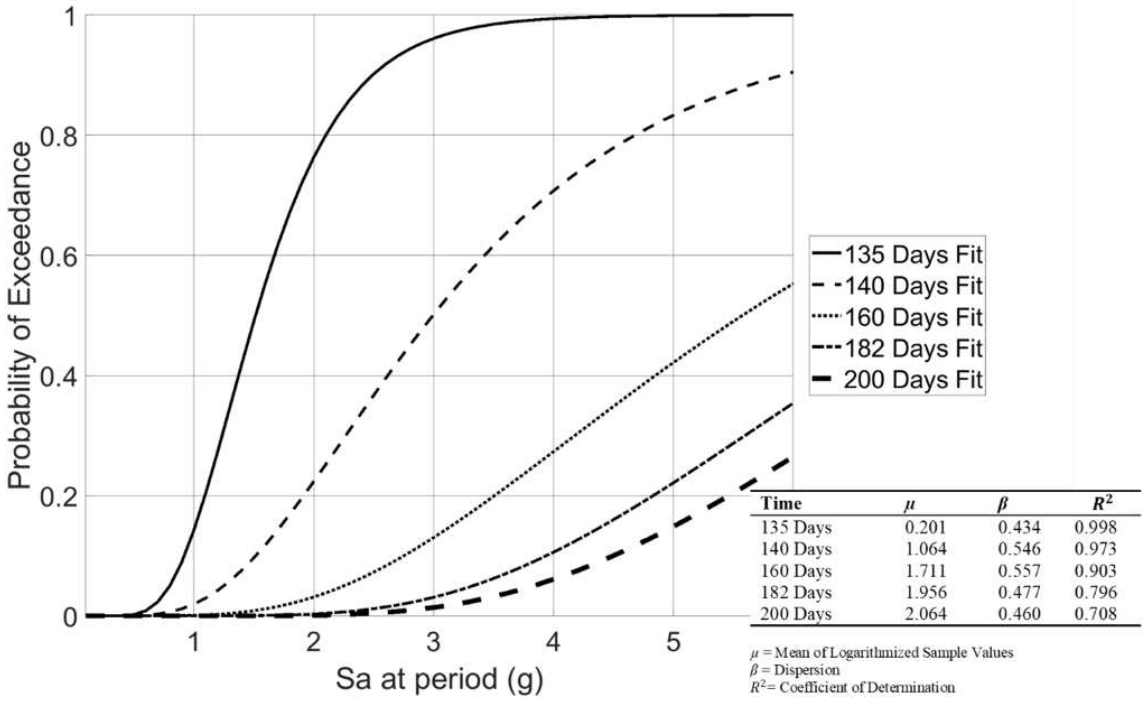

Time	μ	β	R^2
135 Days	0.201	0.434	0.998
140 Days	1.064	0.546	0.973
160 Days	1.711	0.557	0.903
182 Days	1.956	0.477	0.796
200 Days	2.064	0.460	0.708

μ = Mean of Logarithmized Sample Values
β = Dispersion
R^2 = Coefficient of Determination

Figure 9: Functional recovery TTF fragility curves

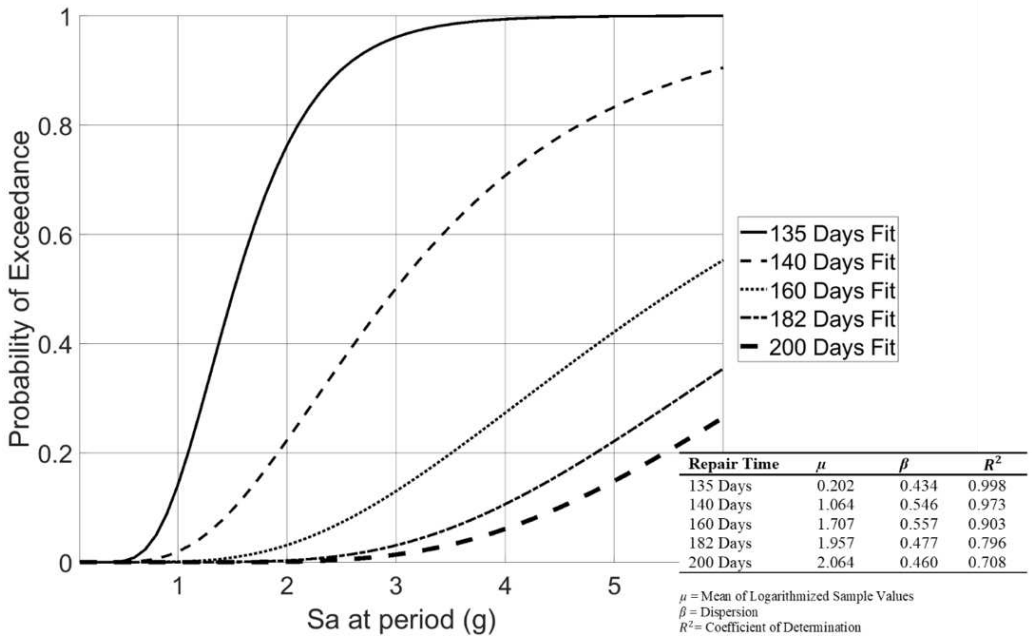

Repair Time	μ	β	R^2
135 Days	0.202	0.434	0.998
140 Days	1.064	0.546	0.973
160 Days	1.707	0.557	0.903
182 Days	1.957	0.477	0.796
200 Days	2.064	0.460	0.708

Figure 10: Full recovery TTF fragility curves

The fragility curves for Functional recovery and Full recovery are observed to be nearly identical; the only visible difference is for the 135 and 160 day fit data. This result is entirely due to the component selection and its corresponding repair class associations. Full recovery is defined as the restoration of the structure to its pre-event level, which corresponds to the repair of all components in repair classes 1, 2, and 3; while Functional recovery is defined as the minimum amount of repair needed to restore functionality to the structure, which corresponds to the repair of all components in repair classes 2 and 3. Further investigation of the behavior of the model suggests that at larger spectral accelerations (larger damage states), all components are more heavily damaged and thus fall into repair class 2 or 3 (Table 5). This means that by definition, at larger spectral accelerations, Full recovery is equal to Functional recovery. For moderate spectral accelerations, HVAC components do not have a damage state for repair class 1, and are instead always considered repair class 2 (Table 5). This is important to note because these components have long lead times associated with them, meaning that repair class 1 components can be repaired

while waiting for the repair class 2 components to arrive, thus leading to the functional recovery and full recovery being equivalent. Finally, at lower spectral accelerations the HVAC components will not be damaged, while several components will be in their repair class 1 damage state. This leads to the Re-occupancy and Functional recovery being equivalent, while the Full recovery is greater. Recalling the observed difference between the Functional recovery and Full recovery 135 days and 160 days TTF fragility curves and combining this observation with the previously discussed lower sample densities at quicker TTF values, one can conclude that the demonstrated difference between the TTF fragility curves is due to samples at low spectral accelerations affecting the fit for both 135 and 160 days respectively. Functional recovery and Full recovery are not expected to be so similar for every structure; incorporation of more resilient components, repair class 1 components with long lead times, different repair class 2 components, among other things could all differentiate the Functional recovery and Full recovery significantly.

Closing

The methodology laid out in this chapter allows for the development of TTF fragility curves that incorporate both structural and non-structural components, as well as a variety of uncertainties. The primary result is a methodology that merges a relatively deterministic REDi Downtime Assessment Methodology and a stochastic FEMA P-58 Methodology into a multi-layered Direct Monte Carlo Simulation to simulate time to achieve different levels of system recovery. Families of fragility curves representing those building states can provide, at a glance, a fairly comprehensive and clear view of the probability of a structure over a variety of different demand parameters, lending itself well to its incorporation into a larger decision framework.

The rocking wall system reduces the damage to the structural systems of the building and

almost entirely eliminates residual drift, but with the drift criteria similar to other systems, it does little to reduce the drift induced damage for non-structural components. While the structural components remain mostly undamaged (for practical considerations), the rocking wall system does not reduce damage for most traditional non-structural elements, demonstrating a need to incorporate more deformation compatible non-structural components to improve the resilience of the system. Additionally, while the system here incorporated dropped suspended ceilings, in many cases mass timber buildings less than 6 stories do not incorporate suspended ceilings, which would reduce the TTF of the structure. Currently, the model estimates the TTF for different recovery levels, allowing for flexibility in the determination of resilience objectives. Additionally, the repair sequencing used in the example was a relatively unmodified implementation of REDi, and while fairly comprehensive, the methodology is not beholden to this type of repair sequencing. It would be possible to modify or completely replace that procedure with a different downtime estimation procedure as more detailed information becomes available. Comprehensively, the effectiveness and potential of the methodology have been demonstrated by the example herein, but areas in which more research is needed have been revealed. Specifically, the effects of the selected ground motions, analysis type, and Building Performance Model complexity needs to be further investigated; and further development of fragility curves for mass timber products and additional resilient non-structural components are needed.

CHAPTER 4 – NAIL LAMINATED AND DOWEL LAMINATED DIAPHRAGM TEST SETUP

Introduction

As a portion of the larger NHERI TallWood ten-story project, dowel laminated timber (DLT) and nail laminated timber (NLT) diaphragms designs were tested to evaluate their performance and suitability for inclusion in the ten-story test building. Additionally, the testing provided an opportunity to develop fragility curves for the diaphragm designs with the objective of addressing some of the deficit of the mass timber fragility curve inventory, and for the incorporation into the TTF model.

Nail laminated timber is a structural system that is manufactured by fastening dimension lumber stacked on their edge together into laminations using nails, spikes, or screws. NLT is considered a one-dimension additive process, meaning that the grains of the laminations run parallel with the lengths of the members. The result of this manufacturing method are large, flat structural components primarily used for diaphragms. NLT has been in use since at least the 19th century as floor systems, colloquially named “mill construction”, in cotton and sawmills in the Northeastern United States [13]. The widespread use of NLT in these industrial applications led to the development of a design guide by the National Lumber Manufactures Association entitled “Heavy Timber Mill Construction Buildings” [13]. However, NLT was not limited to mill buildings, and has been used as bridge and building diaphragms for centuries. More recently with the increasing use of other mass timber products (such as CLT, glulam, mass plywood panels, etc.) NLT has seen a reemergence in new applications such as diaphragms in offices, apartments, and mixed-use

buildings and with either the implementation of cross lamination, OSB sheathing, or plywood sheathing, as lateral systems and shear walls. One of the many benefits of mass timber including NLT is the ability to use lesser quality materials to manufacture a quality structural system. An example of this in the NLT context can be found in Derikvand, et al. (2018) [18], where two Australian hardwood species (Eucalyptus nitens and Eucalyptus globulus) primarily used to produce woodchips, were instead used to create various configurations of NLT and NLT-concrete composite (NLTC) floor panels. These panels were then subjected to vibration and four-point bending tests, the results of which showed that the species were indeed capable of being used for NLT panels, with the species being superior to some commercially imported mass laminated timber products. As previously mentioned, other materials can be combined with NLT to provide more effective shear transfer. In Hong, K. E. M. (2017) [33] the performance of the shear connectors between the concrete and NLT in a NLTC panel were investigated. Ultimately, four different truss-plate configurations were tested at a full panel scale under quasi-static monotonic loading to determine the vibration and bending properties. The resulting data showed that the panels slightly exceed the predicted fundamental natural frequency and bending stiffness. Additionally, failure did not occur until 5 to 7 times the required serviceability load. Noticeably absent from contemporary research is robust performance testing of NLT lateral systems (including those using OSB and plywood) for seismic loading. This deficit has real word consequences as many regions that are prime candidates for implementation of NLT are additionally high seismic risk. Currently, such implementation requires a case-by-case design which is typically overly conservative and damages the competitiveness of NLT in seismic regions.

DLT is also a mass timber product growing in popularity, and DLT is manufactured in a similar fashion to NLT, but instead of nails, hardwood dowels are used as fasteners between the laminations. The primary benefits of DLT over NLT are twofold, first dowels can be pushed through 7-10 laminations at a time, resulting in a more efficient manufacturing process. Since the entire panel is wood and does not have any nails, it can be more readily milled and routed, adding extra flexibility and applications. DLT as a structural system was first developed in Switzerland in the early 1990s with some early iterations including steel dowels [13]. In a project funded by the European Union, more traditional techniques of DLT manufacturing were combined with contemporary research on densified wood materials to take advantage of improved physical and mechanical properties and manufacture adhesive free panels [2]. An early design guide implementing steel dowels can be found in Eurocode 5: Design of Timber Structures. British Standards (2004) [11]. A more recent design incorporating Beech dowels can be found in Rombach (2018) [61], with the design being applied in the expansion of Smithers Airport in Canada, with the design work by StructureCraft (2018) [68], as well as the implementation in around another 300 buildings worldwide [1]. Similar to NLT, DLT can be utilized in lateral systems with the addition of additional shear transfer mechanisms (like OSB or plywood). Unlike NLT, there is contemporary research on the seismic performance of DLT. Specifically, in Sandhass and Schädle (2017) the joint behavior of DLT panels with beech dowels was investigated. This was chosen specifically due to the concern that the adhesive free manufacturing of the panels could lead to significantly reduced shear wall capacity, as fasteners inserted perpendicular to the lamination may be placed in the gaps between the individual laminations. The testing showed that depending on diameter, fasteners may only have 25% of the capacity of

fasteners placed directly in wood. Additional monotonic and quasi-static reversed cyclic tests showed stiffness, load carrying capacities, and energy dissipation properties comparable to traditional timber frame constructions Sandhass and Schädle (2017) [63]. Even with more contemporary seismic research, DLT still suffers from research deficits, specifically the effects of different sheathing configurations on the seismic performance of DLT panels.

Specimen Information and Testing Methodology

As stated at the beginning of the introduction, DLT and NLT diaphragms are to be included (one NLT floor and two DLT floors) in the ten-story building test. However, as previously discussed, there is a deficit of seismic research for both NLT and DLT floor diaphragms, so additional information on the performance of both systems was needed before inclusion in the larger test structure. To address the deficit, five floor diaphragms (three DLT, one NLT, and one light frame wood diaphragm) were tested at Colorado State University's Engineering Research Center using a cantilever testbed that will be described in detail later in the Chapter. The diaphragms (excluding the light frame diaphragm) and the NLT/DLT panels were designed and manufactured by StructureCraft in accordance with anticipated demands on the ten-story and by adhering to their design guide [68]. The structural system consisted of three primary parts, the NLT/DLT panels, the OSB sheathing, and the Simpson strong tie strapping. The panels themselves were the primary bearing capacity mechanism, while the straps and OSB sheathing were attached with nail fasteners with the primary purpose of transferring shear. The light frame diaphragm was designed using the 2018 NDS® (National Design Specification®) [45] to be comparable in capacity to the NLT/DLT diaphragms and used dimensional lumber as the primary bearing capacity and OSB sheathing with nail fasteners as the primary shear transfer. Initially, four different NLT/DLT diaphragms, all

sheathed with 11.112 mm (7/16”) OSB, using CMST 12 Simpson Strong Tie straps were to be tested (Tests A-D) with an additional light frame wood diaphragm test as a control. All of the panels (both NLT and DLT) were notched in order to fit into the testbed, 22.2 mm x 609.6 mm (7/8” x 2’) notch was routed around the perimeter of each panel. However, the testbed changed before testing and after routing, rendering the notches unnecessary on three of the four sides. The notches did reduce the potential bearing capacity of the diaphragms, but since bearing capacity was not being tested, it was deemed acceptable. The Test A and B designs consisted of four 2.48 m x 2.13 m (8’-1 13/16” x 7’) panels with 1.112 mm (7/16”) OSB sheathing, cut from 1.22 m x 2.44 m (4’x 8’) sheets to fit the panels as well as the 22.22 cm (8-3/4”) wide infill strips, fastened with 3.33 mm (0.131”) dia. x 63.5 mm (2-1/2”) common nails using 15.24 cm (6”) edge spacing and 30.48 cm (12”) in field spacing. There were also 3 CSMT straps installed on either end of the diaphragm (6 total) perpendicular to the loading direction using 4.11 mm dia. x 63.5 mm (0.161” dia. x 2-1/2”) common nails as seen in Figures 11 and 12.

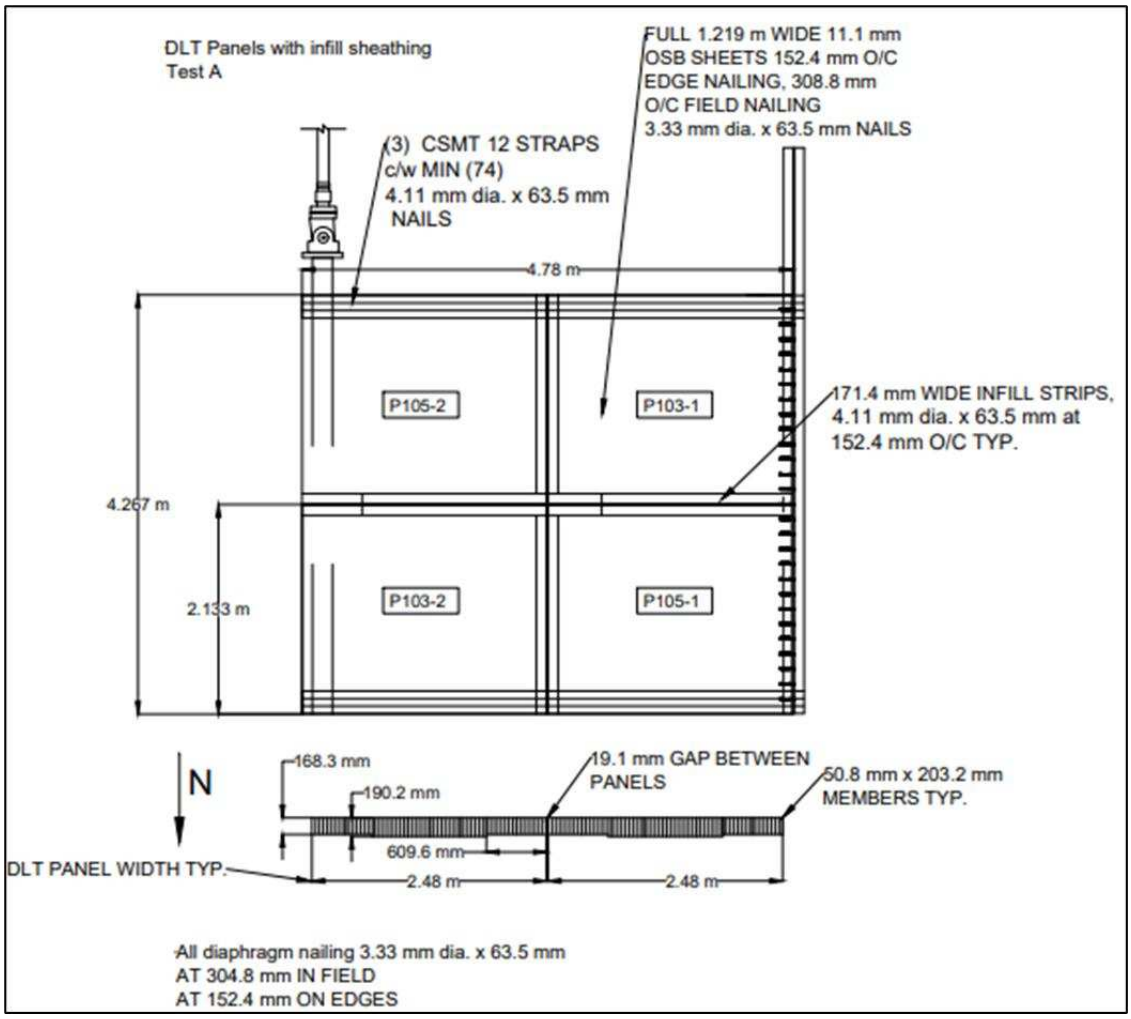

Figure 11: Test A DLT design

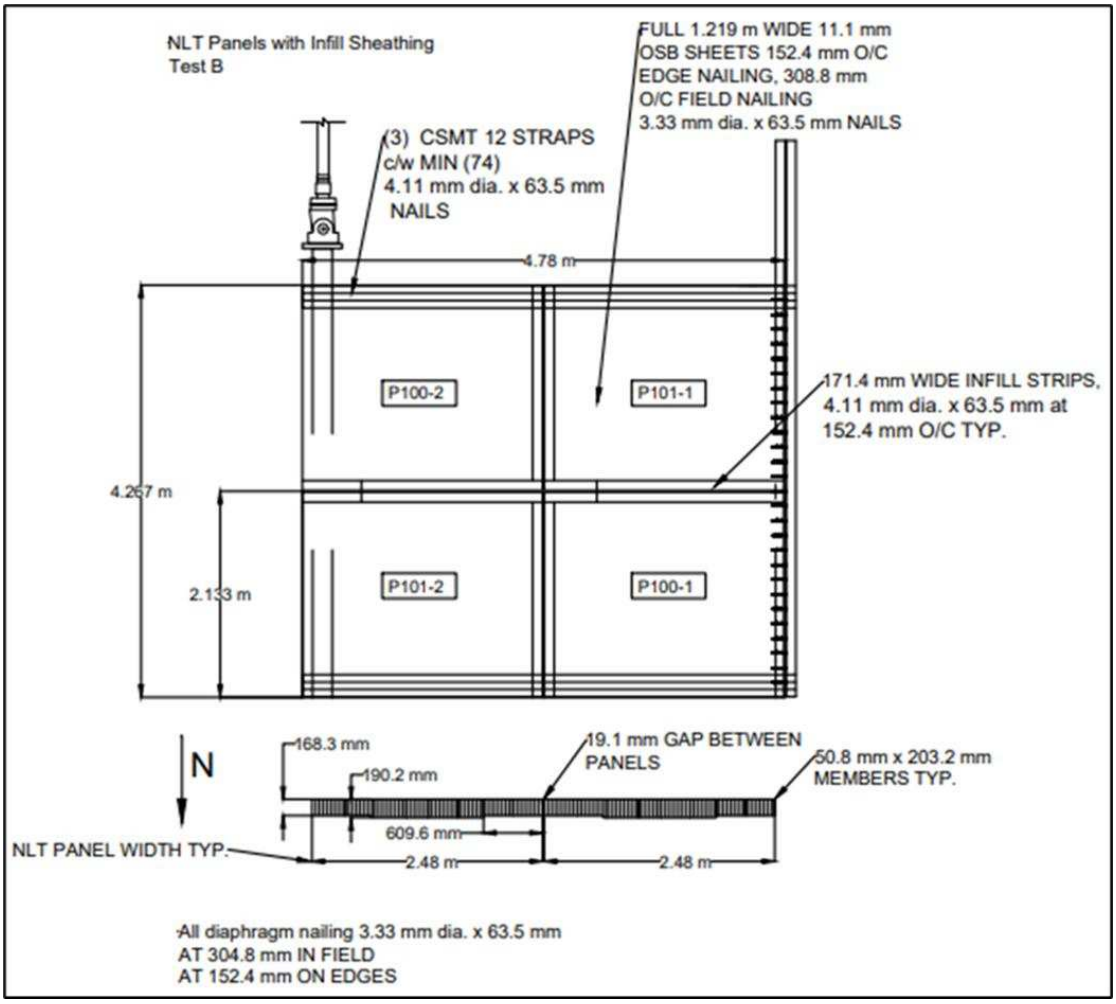

Figure 12: Test B NLT Design

Test C in comparison used the same panel sheathing and infill geometry, OSB thickness, straps, and nails as Tests A and B, but with a nailing pattern of 6.35 cm (2-1/2”) edge spacing and 304.8 mm (12”) in field spacing. In addition, extra 45-degree SCHMID Rapid VG (FT-CL) 6 mm x 200 mm screws were installed, for additional shear capacity in the panels, in all four panels along the diaphragm joint parallel to the loading. The design of Test D used the same OSB thickness, nail size, nail pattern, and straps as Test C, however instead of infill sheathing between the panels, a running bond (staggered) sheathing geometry was used. The design for both Test C and D can be seen in Figures 13 and 14.

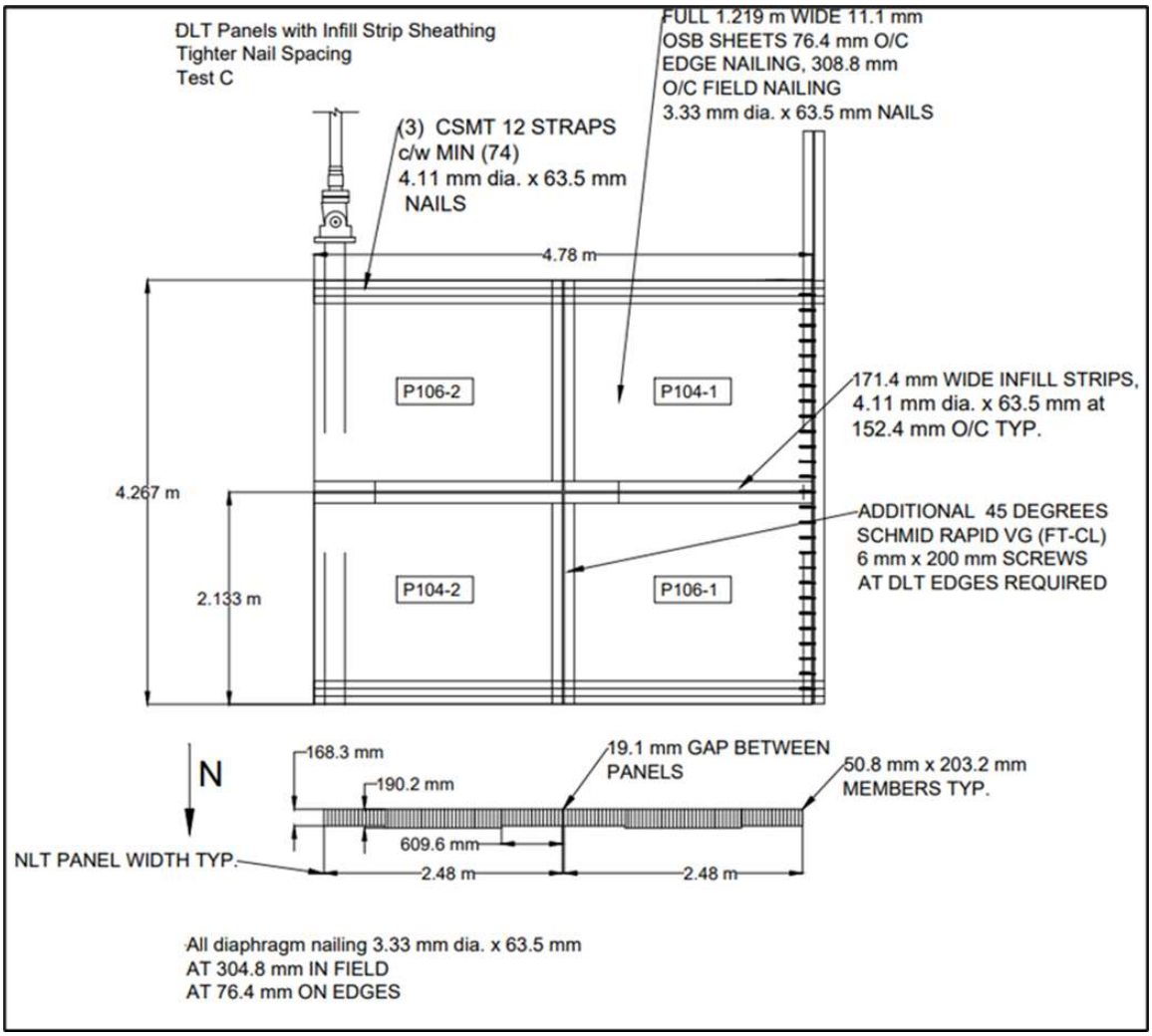

Figure 13: Test C DLT design

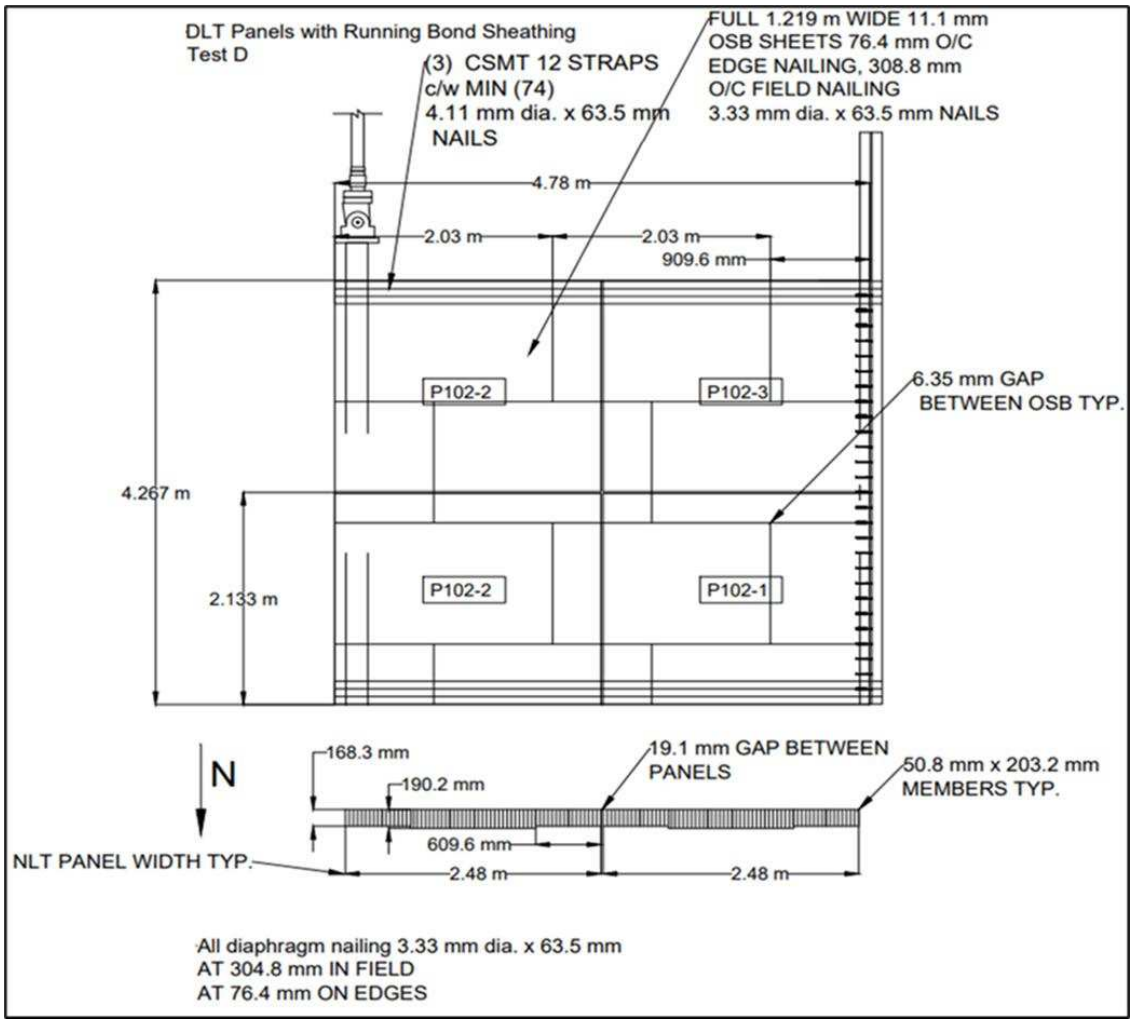

Figure 14: Test D DLT design

For the light frame design, in order to have comparable capacity to the NLT/DLT diaphragms and to connect well to the testbed, some additional considerations were needed. The frame consists of 101.6 mm x 254 mm (4" x 10") header joists (actual size of 88.9 mm x 234.95 mm [3-1/2" x 9-1/4"]) and 50.8 mm x 254 mm (2" x 10") floor joists (actual size of 38.1 mm x 234.95 mm [1.5" x 9-1/4"]). The rim joists were two different sizes (due to needing to fit in the web of the steel W fixed beam), with the rim joist attached to the fixed beam being a triple 50.8 mm x 152.4 mm (2" x 6") joist (actual size of 38.1 mm x 139.7 mm [1-1/2" x 5-1/2"]). In comparison, the rim joist on the free end consisted of a triple joist with the same size members as the floor joists. The sheathing

consisted of 15.08 mm (19/32”) thick structural OSB sheathing cut to size and installed in a staggered pattern. 50.8 mm x 101.6 mm (2” x 4”) blocking (actual size of 38.1 mm x 88.9 mm [2-1/2” x 5-1/2”]) was used between the floor joints along the joints of the OSB sheathing. A 3.58 mm dia. x 76.2 mm (0.141” dia. x 3”) common box nail was used to secure the OSB sheathing to the joists in a 101.6 mm –152.4 mm-152.4 mm (4”-6”-6”) edge nailing pattern and 304.8 mm (12”) in field spacing. To help transfer the shear from the diaphragm into the fixed beam, a custom connection consisting of a 12.7 mm (0.5”) thick 1.3 m (4’-4 1/2”) long steel plate with four rows of 6.35 mm dia. X 88.9 mm (0.25” dia. x 3.5”) SDS screws (88.9mm [3.5”] O/C) was installed on either side of the diaphragm perpendicular to the actuator loading. The design for the light frame wood diaphragm can be seen in Figure 15.

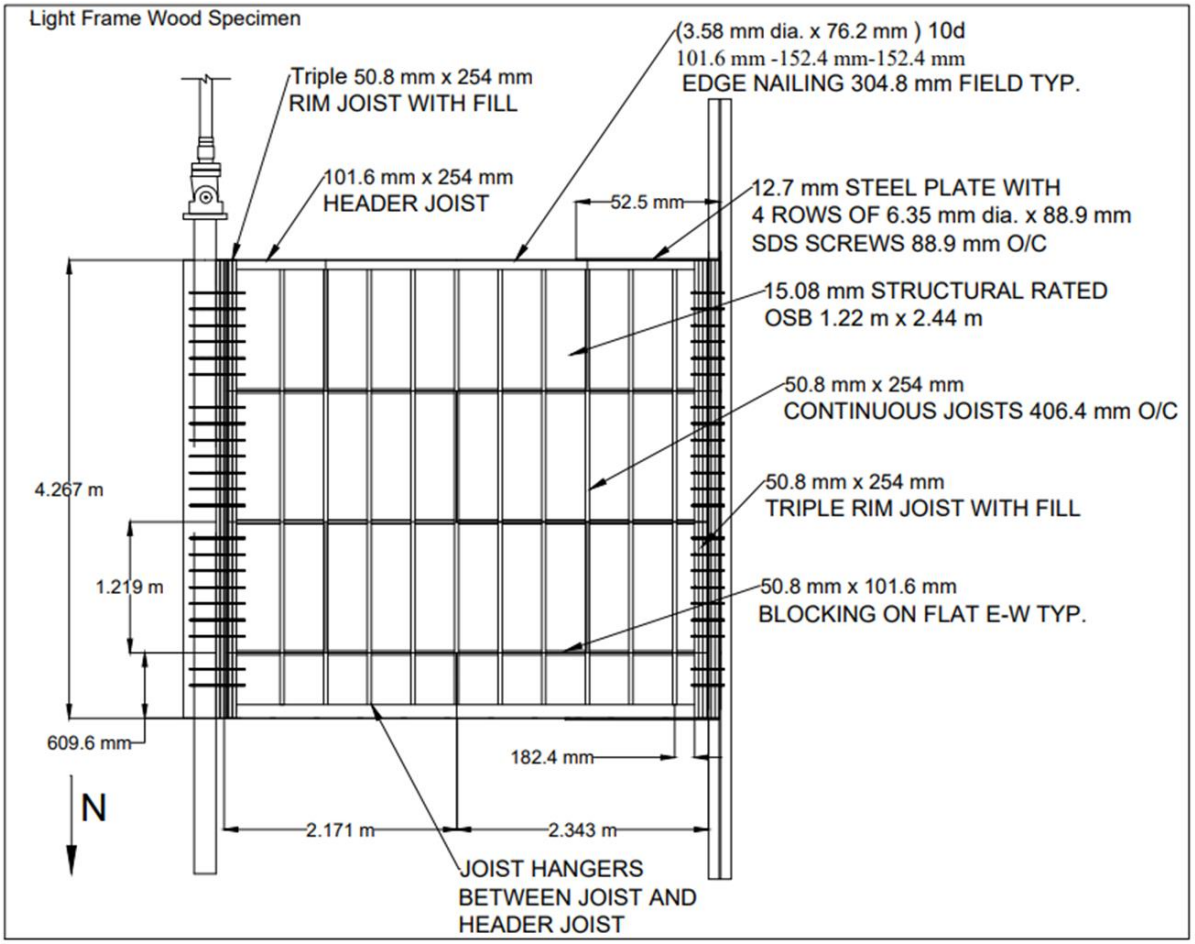

Figure 15: Light frame wood design

As previously mentioned, there were 4 NLT/DLT designs, however during Test C some localized dowel failure was observed, so the DLT panels for test D were coopted and another test using the Test C configuration was run instead. This test will be referred to as Test C1.

Testbed and Loading Protocol

Each of the five diaphragms were tested as cantilevers using the same experimental test frame. The test frame was located on a strong floor and consisted of a steel W-beam fastened to strong floor as the fixed end of the cantilever, and on the other end of the cantilever a support constructed of HSS beams was fastened to the floor. Rollers were then placed on top of the support to simulate

a free end. Intermediately between the free end support and the fixed beam were HSS sections welded together and fastened to the floor. The diaphragms were not secured to the HSS sections allowing free in plane movement, but the HSS sections restricted out of plane movements, simulating collector beams. The fixed beam, the HSS support, and the intermediate sections can be seen in Figure 16.

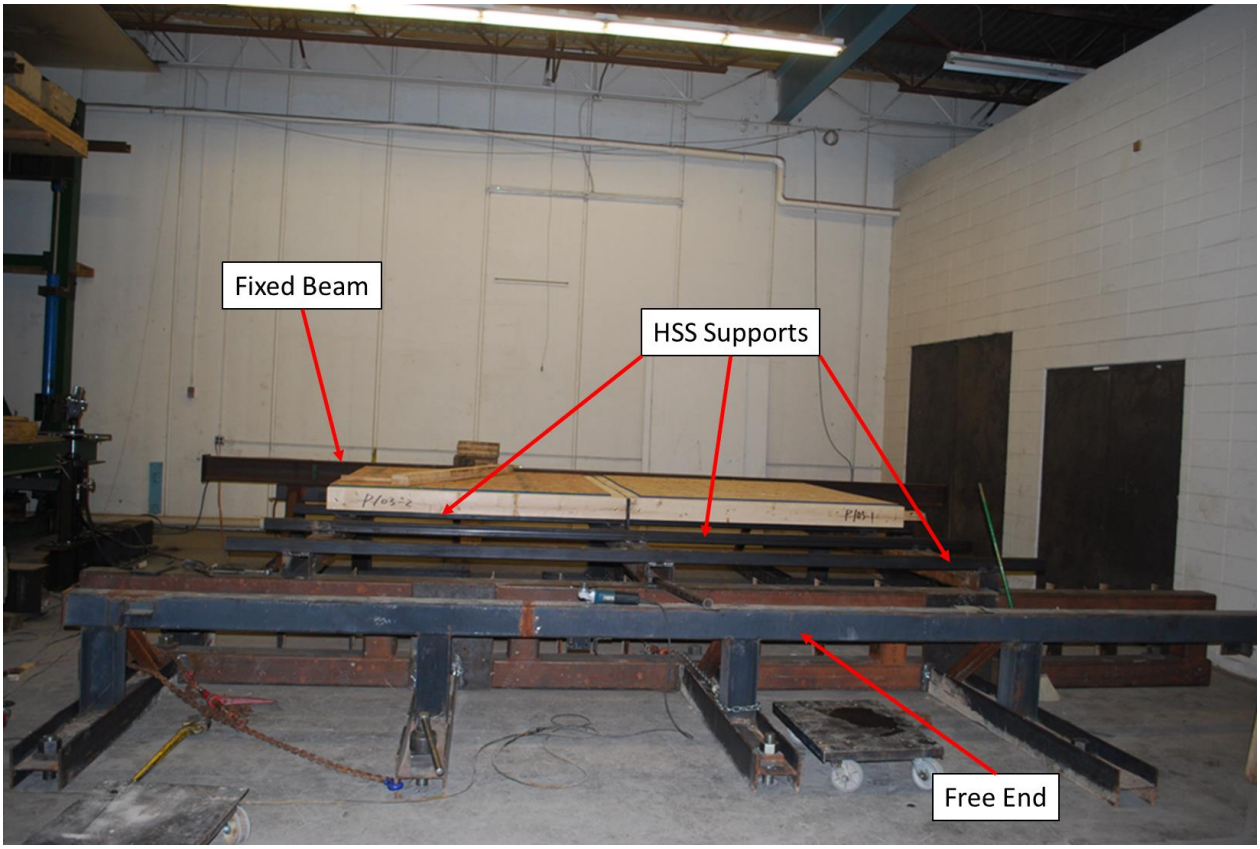

Figure 16: Test frame with partially installed diaphragm: fixed beam (far); free end (close)

In addition to the fixed beam and HSS support, a load beam consisting of HSS sections and two L-shape steel angles was attached to the diaphragm using SDS screws to transfer load from the actuator into the diaphragm. This load beam was also the contact point between the roller and the diaphragm, Figure 17 shows the test frame with the load beam attached to the diaphragm.

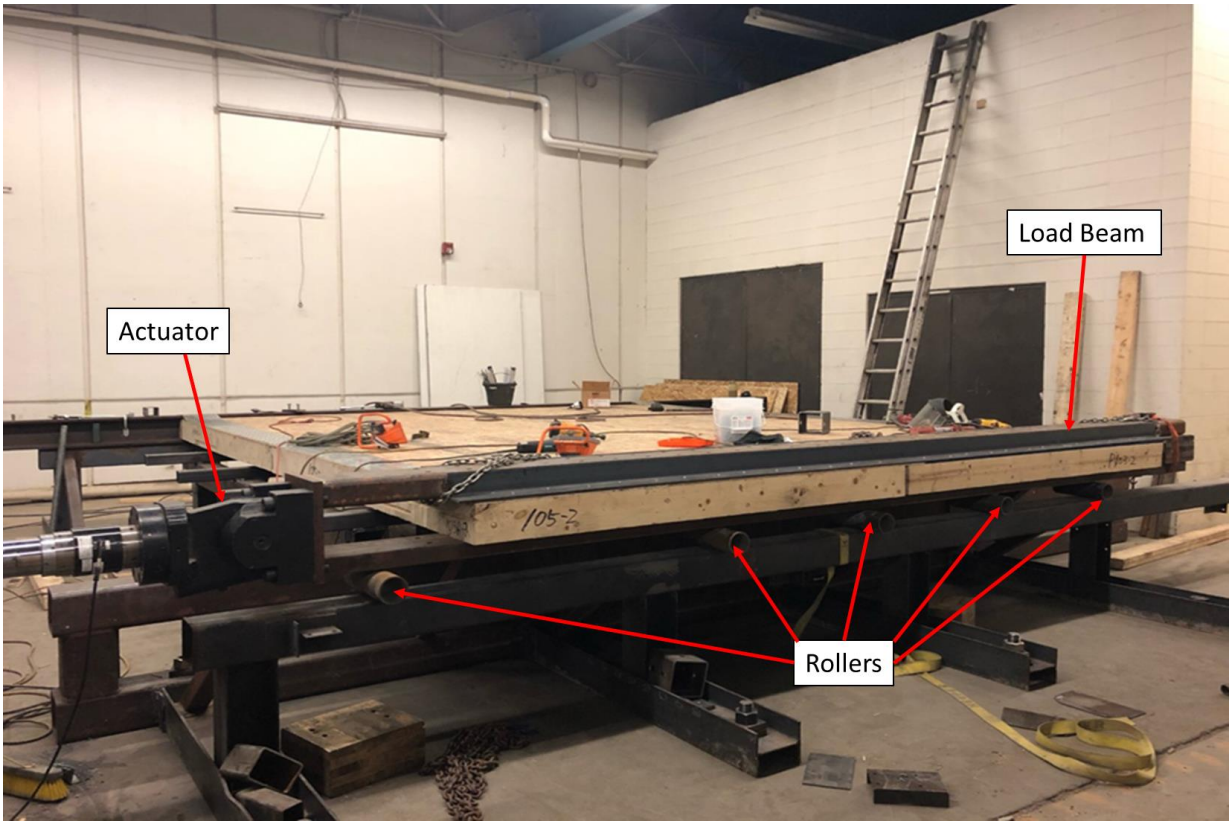

Figure 17: Test frame: load beam, actuator, and rollers

The actuator used in testing was an MTS systems model 201.6 and was attached to the diaphragm using the load beam as previously described and seen in Figure 17. The actuator reacted against a steel W beam anchored into a concrete slab and welded to two other steel W beams. The loading protocol used in the testing was a monotonic and quasi-static reversed cyclic protocol developed using the CUREE methodology for wood framed structures [36]. For Test A and B, a reference displacement of 152.4 mm (6") was used; and for Test C, C1, and the light frame wood diaphragm, a reference displacement of 101.6 mm (4") was used, based on what was learned with Test A and B. The loading table and plotted protocol for a reference displacement of 152.4 mm (6") can be seen in Table 7 and Figure 18 respectively. Similarly, the loading table and plotted protocol for a

reference displacement of 101.6 mm (4”) can be seen in Table 8 and Figure 19 respectively.

Table 7: 152.4 mm (6 in) loading protocol

Reference Displacement		152.4 mm	6 in.
Cycles (Hz)	0.05 xΔ	Displacement (mm)	Displacement (in)
2	0.050	7.62	0.30
2	0.038	5.72	0.23
1	0.075	11.43	0.45
2	0.056	8.57	0.34
1	0.100	15.24	0.60
2	0.075	11.43	0.45
1	0.200	30.48	1.20
2	0.150	22.86	0.90
1	0.300	45.72	1.80
2	0.225	34.29	1.35
1	0.400	60.96	2.40
2	0.300	45.72	1.80
1	0.700	106.68	4.20
1	0.525	80.01	3.15
1	1.000	152.40	6.00
1	0.750	114.30	4.50
1	1.150	175.26	6.90
1	0.863	131.45	5.18
1	1.300	198.12	7.80
1	0.975	148.59	5.85
1	1.450	220.98	8.70
1	1.088	165.74	6.53
1	1.600	243.84	9.60
1	1.200	182.88	7.20
Total Time (sec)		620	

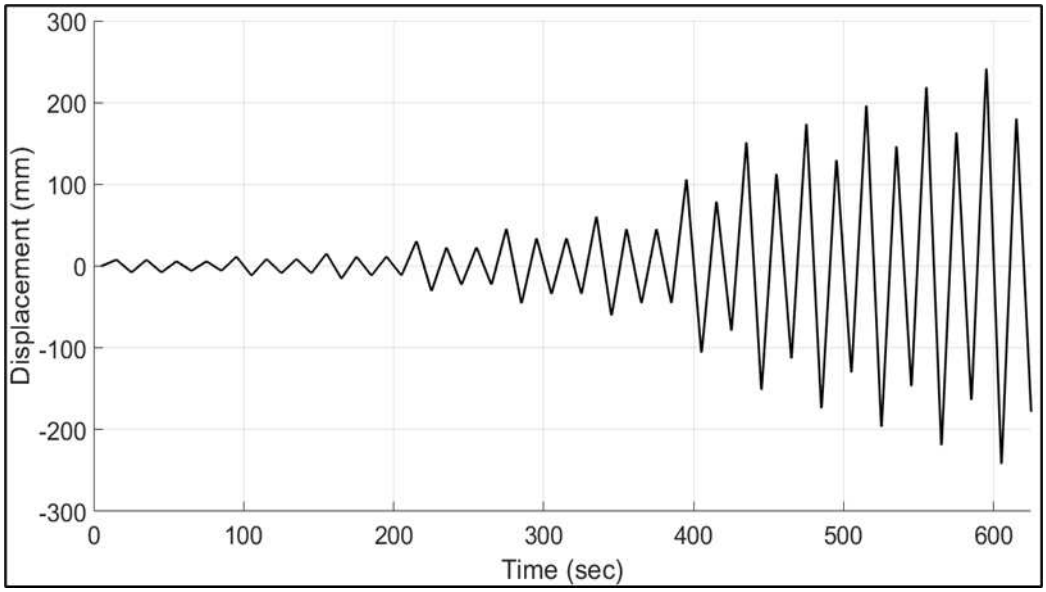

Figure 18: 152.4 mm (6 in) loading protocol

Table 8: 101.6 mm (4 in) loading protocol

Reference Displacement		101.6 mm	4 in.
Cycles (Hz)	0.05 xΔ	Displacement (mm)	Displacement (in.)
2	0.050	5.08	0.20
2	0.038	3.81	0.15
1	0.075	7.62	0.30
2	0.056	5.72	0.23
1	0.100	10.16	0.40
2	0.075	7.62	0.30
1	0.200	20.32	0.80
2	0.150	15.24	0.60
1	0.300	30.48	1.20
2	0.225	22.86	0.90
1	0.400	40.64	1.60
2	0.300	30.48	1.20
1	0.700	71.12	2.80
1	0.525	53.34	2.10
1	1.000	101.60	4.00
1	0.750	76.20	3.00
1	1.150	116.84	4.60
1	0.863	87.63	3.45
1	1.300	132.08	5.20
1	0.975	99.06	3.90
1	1.450	147.32	5.80
1	1.088	110.49	4.35
1	1.600	162.56	6.40
1	1.200	121.92	4.80
2	1.750	177.80	7.00
1	1.313	133.35	5.25
1	1.900	193.04	7.60
1	1.425	144.78	5.70
1	2.050	208.28	8.20
1	1.538	156.21	6.15
1	2.200	223.52	8.80
1	1.650	167.64	6.60
1	2.350	238.76	9.40
1	1.763	179.07	7.05
Total Time (sec)		840	

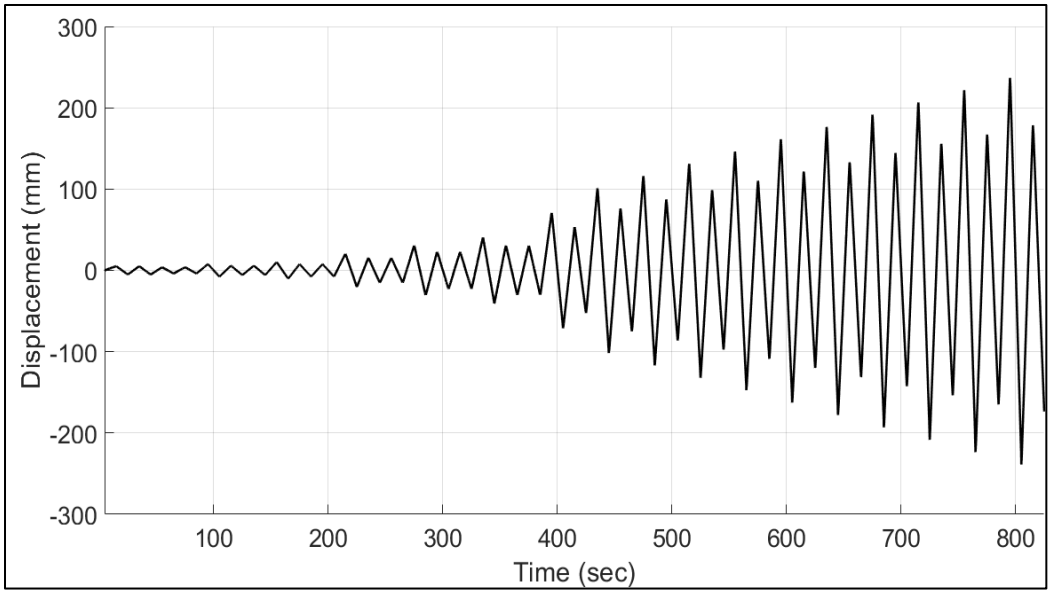

Figure 19: 101.6 mm (4 in) loading protocol

Instrumentation

The primary instrumentation across all the testing were string potentiometers, specifically Measurement Specialties SM-12 and SM-25 string potentiometers. The instrumentation plan was the same for Tests A-C1, with 12 total string potentiometers labeled SP01-12. The diaphragm global deformation was measured using SP01-02, however due to the presence of the load beam and W-beam, the instruments could not be placed exactly at the corners of the diaphragm. The inter-panel deformation was measured on one panel per test with SP10-11, with the placement locations being limited by the CMST 12 straps and the fixed W-beam. Displacement across the infill strip was measured in both directions and on both the infill parallel to the actuator (SP03-04), and perpendicular to the actuator (SP08-09). A piece of dimensional lumber was placed across the infill to provide an anchor point for the string potentiometers on both infills measuring the relative parallel displacements of the panels. The displacement profile was generated using a line of string potentiometers (SP05-07) anchored on one end by the actuator and on the other end by the fixed beam. The string potentiometers were secured to a lumber member attached to the fixed

W-beam, but otherwise unattached to the diaphragm. SP12 was attached to the fixed beam to measure any movement of the flange of the W-beam during testing. It should be noted that due to a recording error, SP11 and SP12 are unavailable for Test A. The locations of each of the string pots for Tests A-C1 can be seen in Figure 20.

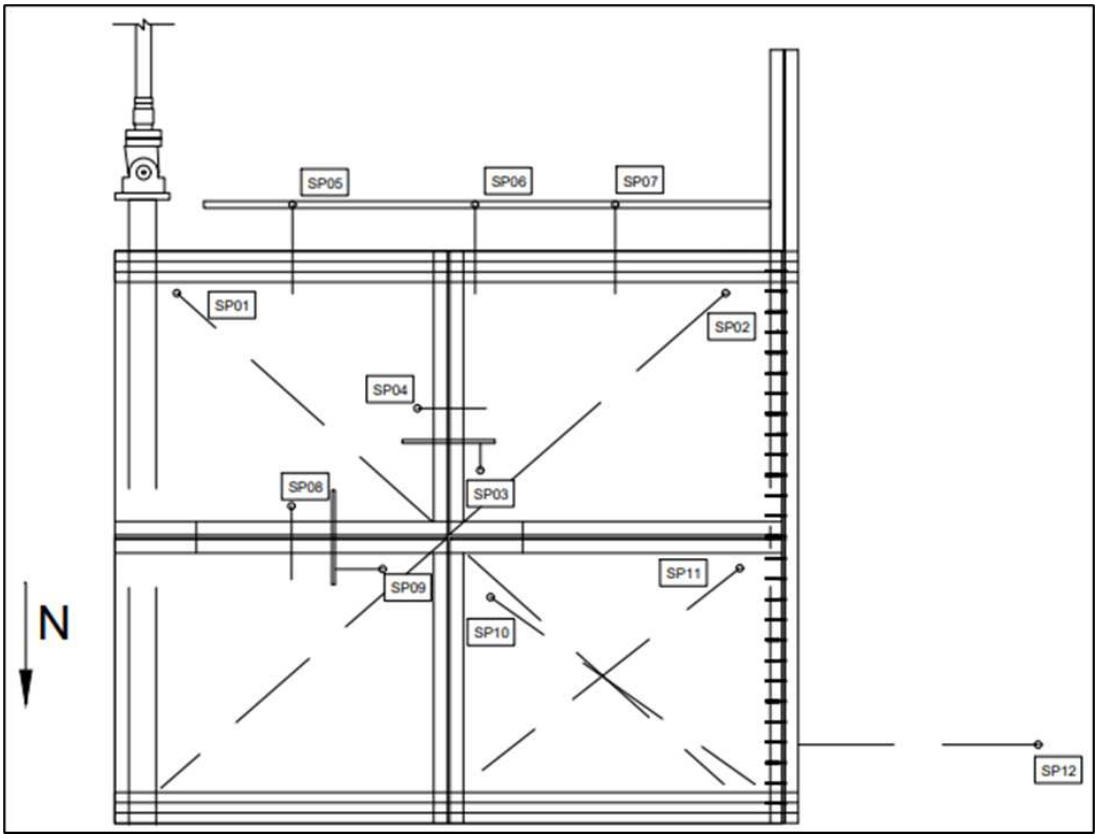

Figure 20: Instrumentation Tests A-C1

For the light frame wood diaphragm instrumentation, since there were no panels or infill strips, string potentiometers SP03, SP04, SP08, SP09, SP10, and SP11 were in different locations than in the NLT/DLT testing. SP03 and SP04 were used to measure displacement on the north-south, east-west OSB sheathing joint on the south side of the diaphragm, while SP10 and SP11 did the same on the north side of the diaphragm. SP08 was used to measure the displacement at the central most OSB sheathing joint perpendicular to the loading direction, while SP09 was added to the

displacement profile string potentiometers (SP05-07). The remaining string potentiometers (SP01-02, SP05-07, and SP12) were in the same locations as the previous tests. The full instrumentation plan for the light frame wood diaphragm can be seen in Figure 21.

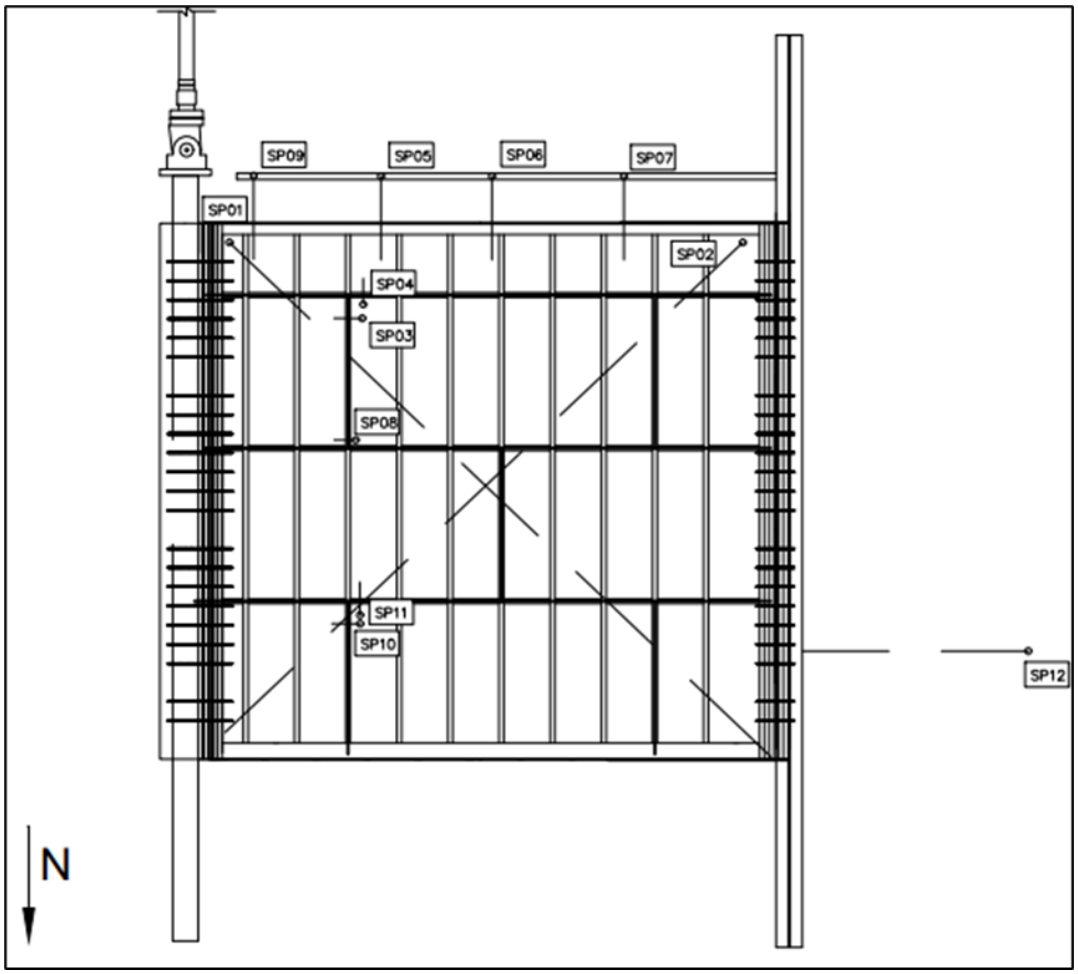

Figure 21: Instrumentation for light frame wood test

CHAPTER 5 - NAIL LAMINATED AND DOWEL LAMINATED DIAPHRAGM TEST RESULTS

Fixed-Beam Assumption

As previously mentioned, it was assumed that the steel W-beam anchored into the floor would act as the fixed end for the cantilever testing. To examine the validity of this assumption, a string potentiometer (SP12) was used to measure any potential rotation of the flange of the W-beam. Figure 22 shows the measured displacement of the flange from each of the tests, excluding Test A where there was a recording error, as a time series over the entirety of the test.

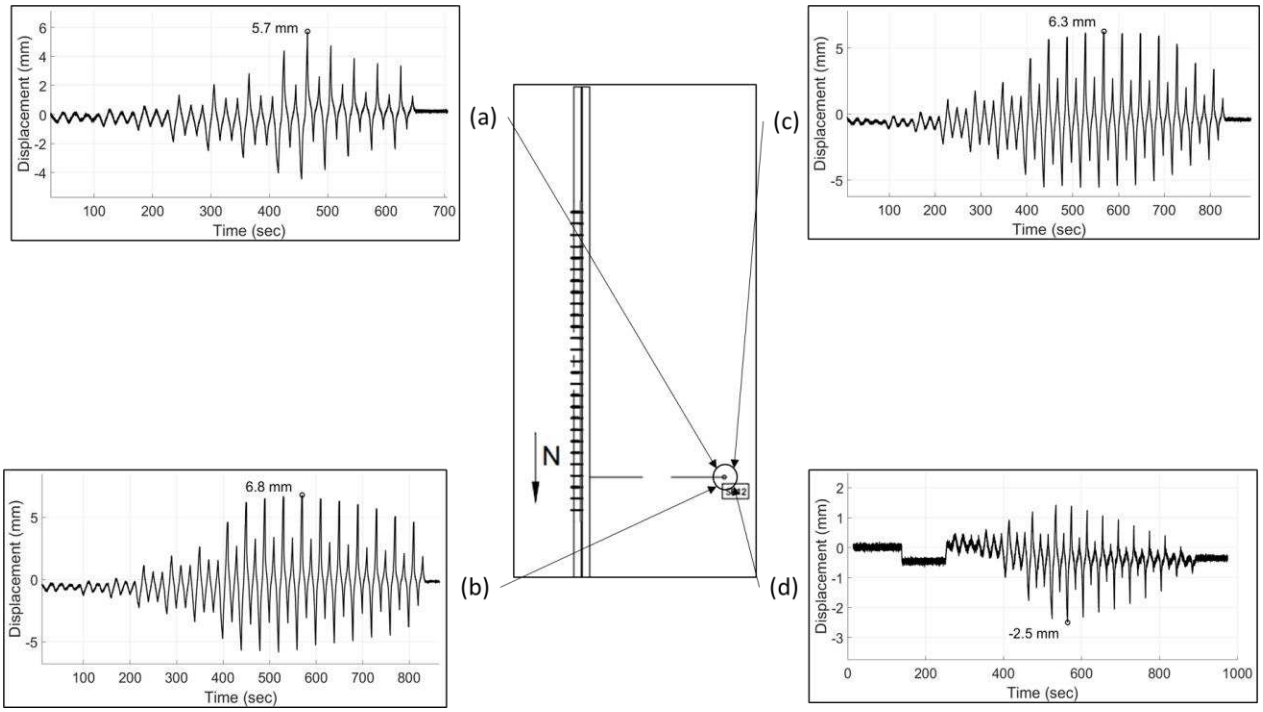

Figure 22: Displacement of fixed beam flange: Test B (a), Test C (b), Test C1 (c), LFW Test (d)

The maximum displacement measured was 6.8 mm (0.27”), observed during Test C. Test C1 had

a similar result with 6.3 mm (0.25”) of displacement. Test B saw a maximum displacement of 5.7 mm (0.22”), and it is a reasonable assumption that Test A would have a displacement of similar magnitude. The light frame wood test had the smallest displacement, measured at 2.5 mm (0.1”). While the displacement of the W-beam is nonzero, with maximum displacements in excess of 200 mm (7.87”) during testing, the assumed fixed nature of the W-beam seems reasonable.

Force-Displacement Hystereses

The primary objective of the testing was to develop a force-displacement hysteresis for several different NLT/DLT diaphragm designs, with the purpose of better understanding the lateral performance and properties of the various designs, which could then be used in both modeling and design efforts, specifically the design efforts of the NLT/DLT diaphragms in the larger 10 story test. The recorded hystereses for each of the first four tests (Tests A-C1) are presented in Figure 23 and Table 9.

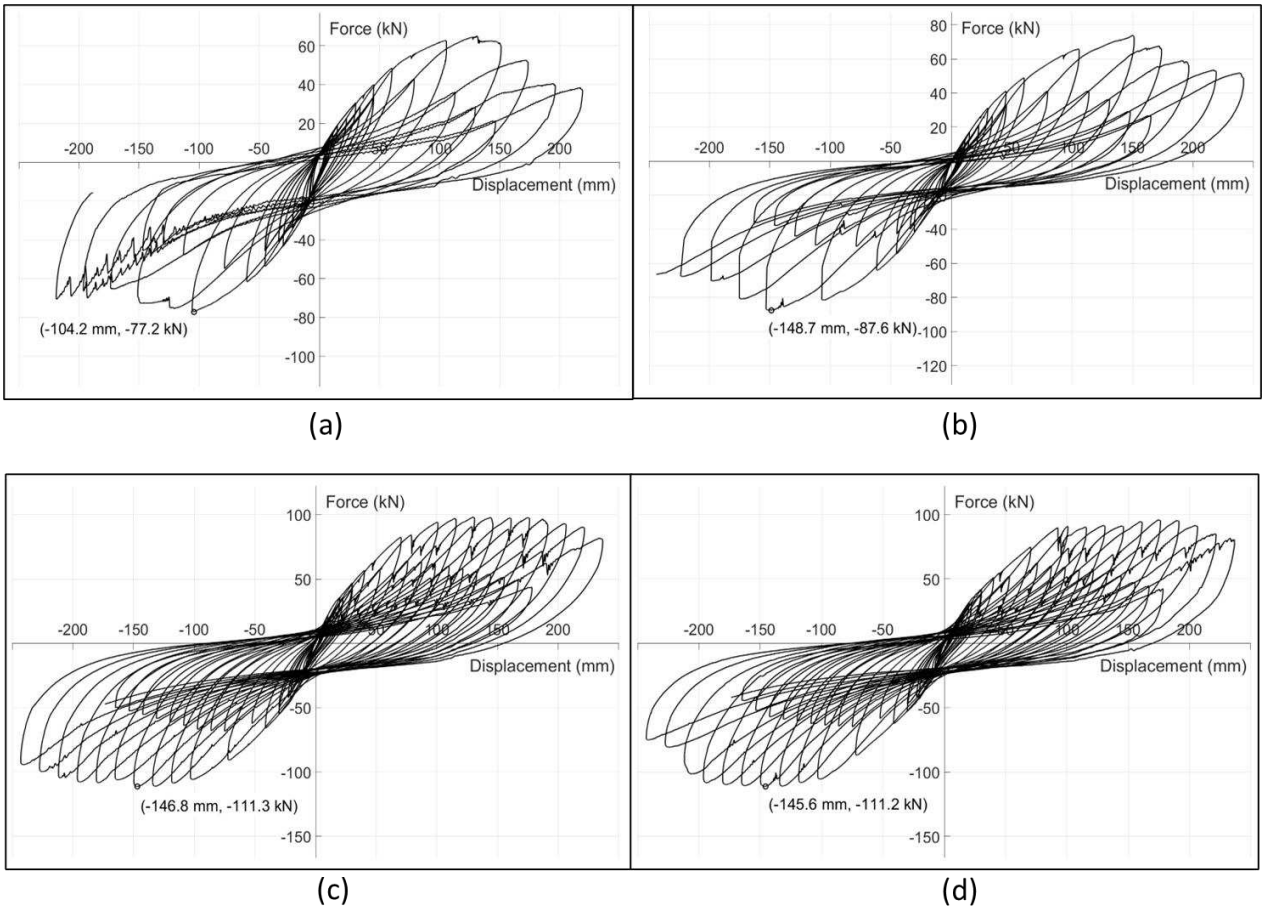

Figure 23: Force-displacement hysteresis: Test A (a), Test B (b), Test C (c), Test C1 (d)

Table 9: Force-displacement hysteresis peaks for Tests A-C1

Test	Peak Force (kN)	Peak Force (kips)	Peak Force Displacement (mm)	Peak Force Displacement (in)
Test A	77.2	17.4	104.2	4.1
Test B	87.6	19.7	148.7	5.9
Test C	111.3	25.0	146.8	5.8
Test C1	111.2	25.0	145.6	5.7

In general, all the diaphragms in the first four tests clearly showed inelastic behavior, with stiffness-softening occurring across all diaphragms. Comparing the DLT and NLT diaphragms in Tests A and B respectively, while the sheathing and fastener design were identical, there are

significant differences in hysteresis. The NLT diaphragm had a larger maximum measured force magnitude than the DLT (87.6 kN [19.7 kips] versus 77.2 kN [17.4 kips] respectively) by around 13%, but while the DLT panel failed before the completion of the protocol, the NLT diaphragm was able to complete the full test protocol. As previously discussed, during Test C, there was localized out of plane deformation observed in the two panels attached to the fixed W-beam, starting at a displacement of around 147.32 mm (5.8”). There was concern that the deformation could impact the results of the testing, so instead of running the Test D design (Figure 14), another test using the Test C design was run instead. Figure 24 shows the observed deformation during Test C.

Figure 24: Observed out of plane deformation during Test C

In terms of capacity, this concern was unfounded. Comparing the hysteresis of Test C to the hysteresis of Test C1, the maximum capacity was almost identical, and occurred at nearly the same time. However, in terms of stiffness-softening, the out of plane deformation seemed to have some effect. Test C1 clearly softened more than Test C after 150 mm (5.9”), and this difference can be explained by the out of plane deformation acting as a form of energy dissipation, delaying further stiffness-softening significantly. Comparing the two different nail patterns tested (Tests A and B had the same nail pattern, and Tests C and C1 had the same nail pattern), as expected, in terms of capacity, the tighter nail patterns performed significantly better. Test C and C1 (DLT) had approximately 44% higher maximum observed load in comparison to Test A (DLT), and approximately 27% higher than Test B (NLT). Also as expected, Test C and C1 were significantly stiffer than Tests A and B. This demonstrates the importance of the sheathing, nails, and the nail pattern to the lateral capacity of the NLT/DLT diaphragm designs. For comparison, Figure 25 and Table 10 show the force-displacement hysteresis for the light frame wood test.

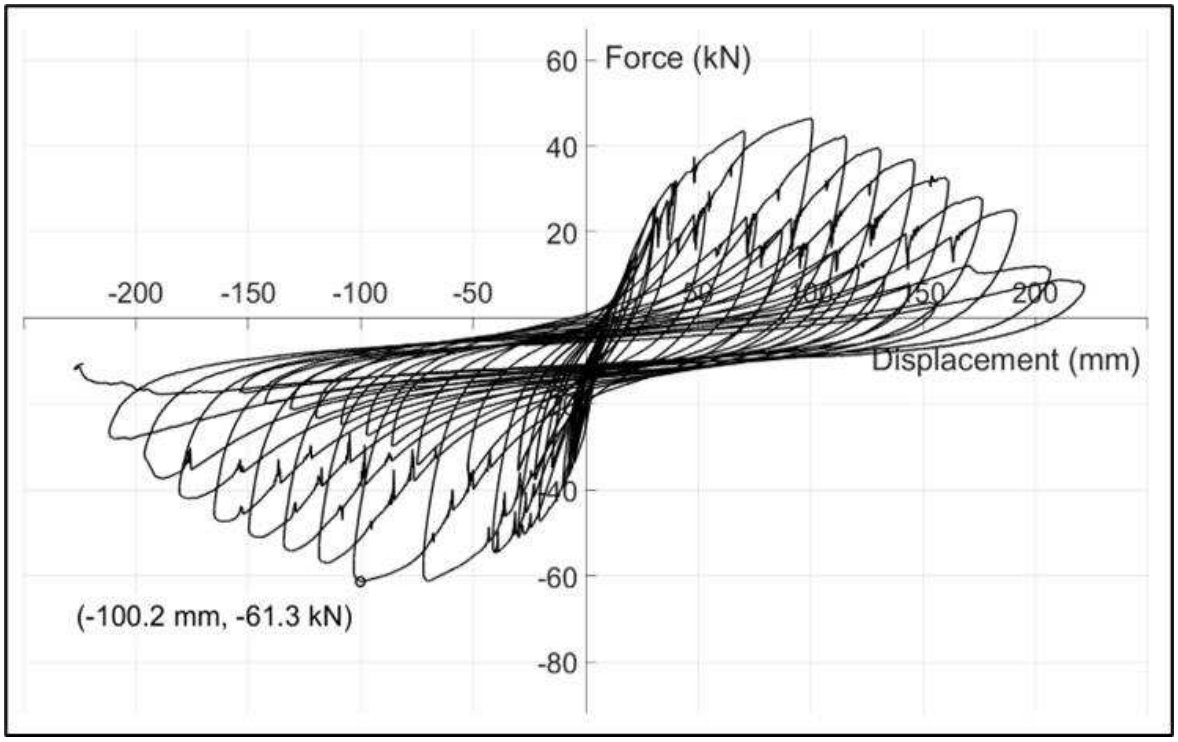

Figure 25: Light frame wood test force-displacement hysteresis

Table 10: Force-displacement hysteresis peak for LFW Test

Test	Peak Force (kN)	Peak Force (kips)	Peak Force Displacement (mm)	Peak Force Displacement (in)
LFW Test	61.3	13.8	100.2	3.9

From Figure 25 and Table 10, it is clear that light frame wood diaphragms struggle to match the capacity of the NLT/DLT diaphragms, with the closest diaphragm being the Test A DLT diaphragm, with almost 26% more capacity. As documented, the light frame wood diaphragm had two custom connections to help better transfer shear into the fixed beam, as well as thicker OSB, larger nails, and a nail pattern most similar to Test C and C1, only reinforcing the capacity disparity observation. In terms of stiffness, the light frame wood diaphragm also clearly began to soften before any of the NLT/DLT diaphragms, however it was able to complete the full test protocol, unlike Test A.

Diaphragm Displacement Time Series and Profile

To construct a displacement profile for each of the tests, a series of string potentiometers (SP05-07) were placed equidistant from the actuator to the fixed W-beam. These string potentiometers measured the global displacements at these points with the fixed beam assumed zero and the actuator data providing the displacement at the free end. Figure 26 shows an example of the time series for SP05-07 for Test A.

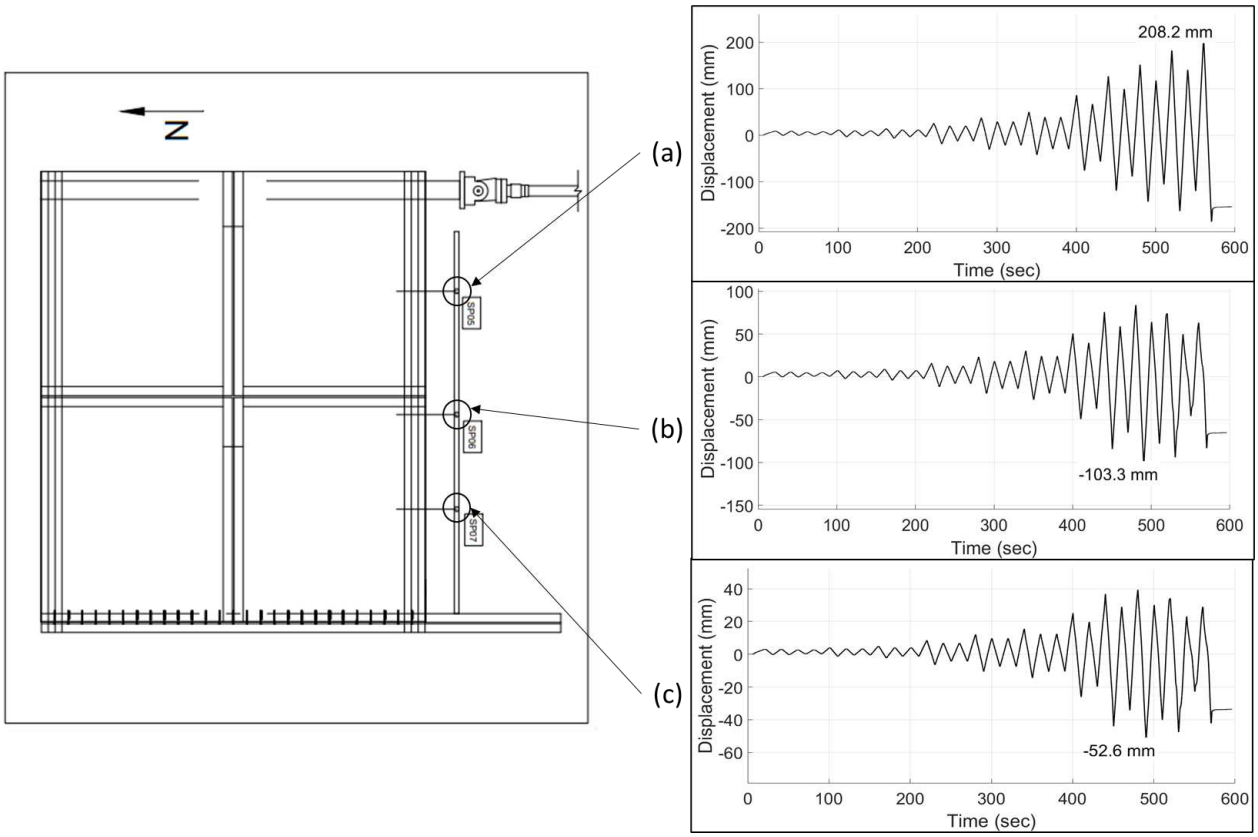

Figure 26: Test A displacement time series: SP05 (a), SP06 (b), SP07 (c)

Examining Figure 26, it can be seen that the peak displacements for SP05 and SP06-07 occur at different times, with an observed maximum displacement of 208.2 mm (8.2") for SP05 at approximately 550 seconds and observed maximum displacements of 103.3 mm (4.07") and 52.6 mm (2.07") for SP06 and SP07 respectively, occurring at approximately 490 seconds. Looking

closer at SP06 and SP07, until the maximum displacement, there is good agreement between all three string potentiometers; the general shape of the time series looks similar, with different magnitudes corresponding to the distance from the actuator (farther from the actuator has smaller displacements). The reason for the poor agreement after this point was observed during testing, the panel SP05 and SP06 was attached to was isolated from the other three panels by the failure of the OSB infill connectors. The test was continued for a few more cycles to ensure failure, but it is clear from Figure 26 when the failure of the diaphragm occurred. Table 11 shows the observed maximums and the time that they occurred for Tests A, B, C, and C1.

Table 11: Peak displacements for SP05-07 for tests A-C1

Test	SP05 Peak Displacement (mm)	SP05 Peak Displacement (in)	SP05 Peak Displacement Time (sec)
Test A	208.2	8.20	550
Test B	206.8	8.14	625
Test C	193.0	7.60	810
Test C1	200.6	7.90	810
Test	SP06 Peak Displacement (mm)	SP06 Peak Displacement (in)	SP06 Peak Displacement Time (sec)
Test A	103.3	4.07	490
Test B	146.2	5.76	625
Test C	141.5	5.57	810
Test C1	171.5	6.75	810
Test	SP07 Peak Displacement (mm)	SP07 Peak Displacement (in)	SP07 Peak Displacement Time (sec)
Test A	52.6	2.07	490
Test B	80.8	3.18	625
Test C	73.6	2.90	810
Test C1	75.6	2.98	810

The observed failure in Test A was not repeated in Test B, so the global displacement string pots have much better agreement, and maximum displacements during the same testing cycle. A maximum displacement of 206.8 mm (8.14”), 146.2 mm (5.76”), and 80.8 mm (3.18”) were observed for SP05, SP06, and SP07 respectively, all occurring at approximately 625 seconds. The results for Tests C and C1 followed previously established patterns and expectations, the maximum displacement for each SP occurred at the same cycle corresponding to the maximum actuator displacement. Test C had a maximum observed displacement of 193 mm (7.6”), 141.5 mm (5.57”) and 73.6 mm (2.9”) for SP05, SP06, and SP07 respectively at approximately 810 seconds. In comparison, Test C1 had 200.6mm (7.9”), 171.5 mm (6.75”), and 75.6 mm (2.98”) maximum displacements for SP05, SP06, and SP07 respectively, occurring also at approximately 810 seconds.

The light frame wood test saw the addition of SP09 to the displacement profile, so unlike Tests A-C1, the order of string potentiometer from the actuator to the fixed beam went as follows: SP09, SP05, SP06, SP07. Similar to Test A, the maximum observed displacements for each of the string pots did not occur at the same time, with the maximum for SP09 and SP05 occurring simultaneously at approximately 810 seconds, while SP06 and SP07 had their maximums occur at approximately 780 seconds and 720 seconds respectively. The magnitudes observed were 174.2 mm, 123.2 mm (4.85”), 66.6 mm (2.62”), and 33.4 mm (1.31”) for SP09, SP05, SP06, and SP07 respectively. The full time series for each of the string potentiometers, as well as their peaks, for the light frame wood test can be found in Figure 27 and Table 12.

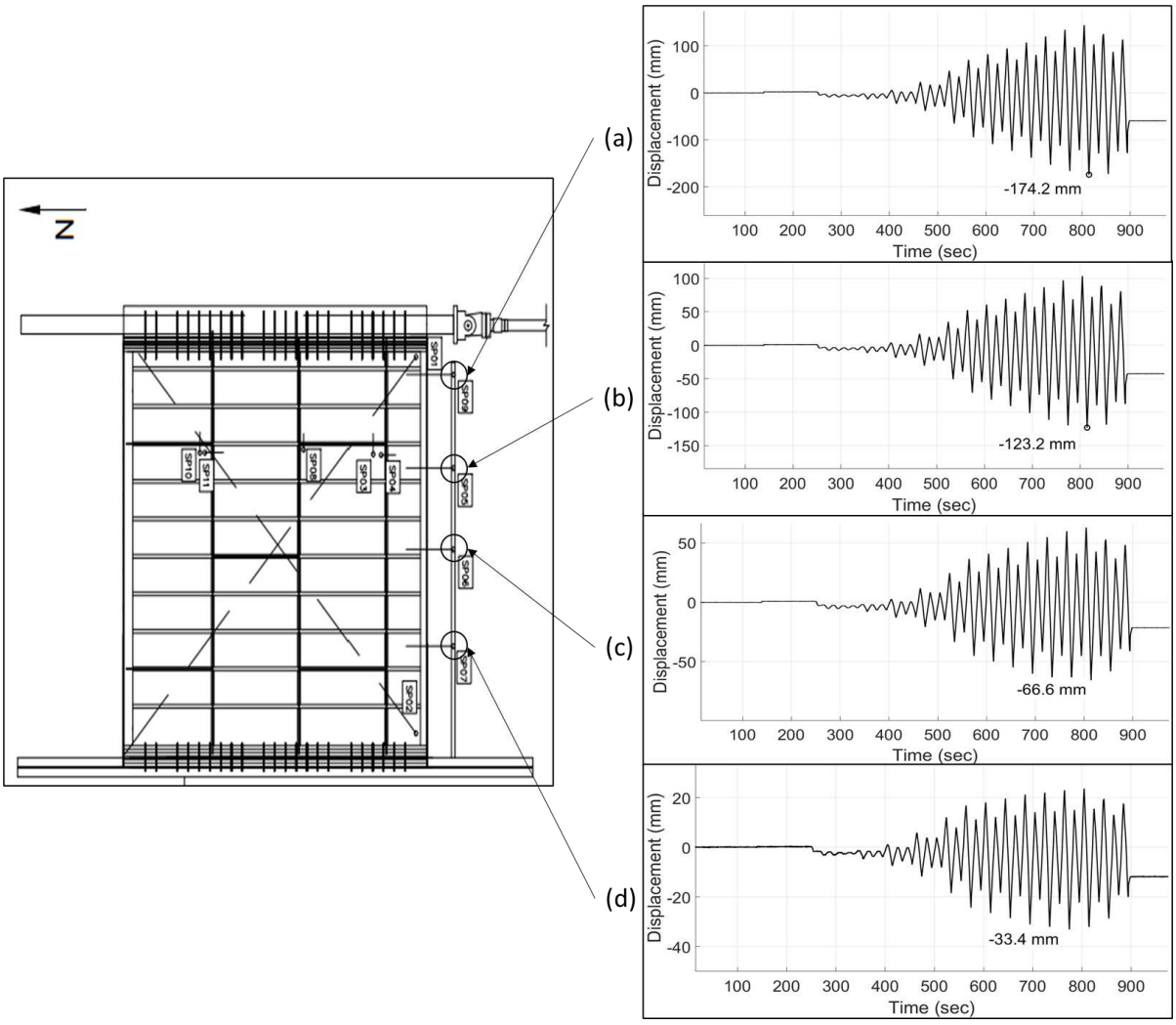

Figure 27: Light frame wood test displacement timeseries: SP09 (a) SP05 (b), SP06 (c), SP07 (d)

Table 12: Peak displacements for SP09 and SP05-07 for LFW test

Test	SP09 Peak Displacement (mm)	SP09 Peak Displacement (in)	SP09 Peak Displacement Time (sec)
Light frame wood	174.2	6.86	810
Test	SP05 Peak Displacement (mm)	SP05 Peak Displacement (in)	SP05 Peak Displacement Time (sec)
Light frame wood	123.2	4.85	810
Test	SP06 Peak Displacement (mm)	SP06 Peak Displacement (in)	SP06 Peak Displacement Time (sec)
Light frame wood	66.6	2.62	780
Test	SP07 Peak Displacement (mm)	SP07 Peak Displacement (in)	SP07 Peak Displacement Time (sec)
Light frame wood	33.4	1.31	720

To better observe and compare the behavior of each diaphragm at maximum actuator displacement, a displacement profile along the diaphragm was created for each test at the corresponding time in the time series, and then plotted against each other. This created a plot of all of the test's displacement profiles in terms of displacement versus location along the diaphragm from the fixed beam to the actuator (with the fixed W-beam acting as the origin). The most immediate and obvious observation was the significant jump created in the Test A profile from the isolation of the panel some of the string potentiometers were connected to. Tests C and C1 also have an approximately 30 mm (1.18") difference in displacement near the OSB infill joint. This is potentially a consequence of the out of plane deformation seen in Test C, but further investigation is required. The full suite of test profile displacements can be seen in Figure 28.

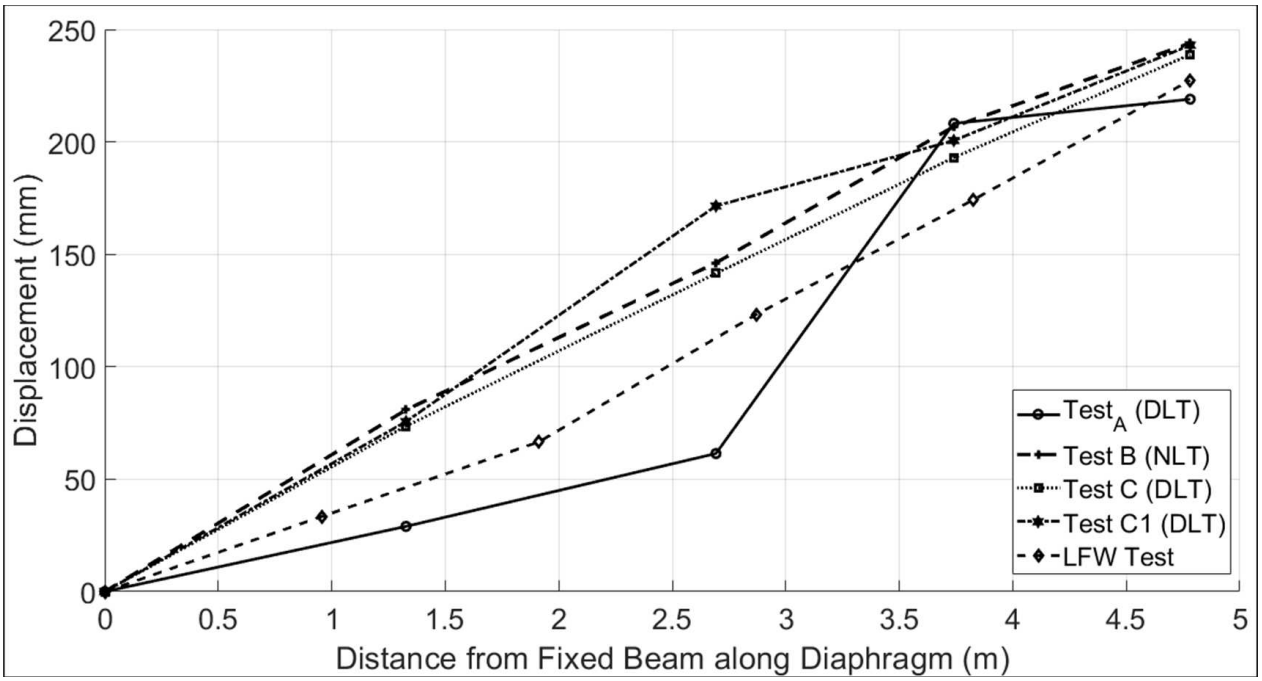

Figure 28: Displacement profile comparison for all tests at maximum observed actuator displacement

Diaphragm Deformation

To construct a more complete picture of each of the diaphragm performance, global diaphragm displacement was measured during each of the tests. This was done using SP01 and SP02, with SP01 placed near the actuator on the south side of the diaphragm and measured diagonally across the diaphragm to the north side of the diaphragm near the fixed W-beam (SE to NW). Conversely, SP02 measured diagonally from the south side of the diaphragm near the fixed W-beam to the north side of the diaphragm near the actuator (SW to NE). The peak diaphragm displacement for each test can be seen in Table 13.

Table 13: Peak observed diaphragm

Test	Peak Diaphragm Deformation (mm)	Peak Diaphragm Deformation (in)
Test A	124.1	4.89
Test B	139.8	5.50
Test C	107.4	4.23
Test C1	113.9	4.48
Light frame wood	113.3	4.46

Test A had a maximum diaphragm deformation of 124.1 mm (4.89") from SP01 (SW to NE) and 118.9 mm (4.68") from SP02 (SE to NW). In comparison, Test B had a maximum diaphragm deformation of 139.8 mm (5.50") from SP01 (SW to NE) and 129.7 mm (5.11") from SP02 (SE to NW). For both Test A and Test B the measured maximum in SP02 was smaller than the measured maximum in SP01, which shows differential deformation of the panels. In Test A, a clear isolation of the southwestern panel (attached to the fixed beam) was observed; in Test B infill sheathing failure was observed, but no individual panel was isolated, so the difference is most likely from the culmination of infill sheathing failure across the diaphragm. On initial observation it appears that Test A had less diaphragm deformation. However, this is misleading; Test A did not complete the full testing protocol, so while Test B had a larger maximum measured deformation, the diaphragm was subjected to a larger maximum displacement than Test A. The effect of the panel isolation in Test A as well as the asymmetrical deformation of Test B can be seen in Figure 29.

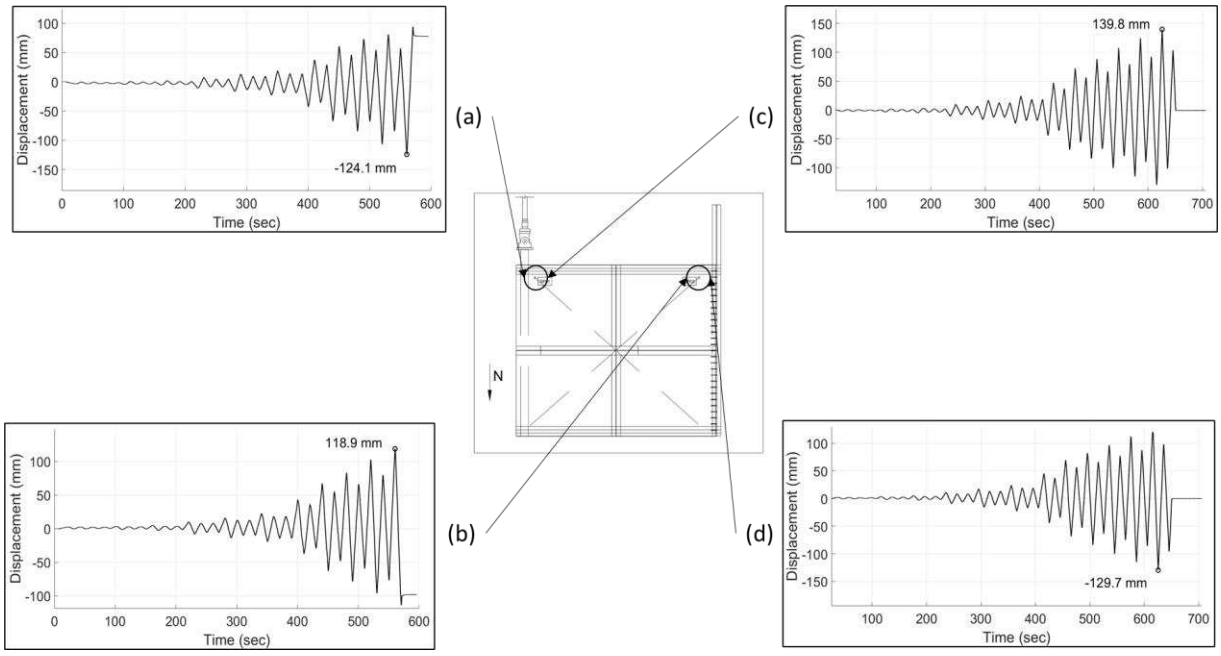

Figure 29: Diaphragm deformation for Test A and Test B: Test A SP01 (SE to NW) (a), Test A SP02 (SW to NE) (b), Test B SP01 (SE to NW) (c), Test B SP02 (SW to NE) (d).

As discussed previously, Test C and C1 had a tighter nail spacing in comparison to Test A and B, which lead to a stiffer diaphragm as shown in Figure 23. So, it would be expected that the stiffer diaphragms of Test C and C1 would show less global deformation in comparison to Test A and Test B. During Test C a maximum diaphragm deformation of 100.1 mm from SP01 (SW to NE) and 107.4 mm from SP02 (SE to NW). In comparison, Test C1 had a maximum deformation of 113.9 mm (4.48") and 113.4 mm (4.46") measured from SP01 (SW to NE) and SP02 (SE to NW) respectively. These align with the expectation of a stiffer diaphragm; however, it is notable that Test C and Test C1 had a significant variation in the maximum measured deformation and differential between SP01 and SP02. Test C1 had a similar differential between SP01 and SP02 (7.4 mm [0.29"]) as was seen in Test A (5.2 mm [0.20"]), while Test C was almost symmetric. Considering as well the almost 7 mm (0.28") difference in maximum measured deformation between Test C and C1, this is most likely a result of the localized out of plane deformation

during Test C that has been discussed. The full time series for Test C and C1 can be found in Figure 30.

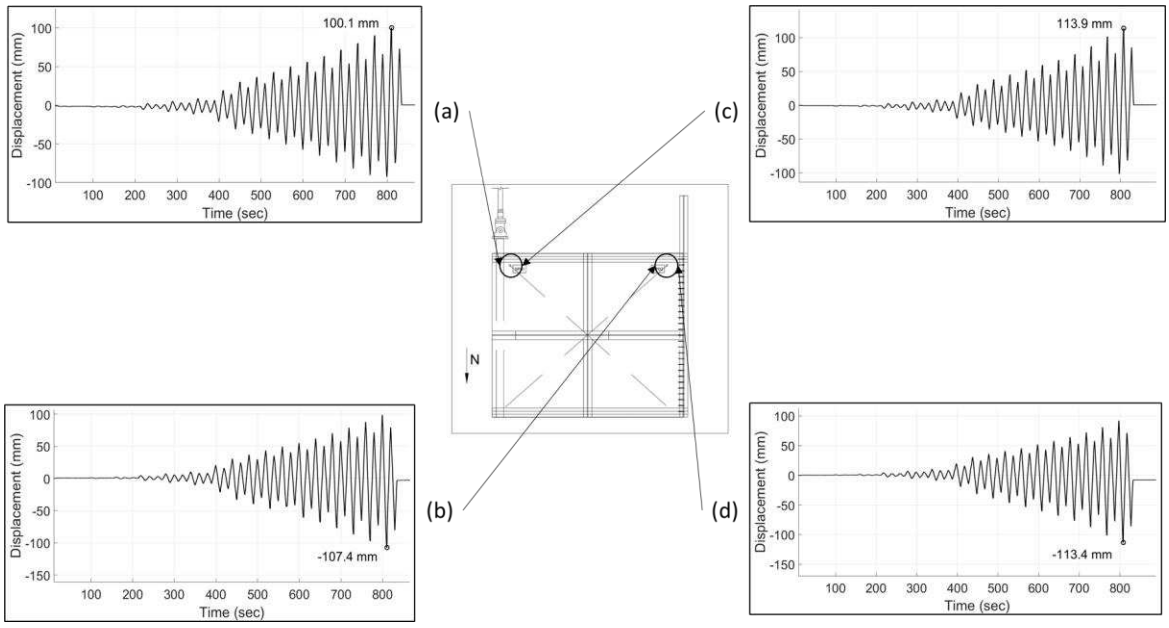

Figure 30: Diaphragm deformation for Test C and Test C1: Test C SP01 (SE to NW) (a), Test C SP02 (SW to NE) (b), Test C1 SP01 (SE to NW) (c), Test C1 SP02 (SW to NE) (d).

The light frame wood test saw a maximum measured displacement of 113.3 mm (4.46") and 96.6 mm (3.8") for SP01 (SW to NE) and SP02 (SE to NW) respectively. Several observations can be made from this: firstly, the maximum measured displacement is more in line with Test C and Test C1 than Test A and B; secondly a significant differential deformation was recorded, more similar to Tests A, B, and C, than C1. This would imply that the light frame diaphragm was stiffer than the NLT/DLT diaphragms in Tests A and B, and this can be confirmed by comparing Figures 23 and 25. Additionally it would imply differential deformation of the panel, which was observed during testing. The full time series for the panel deformation of the light frame wood diaphragm can be seen in Figure 31.

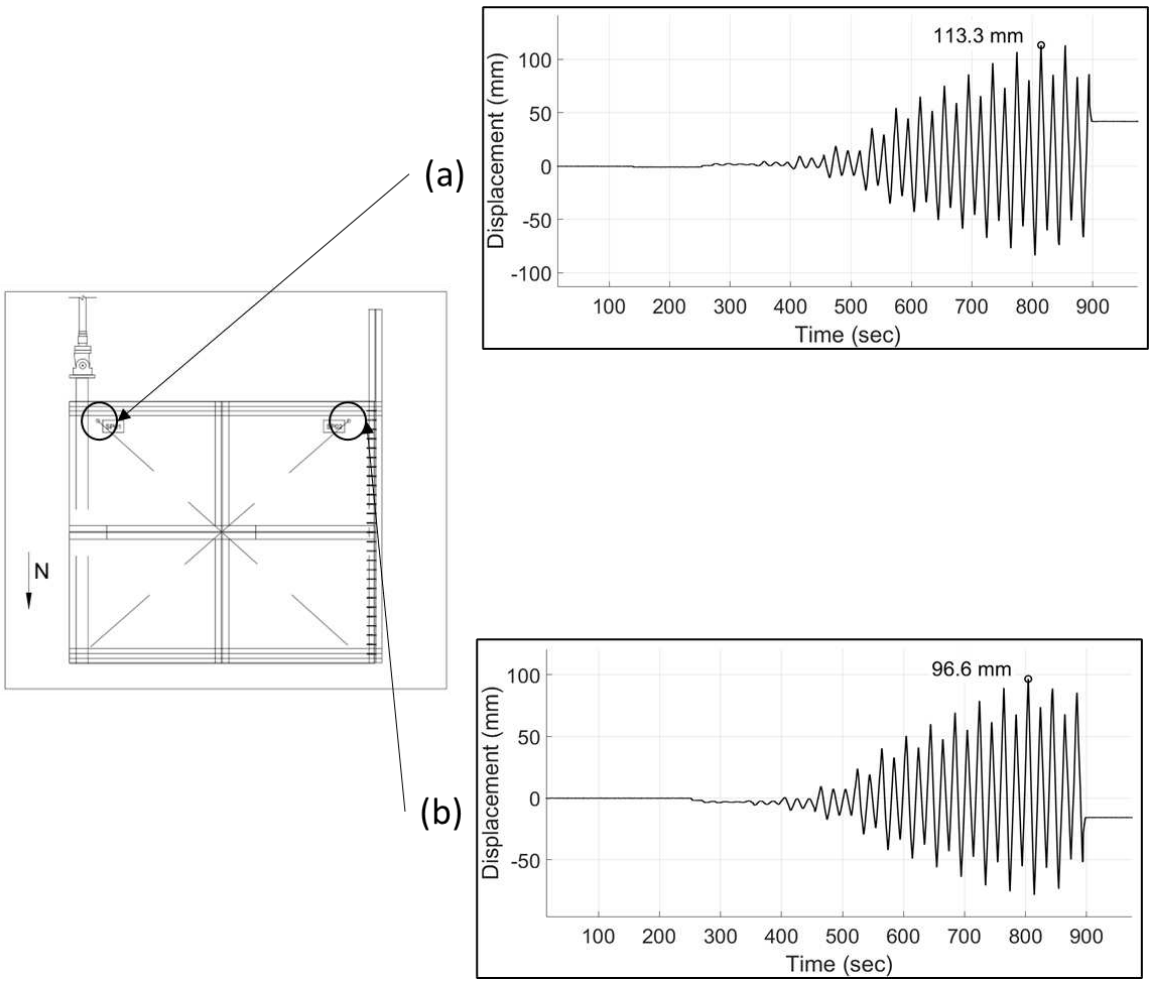

Figure 31: Diaphragm deformation for the light frame wood test: SP01 (SE to NW) (a), SP02 (SW to NE) (b)

Panel Deformation

In addition to the diaphragm deformation, individual panel deformation was of interest. To measure this deformation, SP10 (SE to NW) and SP11 (SW to NE) were placed on the northwestern panel during each test (excluding the light frame wood test). However, during Test A there was a recording error that resulted in the loss of SP11 data for Test A. In addition, during Test B localized OSB sheathing failure affected the measurement of SP11, inflating the measured displacement towards the end of the time series. The time series for Test A and Test B can be seen

in Figure 32 and the peak panel deformation can be seen in Table 14.

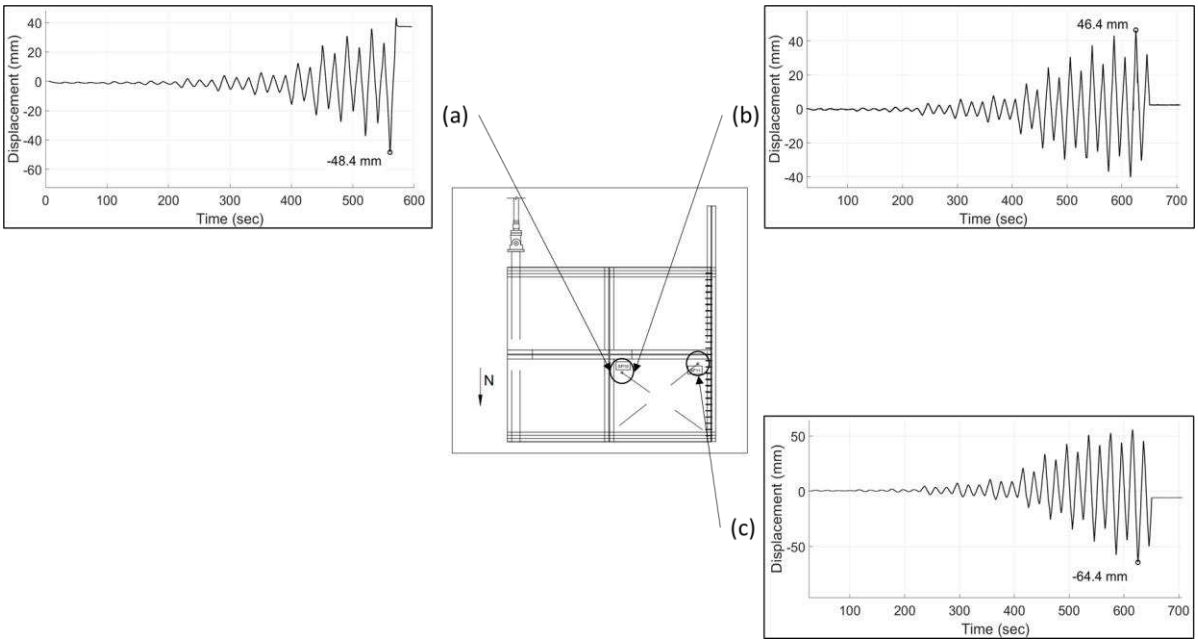

Figure 32: Panel deformation for Test A and Test B: Test A SP10 (SE to NW) (a), Test B SP10 (SE to NW) (b), Test B SP11 (SW to NE) (d).

Table 14: Peak observed panel deformation

Test	Peak Panel Deformation (mm)	Peak Panel Deformation (in)
Test A	48.4	1.91
Test B	46.4	1.83
Test C	58.1	2.29
Test C1	26.2	1.03

The maximum deformation measured in Test A was 48.4 mm (1.91") comparing that to Test B, which had a maximum of 46.4 mm (1.83") (recall SP11 was affected by OSB failure and inflated), a good agreement in the deformation of the DLT and NLT panel can be observed. Test C had a maximum measured panel deformation of 49.3 mm (1.94") and 58.1 mm (2.29") for

SP10 (SE to NW) and SP11 (SW to NE) respectively. Comparing this to Test C1 which had a maximum measured panel of 24.9 mm (0.98”) for SP10 (SE to NW) and 28.2 mm (1.11”) for SP11 (SW to NE), the observed localized out of plane panel deformation is clearly captured. There is a significant disparity between the recorded magnitude of displacements between Test C and Test C1, the difference representing the out of plane deformation. Comparing Test C to Test A and B, less panel deformation was observed in the panels with a tighter nail pattern, which aligns with expectations. The time series comparing Test C and C1 can be found in Figure 33.

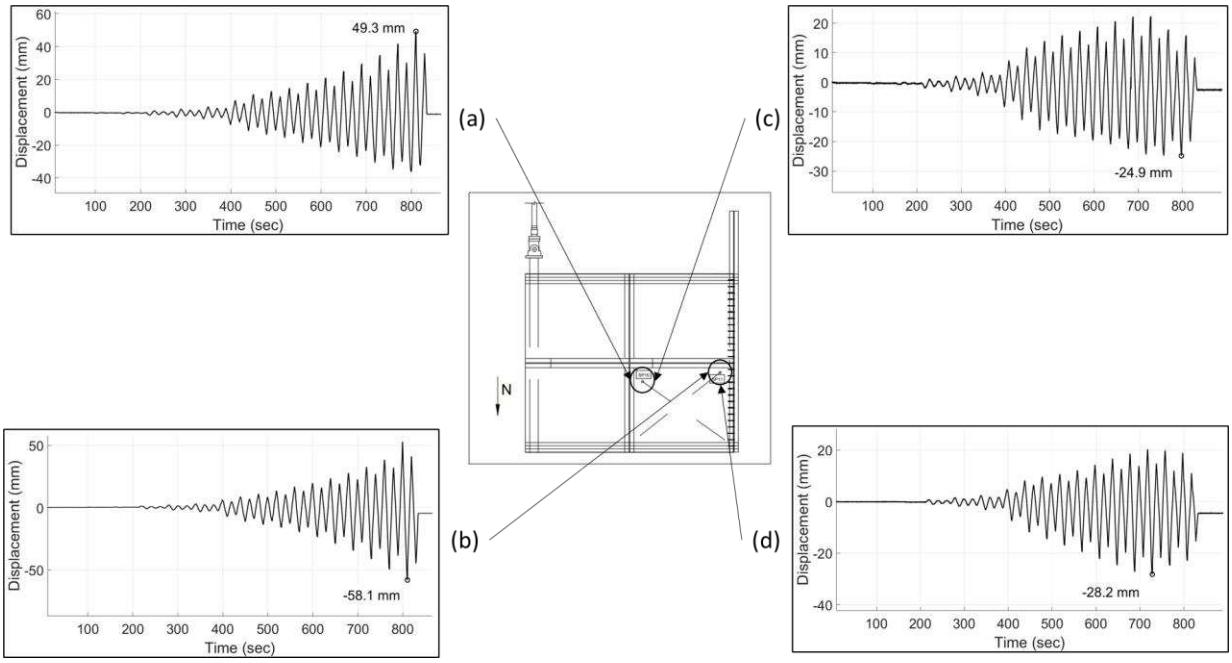

Figure 33: Panel deformation for Test C and Test C1: Test C SP10 (SE to NW) (a), Test C SP11 (SW to NE) (b), Test C1 SP10 (SE to NW) (c), Test C1 SP11 (SW to NE) (d).

Infill Joint and OSB Joint Displacement

The infill displacements for Tests A-C1 were split into two groups as seen in Table 10, parallel (to the actuator loading) infill joint displacement and perpendicular (to the actuator loading) infill joint displacement. Each of these two groups have a perpendicular (to the infill joint) and parallel (to

the infill joint) measurement. The parallel infill joint displacement in Test A saw nail withdrawal affect the results for SP04, the perpendicular (to the infill joint) potentiometer between the southwest and southeastern panel. So, with that in mind, the maximum value of 35.0 mm was measured by the parallel (to the infill joint) string potentiometer (SP03), This measurement captures the failure of the OSB sheathing and the isolation of the southwestern panel, as it was the largest parallel infill joint displacement across the testing as can be seen in Table 10 even though the testing was stopped before the protocol was completed. The maximum perpendicular (to the actuator loading) infill joint displacement was 12.4 mm (0.49”), measured by the parallel (to the infill joint) string potentiometer (SP09). In comparison, the perpendicular (to the infill joint) string potentiometer (SP08) measured a maximum 5.5 mm (0.03”). During Test B, the largest displacement measured at the parallel (to the actuator loading) infill joint was 62.6 mm (2.46”), measured by the parallel (to the infill joint) string potentiometer (SP09). In comparison, the perpendicular (to the infill joint) string potentiometer (SP08) measured a maximum displacement of 38.6 mm (1.52”). These measurements are significantly larger than what would be expected between Test A and Test B, even considering that Test A did not complete the protocol. However, this can be explained by the failure of the perpendicular (to the actuator loading) infill joint, which was observed during the testing. The peak infill deformation for Tests A and B can be found in Table 15.

Table 15: Peak observed infill deformation

Test	Peak parallel infill/joint displacement (mm)	Peak parallel infill/joint displacement (in.)	Peak perpendicular infill/joint displacement (mm)	Peak perpendicular infill/joint displacement (in)

Test A	130.2	5.13	12.4	0.49
Test B	24.4	0.96	62.6	2.46
Test C	8.9	0.35	21.9	0.86
Test C1	31.5	1.24	33.9	1.33
Light frame wood	25.8	1.02	27.8	1.09

During Test C, the maximum measured displacement of the parallel (to the actuator) infill joint was 8.9 mm (0.35”), measured by the parallel (to the infill joint) string potentiometer (SP03). The perpendicular (to the infill joint) string potentiometer (SP04) was affected by nail withdrawal, but even with this, the maximum measured value was less than 8mm. For the perpendicular (to the actuator) infill joint, the maximum measured displacement was 21.9mm (0.86”), measured by the parallel (to the infill joint) string potentiometer (SP09). In comparison, the perpendicular (to the infill joint) string potentiometer (SP08) measured a maximum value of 3.6 mm (0.14”). Comparing the parallel (to the actuator loading) joint to the perpendicular (to the actuator loading) joint, the primary failure of the infill sheathing occurred in the perpendicular (to the actuator loading) infill sheathing. This is confirmed by observations during the testing. For Test C1, the maximum parallel (to the actuator) displacement measurement was 31.5 mm (1.24”), measured by the string potentiometer (SP04) perpendicular to the infill joint. In comparison the parallel (to the infill joint) string potentiometer (SP03) measured a maximum value of 11.8 mm (0.46”). The perpendicular (to the actuator) infill joint maximum displacement value was 33.9 mm (1.33”), measured by the parallel (to the infill) string potentiometer (SP09); the perpendicular (to the infill) string potentiometer (SP08) measured a maximum displacement of 3.6 mm (0.14”). The large differential observed between the two perpendicular (to the actuator) infill joint measurements are explained by observations during testing. There was a crushing failure of the infill sheathing, occurring near the intersection of the two infill joints.

This allowed the infill sheathing to act as a hinge, accounting for the larger parallel (to the infill joint) measurement in comparison to the perpendicular (to the infill joint) measurement. All recorded peak displacement values from Test C and Test C1 can be found in Table 10

For the light frame wood test, there was no infill OSB sheathing, instead relying on a running bond (staggered) OSB sheathing approach. It also did not have any individual panels to measure, meaning the panel deformation string potentiometers (SP10 and SP11) could be repurposed to measure individual OSB joints. For ease of reference, the three measured OSB joints will be referred to Joint 1, Joint 2, and Joint 3; with Joint 1 being the southernmost joint measured by string potentiometers SP03 and SP3, Joint 2 being the center joint measured with string potentiometer SP08, and Joint 3, the northernmost joint, measured by string potentiometers SP10 and SP11. Figure 21 can be referenced for the location of Joint 1, 2, and 3, as well as the string potentiometer locations. The largest displacement measured at Joint 1 was 20.9 mm (0.822”), measured by string potentiometer SP03 which measured perpendicular to actuator loading. The string potentiometer measuring parallel to the actuator loading (SP04) recorded a maximum displacement of 13.4 mm (0.53”). Joint 2 only had a string potentiometer measuring perpendicular to the actuator loading (SP08), and its maximum recorded displacement was 12.2 mm (0.48”). Joint 3, similar to Joint 1, had a maximum displacement measured by the string pot measuring parallel to the actuator loading (SP11). The maximum displacement measured by SP11 was 27.8 mm (1.09”), in contrast the perpendicular to actuator loading string potentiometer (SP10) recorded a maximum displacement of 25.8 mm (1.02”). Comparing Joint 3 and Joint 1, it is clear that Joint 3 experienced larger displacements in both the parallel and vertical directions, however the parallel component was larger at both joints. Conversely, Joint 2

experienced less displacement than either of the perpendicular components of Joint 1 or Joint 3. The peak displacement values for the light frame wood test can be found in Table 10

Damage States and Fragility Curves

As mentioned in the introduction of the NLT/DLT testing, the primary objective of the testing was to explore and evaluate the lateral performance of various NLT/DLT diaphragms with different sheathing connection configurations. However, the testing also provided the opportunity to observe how the diaphragms were damaged throughout testing and to develop damage states for the NLT/DLT diaphragms. This was accomplished by pausing the test in intervals and taking pictures in pre-defined locations, allowing for both the identification of the damage states as well as when they occurred. These damage states can then be used to create basic fragility curves for use in the TTF methodology. It would be possible to develop damage states for the light frame wood diaphragm as well, however the primary focus of this study was NLT/DLT diaphragms.

Four basic damage states were identified during the testing of the NLT/DLT diaphragms: Damage State 1 (DS 1), Damage State 2 (DS2), Damage State 3 (DS3), and Damage State 4 (DS4). DS1 was defined as: “nails begin to withdraw in OSB and straps”, DS2 as: “excessive nail withdrawal in OSB and straps, and some OSB crushing”, DS3 as: “Complete nail withdrawal in OSB and crushing failure of OSB”, and DS4 as: “Strap buckling”. An example of each of these damage states can be seen in Figure 34.

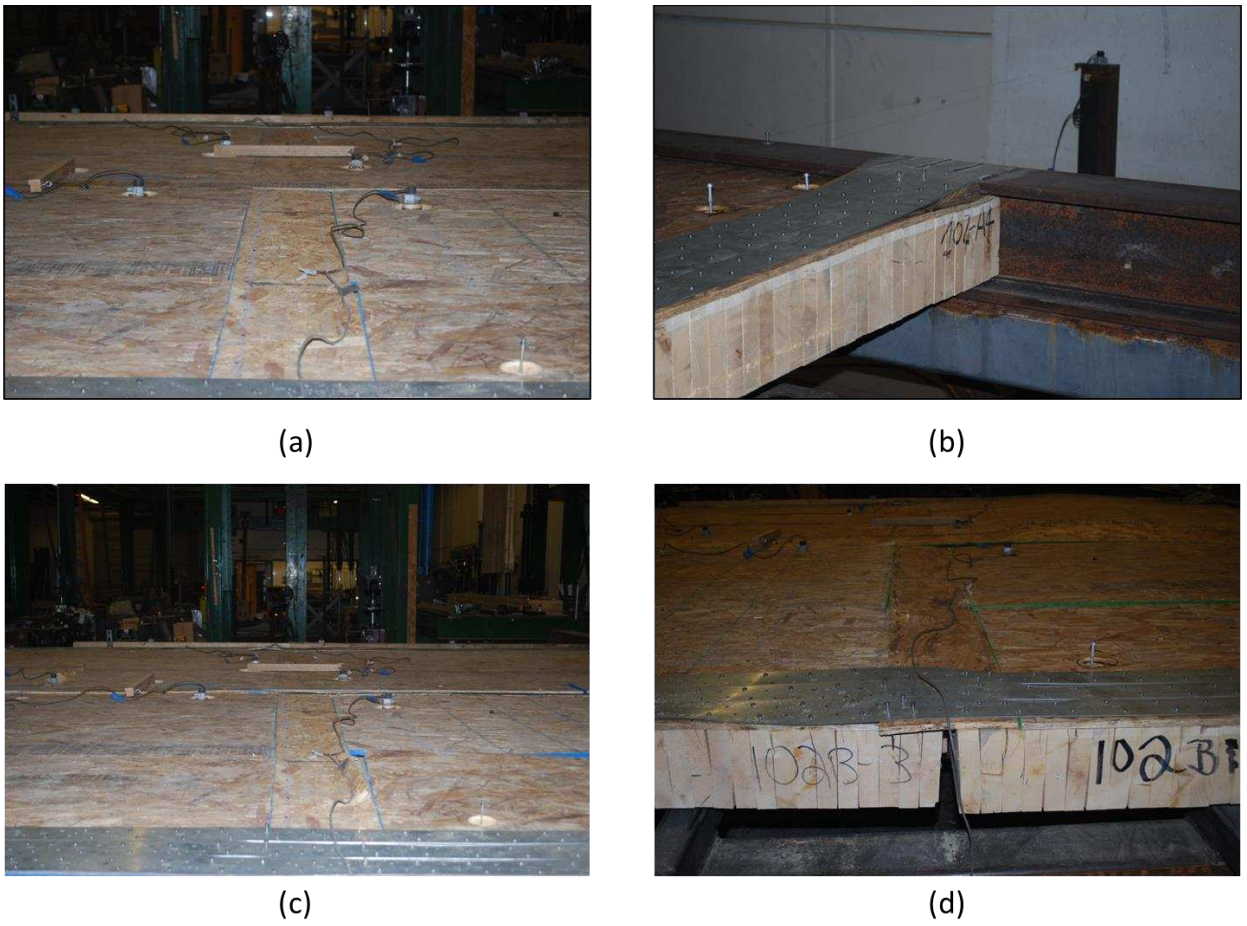

Figure 34: Damage state example photos: (a) DS1, (b) DS2, (c) DS3, (d) DS4

With the damage states identified, the next step was to select an engineering demand parameter to correspond to each of the damage states. Most existing damage states usually involve either inter-story drift or floor acceleration. However, neither of these measures are an adequate representation of the mechanisms behind the failure states observed in a diaphragm. Instead, diaphragm drift (%) was chosen as the best engineering demand parameter. Diaphragm drift is similar to inter-story drift in that it is a ratio of displacement to a length/height, however instead of the height of the story, the length of the diaphragm (perpendicular to the loading) was used, taking the form of:

$$DD = \frac{\Delta}{L} \qquad (6)$$

where Δ is the displacement of the diaphragm, L is the length of the diaphragm perpendicular to the loading, and DD is the diaphragm displacement (%). This can also be thought of as differential drift if the diaphragm was not a cantilever test configuration. As previously mentioned, the test was paused at various intervals during the testing to take photos. For the 152.4 mm (6") reference displacement, the test was paused at: 20.32 mm (0.8"), 40.64 mm (1.6"), 71.12 mm (2.8"), 101.6 mm (4"), 116.84 mm (4.6"), 132.08 mm (5.2"), 147.32 mm (5.8"), 162.56 mm (6.4"), 177.8 mm (7"), 193.04 mm (7.6"), 208.28 mm (8.2"), 223.52 mm (8.8"), and 233.68 mm (9.2"). Similarly, for the 101.6 mm (4") reference displacement, the test was paused at: 30.48 mm (1.2"), 60.96 mm (2.4"), 106.88 mm (4.2"), 152.4 mm (6"), 175.26 mm (6.9"), 198.12 mm (7.8"), 220.98 mm (8.7"), and 243.84 mm (9.6"). While the observation wasn't continuous, and the 101.6 mm (4") is less granular than the 152.4 mm (6"), there is still sufficient granularity for the purpose of finding damage states. With the framework in place, it was possible to identify the displacement for each test where each damage state occurred and convert it into diaphragm drift. Table 16 shows the results of these efforts.

Table 16: Observed Damage States for Tests A-C1

Test	DS1 (% Diaphragm Drift)	DS2 (% Diaphragm Drift)	DS3 (% Diaphragm Drift)	DS4 (% Diaphragm Drift)
Test A	1.22	2.13	3.51	3.97
Test B	1.22	2.13	3.51	3.97
Test C	1.42	2.95	3.87	4.18
Test C1	1.42	2.95	3.87	4.18

DS1 = Nails begin to withdraw in OSB and straps

DS2= Excessive nail withdrawal in OSB and straps, and some OSB crushing

DS3= Complete nail withdrawal in OSB and crushing failure of OSB

DS4= Strap Buckling

The first obvious observation is that Test A and B had each damage state occur at the same time, and Test C and C1 did as well. It is not a surprise that C and C1 performed similarly, even with the localized panel deformation, since they have the same design. What is interesting however, is that the NLT and DLT diaphragm had damage states occur at the same time. Upon closer inspection this makes sense. While the NLT diaphragm in Test B had a larger capacity than the DLT diaphragm in the testing, the sheathing, nails, nail pattern, and strapping were identical, and since all of the damage states were based on those components, as well as displacement based, it makes sense that they would perform similarly. Due to this, it was decided that it would be possible to represent the damage states in terms of the sheathing, straps, and nail pattern, rather than the diaphragm material.

With a need to incorporate the NLT/DLT diaphragms into the TTF model, two fragility curves were developed based on the sheathing, straps, and nail pattern using the same assumptions as the CLT rocking presented earlier. Specifically, the diaphragm drift limit was assumed to represent the mean value in a lognormal fragility curve, and a dispersion value of $\beta = 0.3$ was selected to represent the expected variation in the diaphragm drift limit states. While this is not the best possible estimate, it will suffice until further modeling and testing is done to perform a normal statistical analysis and curve fit. The two resulting fragility curves can be seen in Figure 35.

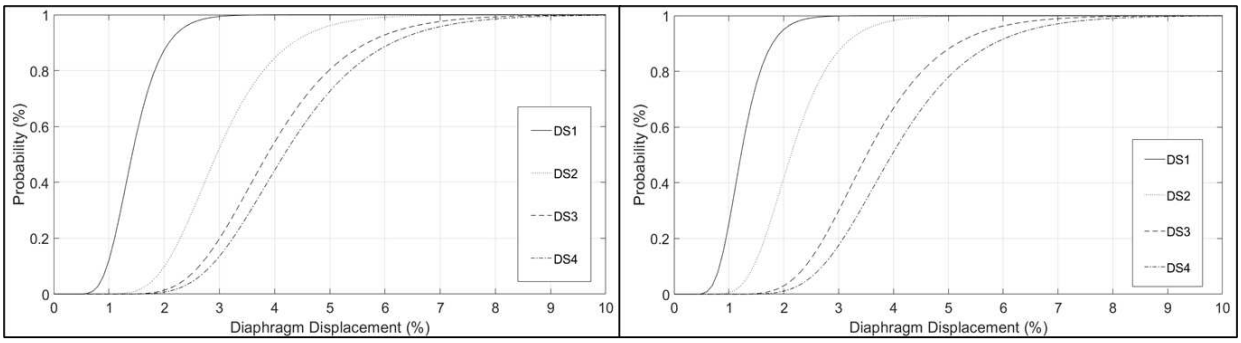

Figure 35: Fragility Curves: (a) 63.5 mm (2.5") O/C nail pattern, (b) 152.4 mm (6") O/C nail pattern

Closing

Presented in this chapter were the results of NLT/DLT diaphragm testing and the development of initial fragility curves for the diaphragm systems. The primary observations of the testing were that the NLT diaphragm had approximately 10% more lateral capacity than a DLT diaphragm of the same design. Whether this is worth the extra manufacturing effort, or the additional carbon cost is left up to the designer. As expected, the DLT diaphragm with a tighter nail pattern did indeed produce a stiffer, higher capacity diaphragm (approximately 40% more capacity) than the original DLT diaphragm tested. In addition, a light-frame wood diaphragm was tested as a comparison. It was found that light-frame wood construction has difficulty achieving similar lateral capacities to even the lowest capacity NLT/DLT diaphragm. Besides the capacity testing, damage states were developed related to the panels, and since the lateral failure modes correspond primarily to the sheathing, nails, nail pattern, and strapping, fragility curves based on these components were developed. The testing here also informed the larger 10 story testing that is ongoing as of the writing of this dissertation. Initial plans to have the DLT/NLT diaphragms on the top two floors were changed to the 7th and 8th floors based on the capacity testing presented

here and concerns over the ability of the diaphragms to handle the large forces present on the 9th and 10th floors. The development of the initial fragility curve estimates also demonstrate a need for numerical modeling and additional experimental testing of these diaphragms in order to develop a better estimate for their respective fragility curves. While the NLT/DLT diaphragms are not directly incorporated in the database and design guidance discussed in Chapters 6 & 7, there are future plans to incorporate them into designs to incorporate into the design guidance in Chapter 7 and the database in Chapter 6.

CHAPTER 6 – APPLICATION AND EVALUATION OF TTF TO ARCHETYPES FOR DESIGN GUIDANCE

Introduction

Chapter 3 demonstrated the application of the TTF methodology to predict the functional recovery of a single two-story design that was tested in the summer of 2017. While valuable, the time and computational resources to develop TTF is beyond what the average design engineer would likely be willing to (or could) invest until it is operationalized or codified. Codification of a new design approach takes years to complete, but the potential application to this problem in the shorter term is the development of a database containing TTF evaluations for a variety of archetypes and designs from which a design engineer could input parameters and receive TTF estimates without an intensive computational commitment. The design will still meet current code requirements and provide guidance to engineers and building owners. With this in mind, a database of various designs for three archetypes of mixed-use buildings utilizing the CLT rocking wall lateral system presented in Chapter 3 were developed to provide a guidance portfolio for engineers considering using functional recovery requirements for their PT CLT buildings. Two, six, and ten stories were primarily selected to coincide with full scale experimental testing that has or will take place by the end of the 2023. The two-story testing is already well documented in Pei (2019) [52], and the ongoing ten-story testing has been mentioned several times previously. However, as additional project, the top four floors of the structure will be removed, and additional testing with a six-story structure will be conducted. These three tests will provide anchor points and essentially partial experimental validation of a design for each archetype in the database, as well as represent a wide range of potential applications for the CLT rocking wall system. In this Chapter several of the

designs for each archetype are compared and general performance trends are established based on the methodology presented in this dissertation. The full database including the performance for each design can be found in the Appendix.

Design Selection

A variety of designs were considered for each archetype (two-story, six-story, and ten-story), however the changes were primarily focused on the lateral system. As a refresher, the CLT rocking wall consists of three primary components, the CLT panels, the post-tensioning rods, and the UFP devices. Within these components, four different variables were investigated: CLT panel width, CLT panel thickness, number of UFPs per wall, and diameter of post-tensioning rods. For each of these variables, three variations were selected to represent the range of possible values for each variable as can be seen in Table 17.

Table 17: Design Variations in CLT Rocking Wall Design

Component	Component Variation 1	Component Variation 2	Component Variation 3
CLT Panel Width	127 mm (5')	254 mm (10')	508 mm (20')
CLT Panel Thickness	5 ply	7 ply	9 ply
Number of UFPs per Wall	2	3	4
Diameter of Post-Tensioning	15.8 mm (0.625")	31.75 mm (1.25")	50.8 mm (2")

There are several important things to note about the different component variations. A design combining every component variation from each component was considered; for example, a design was considered with component variation 1 for CLT panel width (127mm [5']), component variation 2 for CLT panel thickness (7 ply), component variation 3 for the number of UFPs per wall (4), and component variation 1 for the diameter of post-tensioning rods (15.8 mm [0.625"]).

This equates to a total of 3^4 designs for each building height (two-story, six-story, and ten-story), with a total of 243 (3^5) designs considered, which can be found in Tables 23-25 in the Appendix. The lower bound of the design space was selected using the design of the two-story CLT rocking wall building presented in Chapter 3. This is because the two-story was designed using a performance-based design method to meet drift requirements so a smaller component combination would not meet the same drift requirements for any greater building height and are not necessary to include. Thus, the components sizes in variation 1 represent the design for the two-story building analyzed in Chapter 3. The upper bound of the components were selected on an individual basis, with the objective to represent the largest realistic size for each of the components. While the maximum width of a panel is not limited to 6.1 m (20'), this was selected as the upper bound to represent what would be reasonably considered for two-story and six-story designs. The CLT panel thickness is also limited by the size of the press, and 9 ply is as thick as the vast majority of CLT panel manufacturers produce as of 2022. The maximum number of UFPs were selected based on a standard story height, assumed configuration (same as the two-story design), and the development area that they require for maximum effectiveness, with 4 UFPs per wall being the maximum. The upper bound of the post-tensioning rod was selected using the Simpson Strong Tie catalog of threaded rods (which were used in the two-story testing), with the largest offered selection having a gross diameter of 50.8 mm (2"). In addition to the selection of the bounds for design variables, another important note is that CLT panel width as seen in Table 17 refers to the width of a single CLT panel, while the rocking wall itself is composed of two CLT panels. So, for example, a CLT panel width of 127mm (5') would have a total rocking wall width of approximately 254 mm (10'). The purpose of component variation 2 is to represent the median of the upper and lower bounds for each component, and the incorporation of all three variation will

capture the entire breadth of possible design combination for all three building heights.

Time-to-Functionality Method Application

Fragility Curve Selection

Similar to what was presented in Chapter 3, the Time to Functionality Methodology was applied to each of the 243 considered designs using the component variations presented in Table 17. Each of the designs were assumed to be mixed-use buildings, and since the non-structural components selected for the two-story were done by considering their applicability to a ten-story structure, the same set of non-structural components was selected. However, the quantities were estimated accounting for the additional floors for the six and ten-story respectively as shown in Table 5. The structural system has the same basic components throughout all of the different design considerations, and while the different sizes of components may affect the fragility curve slightly, there is no data to construct other fragility curves accounting for this difference, so the original fragility curve developed in Chapter 3 was used. Additionally, the time consequence functions would change drastically between the different building heights, and like the two-story, there is a severe lack of data to develop time consequence functions. Because of this, the time consequence functions for a reinforced concrete rocking wall that are present in the PACT database was used as a surrogate time consequence function for the CLT rocking walls.

Building Performance Model and Ground Motion Selection

The building performance model varies for each of the 238 different designs, but they share a similar modeling philosophy and approach. The basis of the models is the same as the model used in Chapter 3, developed by Wichman et. al (2022) [76], as seen in Figure 4. The model was

expanded to incorporate the different variations in component size and locations and was further extrapolated to six and ten-story models for their respective designs. This model was chosen over others due to the fact it is one of very few CLT rocking wall models that has been validated experimentally and since it is a 2D model, it was significantly easier to construct all the required variations. Additionally, the run time and resource use for the model was significantly less than a comparable 3D model, which was considered valuable for the number of nonlinear time histories being incorporated in the guideline for development. FEMA P695 (FEMA [2009] [24]) far-field ground motions and an incremental dynamic analysis (IDA) (Vamvatsikos, et al., 2002) [73] were selected again for similar reasons as presented in Chapter 3 (general applicability, availability, and widespread usage).

Repair Sequencing

The repair sequencing for each of the different design considerations used the same basic rules and assumptions discussed in Chapters 2 & 3, and the Repair Class assumptions in Table 6 were again assumed for each of the designs. Additionally, the same Impending Factors presented in Table 2 were used for each design, and the number of workers per sequence, per floor, and on-site were calculated with the same rules presented in Chapter 2.

Time-to-Functionality Curves

Time-to-functionality as a measure is the time required for a structure to reach a particular recovery level at a defined spectral acceleration with a given probability of exceedance. Thus, by that definition, time-to-functionality is a three-dimensional measure. To present this measure in two dimensions, it is necessary to remove one of the dimensions. In Chapters 2 & 3, the time-to-

functionality dimension was reduced, thus producing curves for individual time-to-functionalities in the spectral acceleration versus probability of exceedance space. It is not necessary to always reduce the time-to-functionality in this way and as an example of this, the re-occupancy time-to-functionality surface for variation 1 is presented in Figure 36.

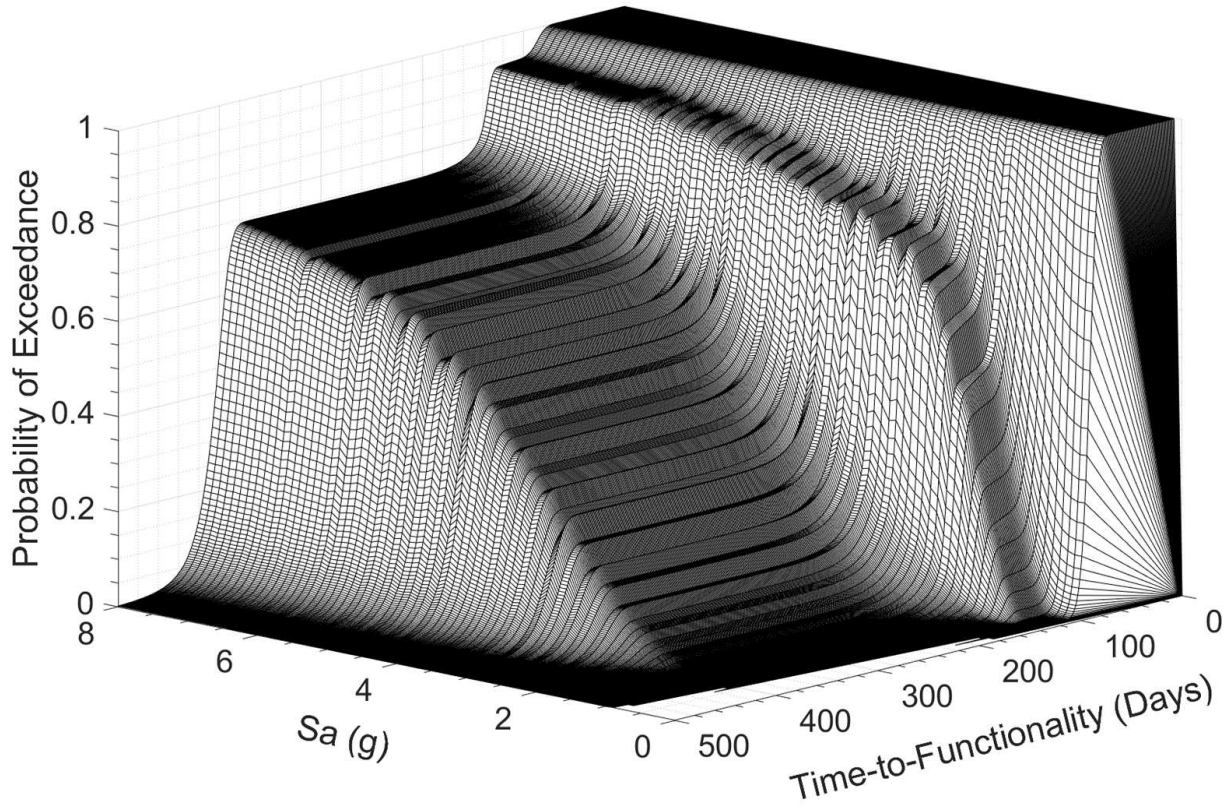

Figure 36: Time-to-Functionality surface for variation 1

In the construction of the database, it was decided to include the surfaces for each recovery level for every design. In the two-dimensional space, instead of reducing the time-to-functionality dimension, the spectral acceleration dimension was reduced. Figure 37 shows the time-to-functionality versus probability of exceedance space for variation 1 at a spectral acceleration of 1 g.

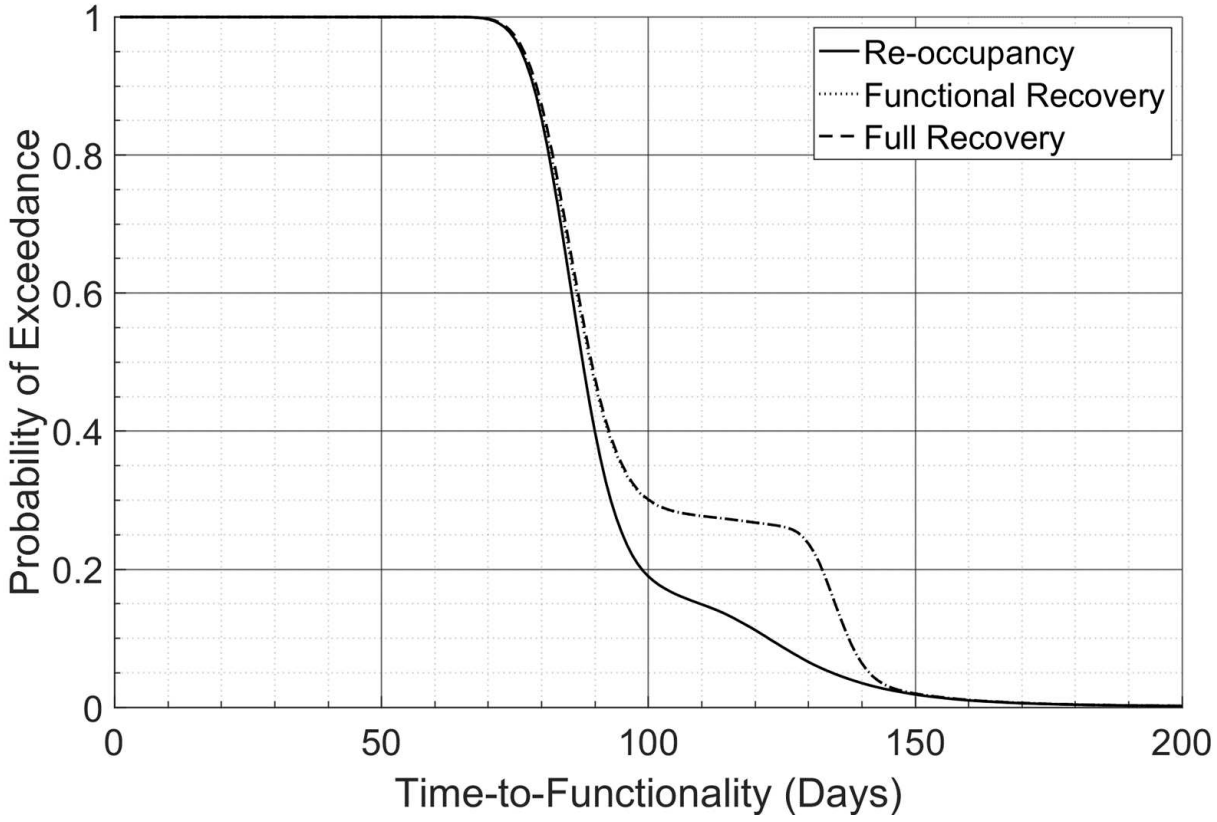

Figure 37: Time-to-Functionality versus probability of exceedance at 1 g Sa for variation 1

Reducing time-to-functionality in this way was done for two reasons: First, a hazard level of particular interest can be isolated effectively from surrounding hazard levels, allowing a designer to only access pertinent information. Secondly, comparisons between individual designs at a given hazard level are much easier to read and differences become much more obvious. The benefits of this reduction strategy will be demonstrated both later in this chapter and in Chapter 7. It should also be mentioned that in this reduction, the lognormal distribution that was assumed in earlier chapters no longer holds; the data was instead plotted directly, bypassing any distribution assumptions.

Evaluation of the TTF Results

Incremental Dynamic Analysis

As laid out in Chapter 2, incremental dynamic analysis is used to obtain the demand parameters for the building by scaling selected ground motions to various hazard levels. Similarly to the two-story example in Chapter 3, the FEMA P695 (FEMA 2009 [24]) far field ground motions were used for the IDA, with a step of 0.1 g Sa, for each of the 238 designs in the database. The floor acceleration was obtained by calculating the maximum acceleration averaged across the diaphragm and walls on each floor. Similarly, the inter-story drift was calculated using the maximum displacement averaged across the two rocking walls. Figure 38 shows an IDA analysis done on a two-story design, with the mean IDA curve in bold.

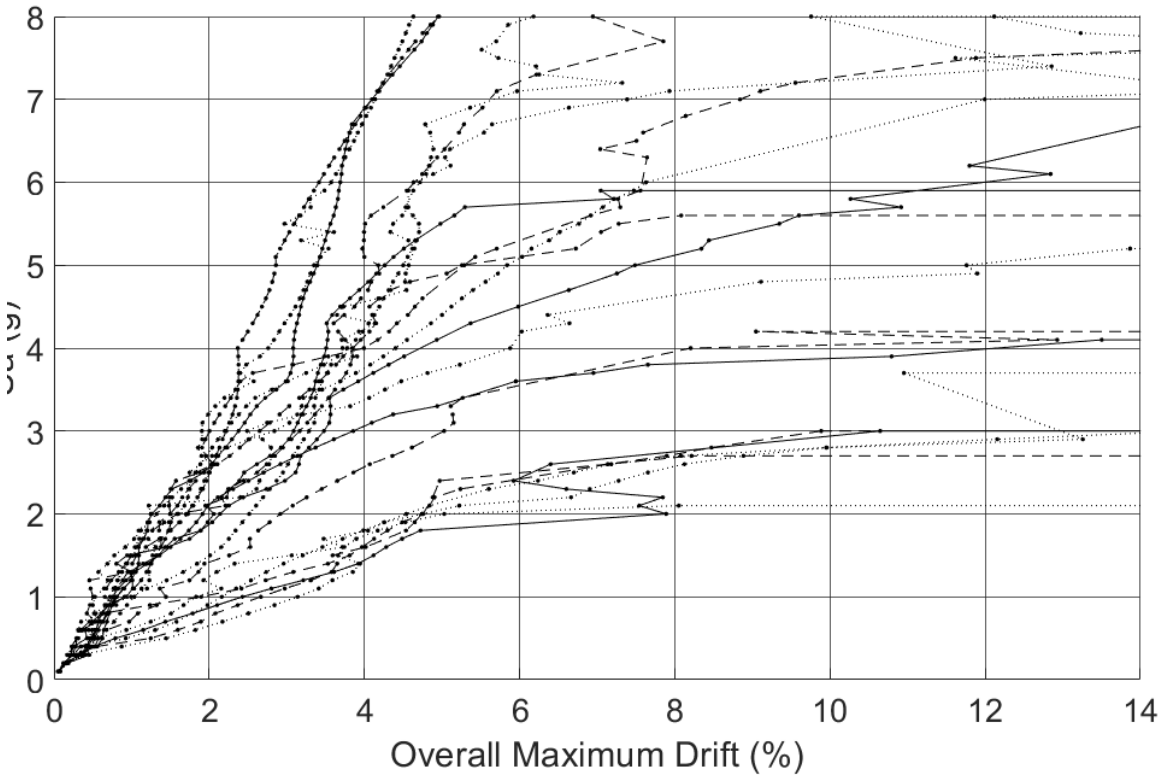

Figure 38: IDA Curve for a two-story design with 127 mm (5') wide and 5 ply thickness panels, 2 UFPs per story, and 15.8 mm (0.625") diameter post-tension rods

This design was selected to illustrate that the IDA curves were developed for each design using an algorithm, so some model runs that would normally be discarded may make their way into the IDA curves. To combat this, 300,000 samples were taken at each considered Sa value during the time-to-functionality methodology, minimizing the effect of a sporadic model run. To provide more context beyond just two-story designs, Figure 39 and Figure 40 show IDA curves for a six-story and ten-story design respectively.

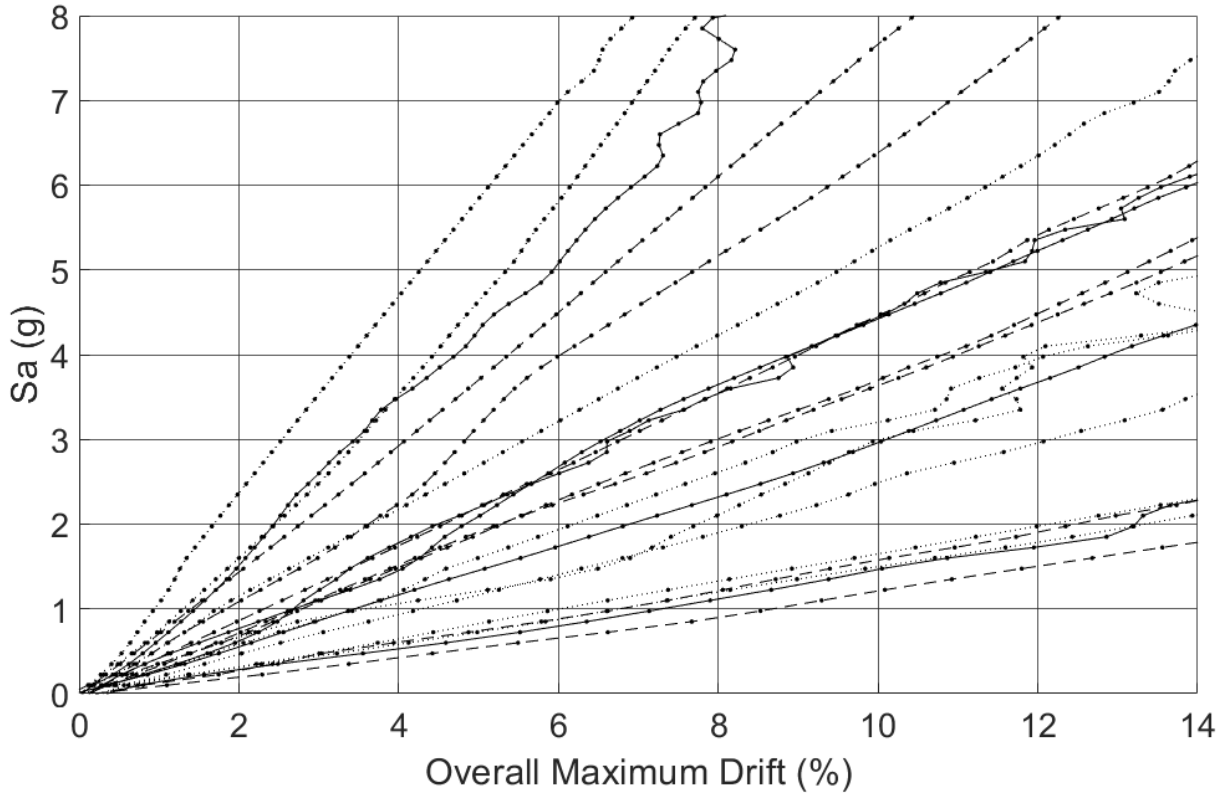

Figure 39: IDA Curve for a six-story design with 127 mm (5') wide and 7 ply thickness panels, 4 UFPs per wall, and 31.75 mm (1.25") diameter post-tension rods

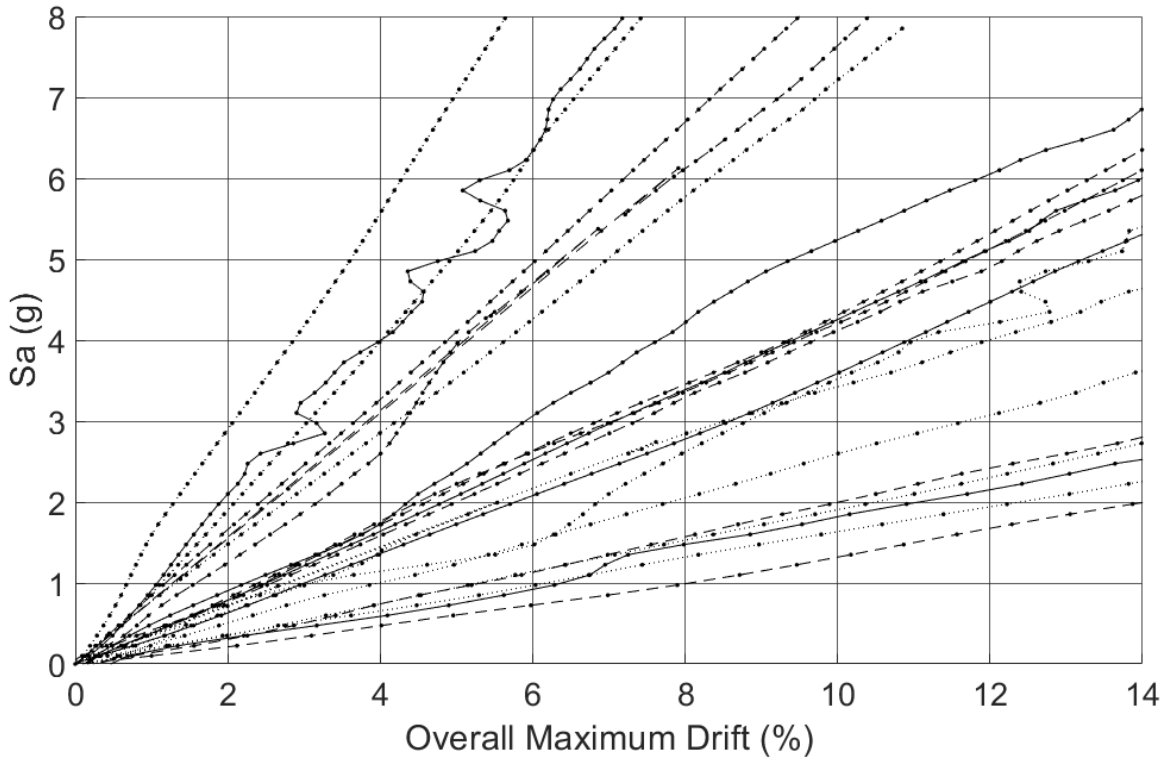

Figure 40: IDA Curve for a ten-story design with 127 mm (5') wide and 9 ply thickness panels, 3 UFPs per wall, and 31.75 mm (1.25") diameter post-tension rods

The scaling used for the IDA curves was capped at 8 Sa, with the corresponding drift uncapped, but limited to 14% on Figures 38-40. It should be noted that mass timber rocking walls that have been tested have shown substantial non-linearity, non-elastic, behavior and the IDA curves constructed during this process have some non-elasticity, but there also seems to be some cases of elasticity. There has been other research done on modeling mass timber rocking walls, such as Sarti, F. et. al (2017) [64]. In this study, models for various configurations of mass timber rocking walls (including a configuration similar to the ones used in this research) were constructed for a 3-story, 6-story, and 10-story archetypes in accordance with FEMA P695. Comparing the IDA curves from that study to the ones presented here, there are both some similarities and some differences. Similarly to the IDA curves here, there are some motions that seem to illicit essentially an elastic response from the structure, while other motions caused a

highly inelastic response. Sarti, F. et al. (2017) [64] did have a larger proportion of inelastic responses than the models in this research; this could mean that the elastic or inelastic response could be a function of the motions that are selected, or it could be that some inelasticity is not fully being accounted for in the models presented here. In either case, further investigation and tuning of the six- and ten-story archetype models is needed, and that opportunity will be provided by the test data of the six- and ten-story full scale tests. It should be noted that these models share the same limitations as the original two-story model in that they cannot accurately model or predict collapse; however, resilience and time-to-functionality recovery targets would occur long before collapse and it was deemed acceptable that collapse could not be accurately predicted with these models. This does mean an analysis incorporating collapse will need to be done sometime in the design of the building; how and when to incorporate this analysis is discussed in Chapter 7.

Time-to-Functionality Curves

The time-to-functionality curves for each of the designs used the plotting strategy discussed in the time-to-functionality method application section earlier in this chapter. Specifically, the time-to-functionality surfaces were plotted and then the Sa dimension was fixed, giving time-to-functionality versus probability of exceedance plots. With a step of 0.1 g Sa from 0.1 g to 8 g would produce approximately 80 individual plots for each recovery level as well as three surfaces (one for each recovery level). To reduce the number of plots, all three recovery levels were plotted on each time-to-functionality versus probability of exceedance plot. However, this still leaves 83 plots for each design, and presenting all of them even in the Appendix would not be feasible. So instead, for brevity, in this chapter the effect of each structural component will be analyzed for

each archetype (two, six, and ten-stories), and the Appendix will contain the three surfaces for each design corresponding to each recovery level, as well as a time-to-functionality versus probability of exceedance plot for 1 g, 1.5 g, and 2 g for each design. These values were selected to encompass what is anticipated to be the greatest area of interest for resilience design, however during an actual design, the full database can be leveraged. The full database has been uploaded and can be access through DesignSafe.

Panel Width in Relation to TTF Performance

To identify and compare the effects of different components on the downtime of the archetype designs, a systematic approach for each component was used. In this approach, the same Sa (1 g) was used across the comparison and a component was selected as a variable (such as panel width) and varied over the designs while every other variable was held constant. The spectral acceleration was selected based on expected design spectral accelerations; the trends established at 1 g reflect the region around it, however significantly lower (such as 0.1 g) or significantly higher (above 2 g) may change the behavior of the components. This approach will allow the direct comparison of performance between the designs and identify trends the component variable had on the TTF performance. The base design from which the panel width was changed was a design with 127 mm (5') wide 5 ply thick panels, 15.8 mm (0.625") diameter post-tension rods, and 2 UFPs per wall. Figure 41 shows the effect of changing the panel width on the TTF performance of the two-story archetype, while Figure 42 and Figure 43 show the effect on the six and ten-story archetype respectively.

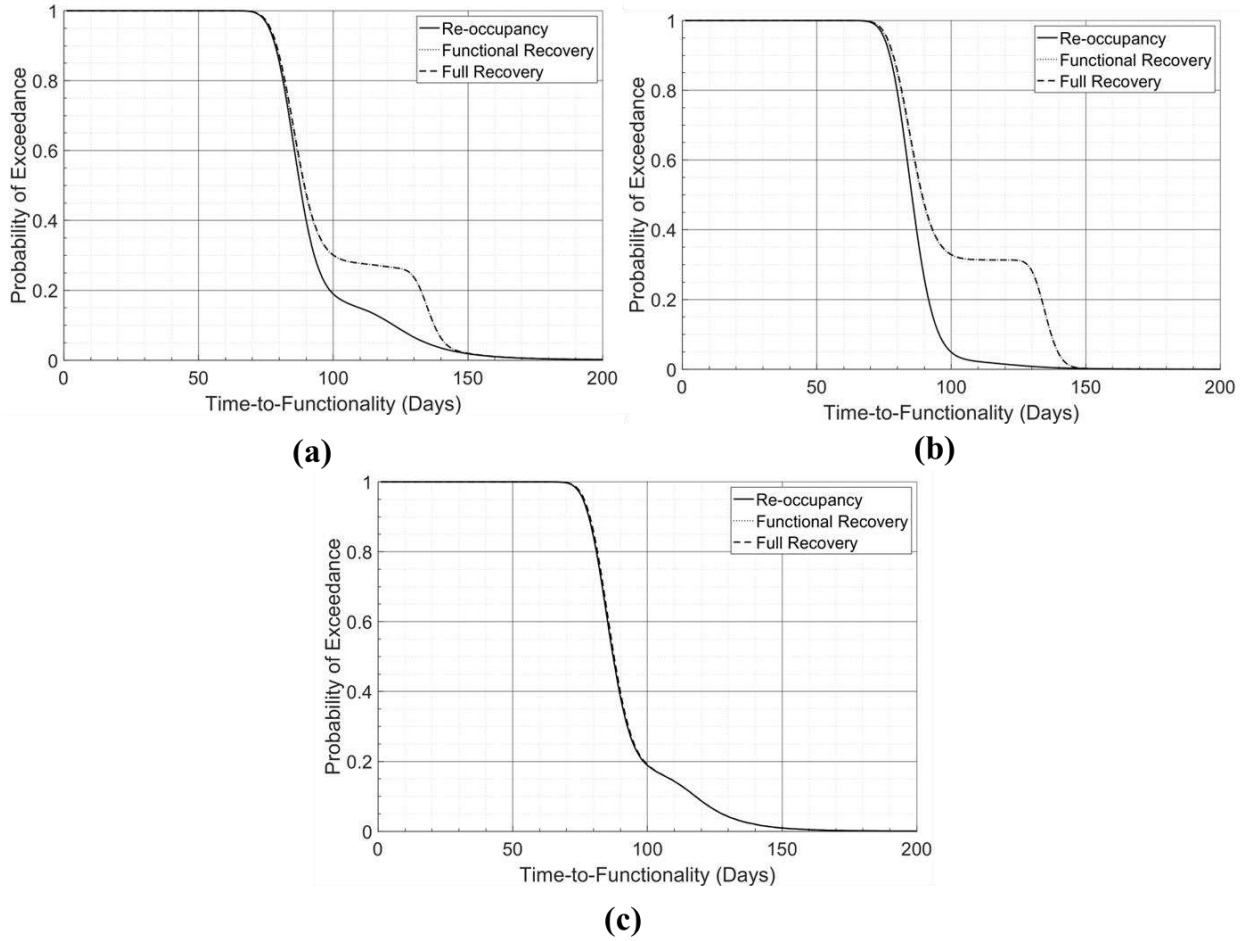

Figure 41: Two-story design with: (a) 127 mm (5') panels, (b) 254 mm (10') panels, (c) 508 mm (20') panels

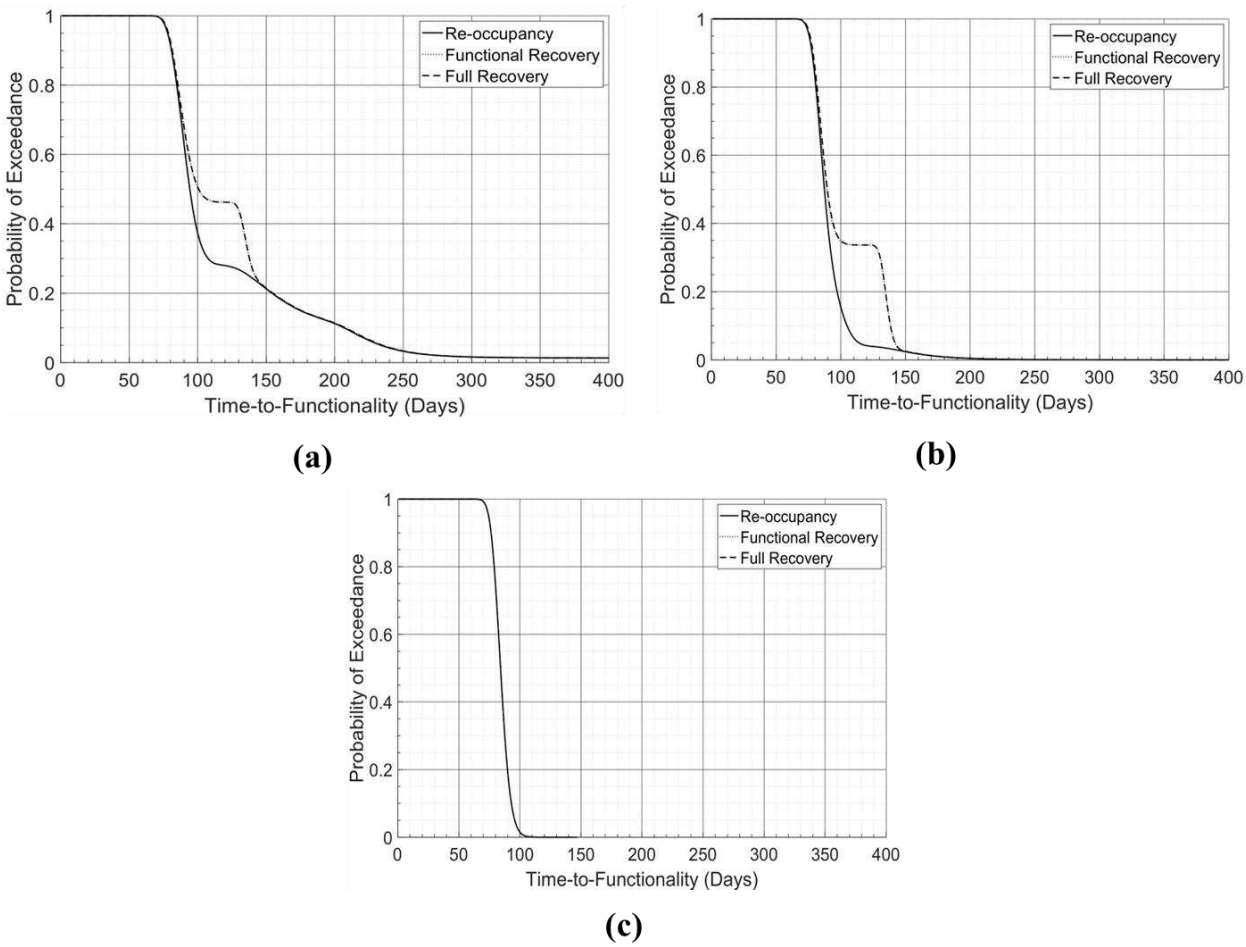

Figure 42: Six-story design with: (a) 127 mm (5') panels, (b) 254 mm (10') panels, (c) 508 mm (20') panels

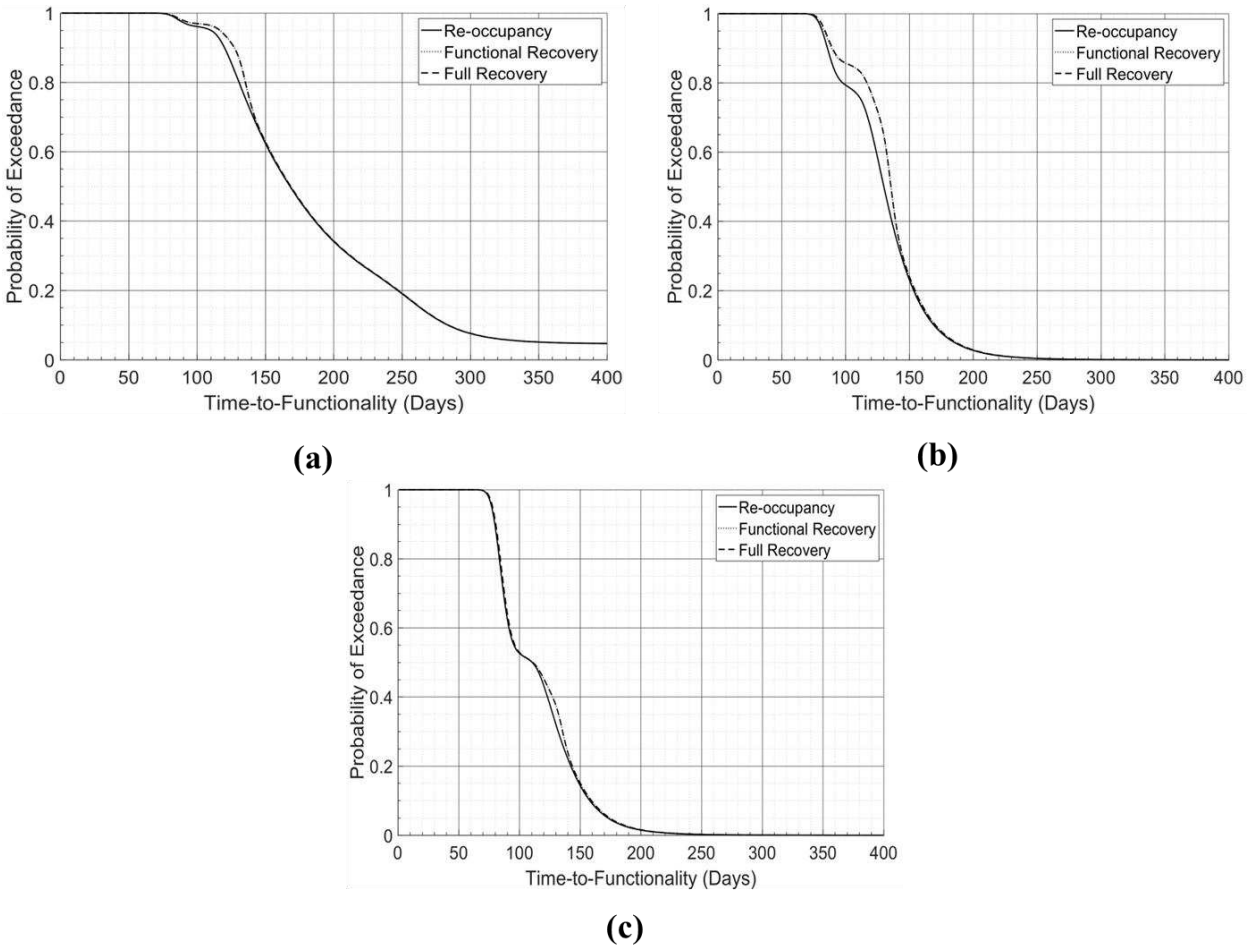

Figure 43: Ten-story design with: (a) 127 mm (5') panels, (b) 254 mm (10') panels, (c) 508 mm (20') panels

The observed behavior seems to be complex and reflects the complicated and nonlinear nature of TTF performance. The clearest observation is that Functional Recovery and Full Recovery are identical for the different archetypes. This was discussed in depth in Chapter 2, but it is essentially the result of component lead times for several components required for Functional Recovery, so the work on components for Full Recovery can be completed before the long lead time components arrive, resulting in Functional Recovery and Full Recovery occurring simultaneously. This is not always the case, but as can be seen, it is quite common for the components selected for the designs. For the two-story archetype it can also be observed in Figure 41 that widening the panels to 254

mm (10') reduced the Re-occupancy downtime but increased the Functional and Full Recovery downtimes. The most likely explanation is that the wider panels reduced the damage on the structural system while increasing the damage to the non-structural components from higher acceleration. Further increasing the width of the panel to 508 mm (20') results in an interesting scenario where all three recovery levels converged, with the Re-occupancy performance decreasing and the Functional and Full Recovery performance increasing in relation to the 254 mm (10') walls. The most likely explanation for this is that a single or perhaps a few components required for Re-occupancy are damaged, but the structural and the rest of the non-structural components are minimally damaged. The time-to-functionality downtime is sensitive to any changes in either floor accelerations or building drift, and this scenario is caused by decreasing the building drift and increasing the floor accelerations. Increasing the width of the CLT panels causes this by increasing the stiffness of the building, and this increased stiffness will decrease the period of the structure, and its ability to respond to the ground motion's excitation. This will ultimately decrease the building drift of the structure but will also increase the floor accelerations. The conclusions one can draw from Figure 41 are nuanced, it seems that for the two-story archetype increasing the wall width can both improve and decrease TTF performance. If Re-occupancy is desired, a 254 mm (10') panel provides the best option, however the other recovery states suffer. The 508 mm (20') panel has the best Functional and Full Recovery performance, but with the walls consisting of two panels, the rocking wall is 1016 mm (40') wide which would conflict with geometric constraints as well as cost in many two-story buildings. The six-story and ten-story archetypes behave in a similar manner as can be seen in Figure 42 and Figure 43, the downtime for all of the recovery states decreases as the width of the panel increases, with all of the recovery levels converging similarly to the two-story at a panel width of 508 mm (20'). It is

also interesting to note that similarly to the two-story archetype, the Functional and Full Recovery seem to diverge more from the Re-occupancy at 254 mm (10'); however, unlike the two-story archetype, the downtime for all the recovery states still decreased. It's clear that increasing the width of the panels has a substantial impact on all archetypes, however the six and ten-story archetypes seem more uniformly affected.

Number of Plys in Relation to TTF Performance

Unlike the width of the panel, in general the number of plys in the panel seemed to have minimal positive effects on the TTF performance across the various archetypes, in fact in some cases it was detrimental to the performance. For the two-story archetype, the most obvious observed trend was that increasing the number of plys in the panel seems to have a marginal effect on Re-occupancy, in fact the TTF performance decreases slightly from 7 plys to 9 plys. Functional and Full Recovery are once again equivalent, but the probability of exceedance increases from 5 to 7 ply, then once again gets marginally worse at 9 plys. It is clear that for the two-story archetype, increasing the number of plys in the panel negatively impacts the TTF performance slightly. Similarly to the width of the panel, increasing the thickness of the panels also increases the stiffness of the building. However, it is clear to see that any positive increase to TTF performance from the decrease in building drift is overcome by the decrease in TTF performance caused by the increased floor acceleration. The six-story archetype saw consistent, if marginal, improvement in Re-occupancy downtime by increasing the number of plys; however, like the two-story the Functional and Full Recovery downtime increased marginally from 5 to 7 plys. Unlike the two-story archetype, the six-story archetype saw improvement across all recovery levels from 7 to 9 plys. The ten-story archetype saw marginal improvement in TFF performance across all recovery levels by increasing

the number of plys. While the improvement was not as significant as the wall width, it was nevertheless consistent, and for much the same reason as the six-story archetype. Figures 44-46 show the results for the two-story, six-story, and ten-story archetypes respectively.

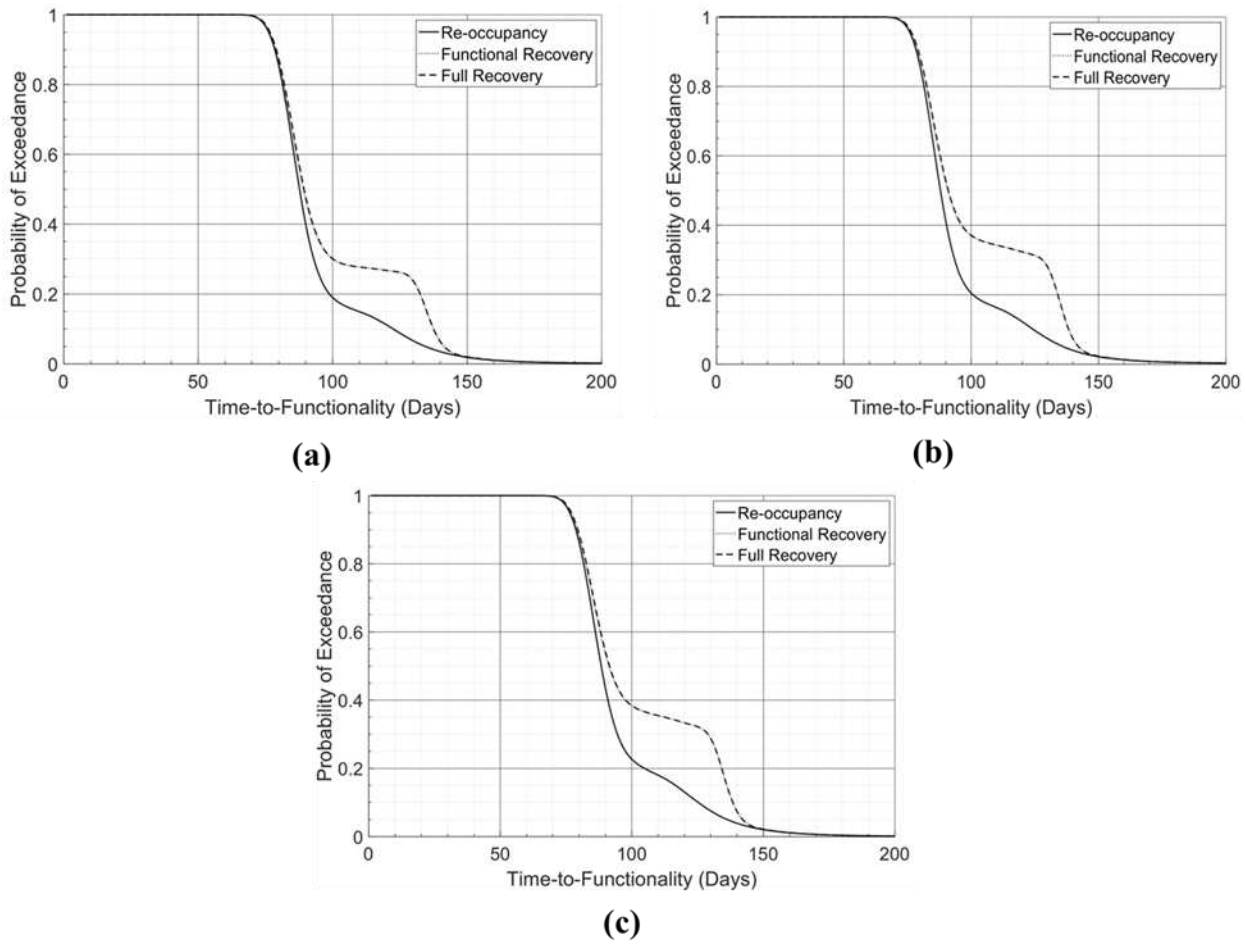

Figure 44: Two-story design with: (a) 5 ply panels, (b) 7 ply panels, (c) 9 ply panels

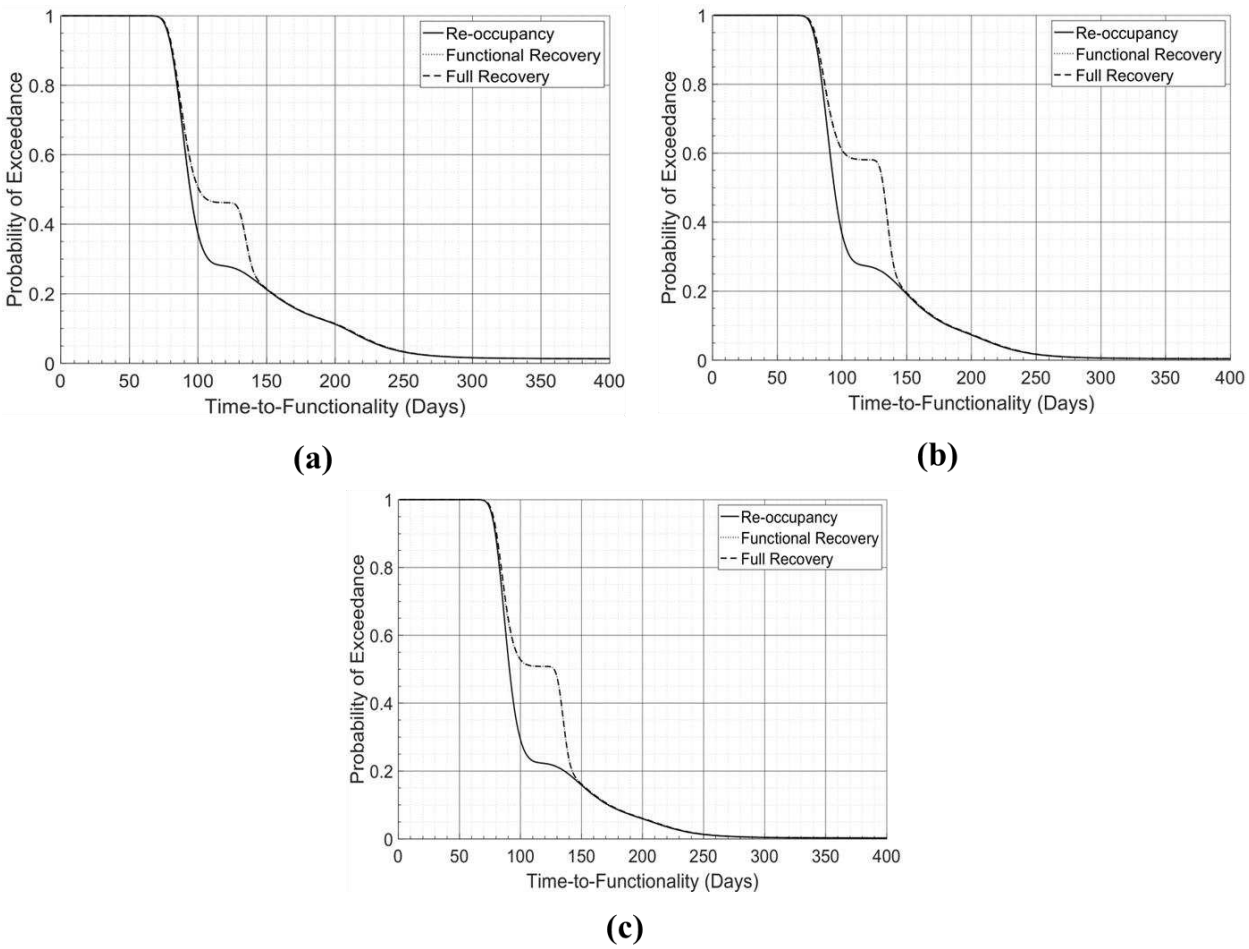

Figure 45: Six-story design with: (a) 5 ply panels, (b) 7 ply panels, (c) 9 ply panels

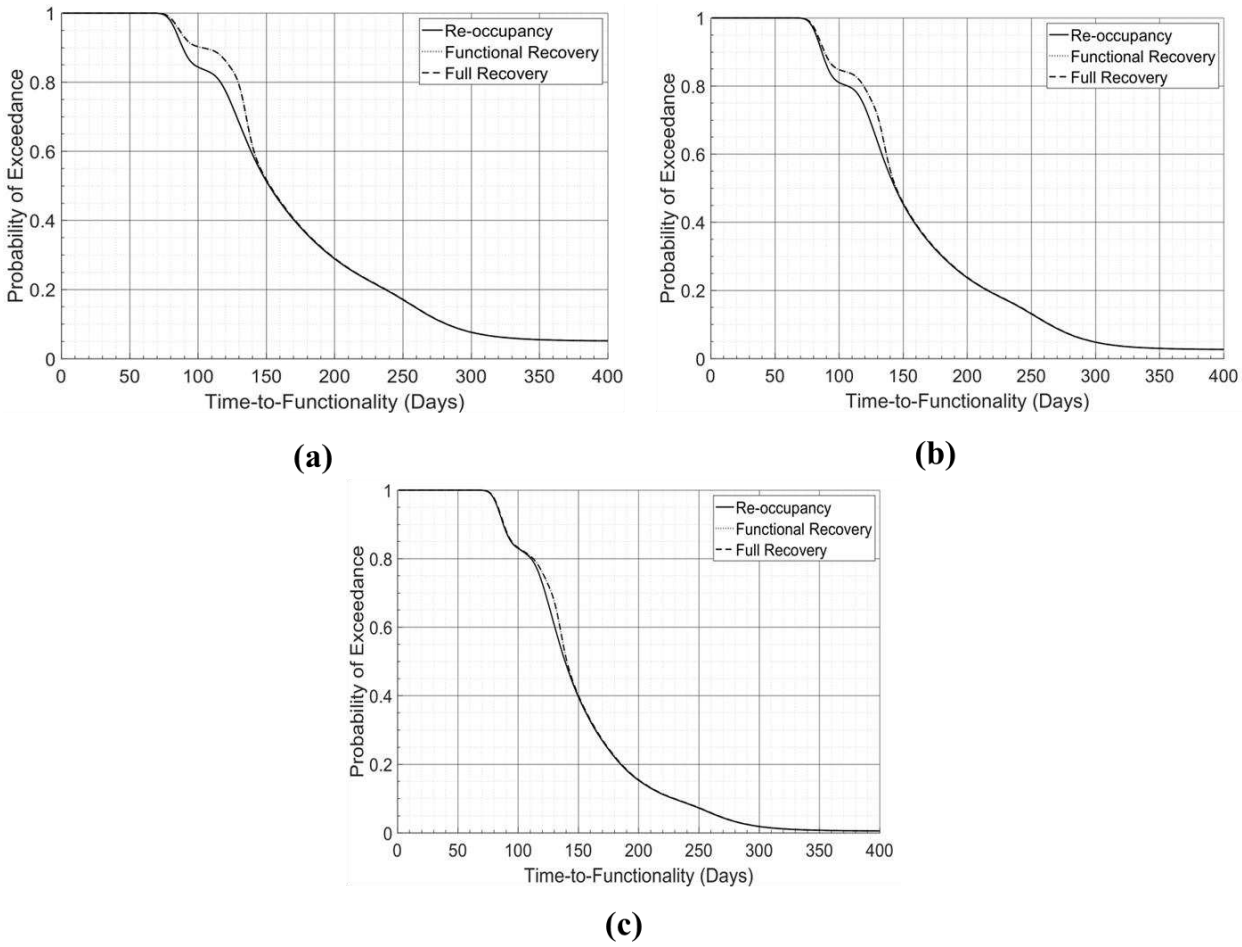

Figure 46: Ten-story design with: (a) 5 ply panels, (b) 7 ply panels, (c) 9 ply panels

The reasons for the behavior of the two-story, six-story, and ten-story archetypes are complex, but are the result of the different responses of the archetypes, and the complex relationship between floor accelerations and inter-story drift and their effect on TTF performance. Similarly to increasing the width of CLT panels, increasing the thickness of the CLT panels will also increase stiffness, decrease the building period, and affect both inter-story drift and floor accelerations. Unlike increasing the width of the CLT panels however, the actual effect on the stiffness of the building is significantly less. For the two-story archetype, that already has relatively low drifts compared to the other archetypes, this slightly increased stiffness (and decreased period) leads to

a marginal decrease in drift which is not significant enough to improve the performance of the drift sensitive components, however the increase in floor accelerations is significant enough to decrease the performance of the acceleration sensitive component in most cases. This explains the minimal positive or even detrimental effect of the thickness of the wall on the two-story archetype TTF performance. Conversely, the six- and ten-story archetypes have much larger drifts than the two-story archetype, and therefore have more TTF performance to gain from a decrease in drift. In both of these cases the increased stiffness (and decreased period) caused by increasing the thickness of panels decreased the drift enough for a measurable improvement in the performance of drift sensitive components, more significantly than it reduced the performance of acceleration sensitive components. The increase in overall TTF performance is still relatively marginal in comparison to increasing the wall width, but it is consistent and measurable, which is demonstrated by the stable, consistent improvement in TTF performance as the panel width increased seen in the six- and ten-story archetypes.

Number of UFPs in Relation to TTF Performance

The number of UFP's had varying effects on the different archetypes, with each of the three archetypes having a different response to increasing the number of UFPs. For the two-story archetypes there were few things that were apparent, like the number of plys, increasing the number of UFPs beyond two decreases the TTF performance of the building, dramatically in the case of four UFPs. Additionally, the recovery levels once again converge much like they did in Figure 41 (c), for many of the same reasons. For the six-story archetype, at first glance the number of UFPs seem to have no effect on the TTF performance of the building, however this is not the case. The Re-occupancy downtime decreases marginally by increasing the number of UFPs to three, while the Full and Functional Recovery downtime increase marginally. Continuing to

increase the number of UFPs to four will once again marginally decrease the Re-occupancy downtime, but the other recovery levels remain the same. For the ten-story archetype, increasing the number of UFPs from three to four visibly improves the TTF performance, but further increasing the number to four worsens the TTF performance. The reason for this is similar to both increasing the panel width and increasing the panel thickness. Like both of those scenarios, adding more UFPs will increase the stiffness of the structure and like the rocking wall mechanism, the UFPs are designed to help dissipate energy. So more UFPs per floor will increase energy dissipation of the system while also increasing the stiffness, which will ultimately reduce drift and increase floor accelerations. Similarly to how the two-story archetype reacted to the increasing the panel thickness, all of the archetypes seem to have some positive TTF performance impacts and some negative impacts from increasing the number of UFPs per floor. This is due to the same reason as the two-story archetype and the panel thickness. The benefit of decreasing the drift does not always outweigh the cost of increasing the floor acceleration, and it seems that all the archetypes are right on the line where the decreasing drift outweighs the increasing floor acceleration. This leads to observed situations where increasing the number of UFPs sometimes increases and sometimes decreases the TTF performance. The behavior of the two-story, six-story, and ten-story can be seen in Figures 47, 48, and 49 respectively.

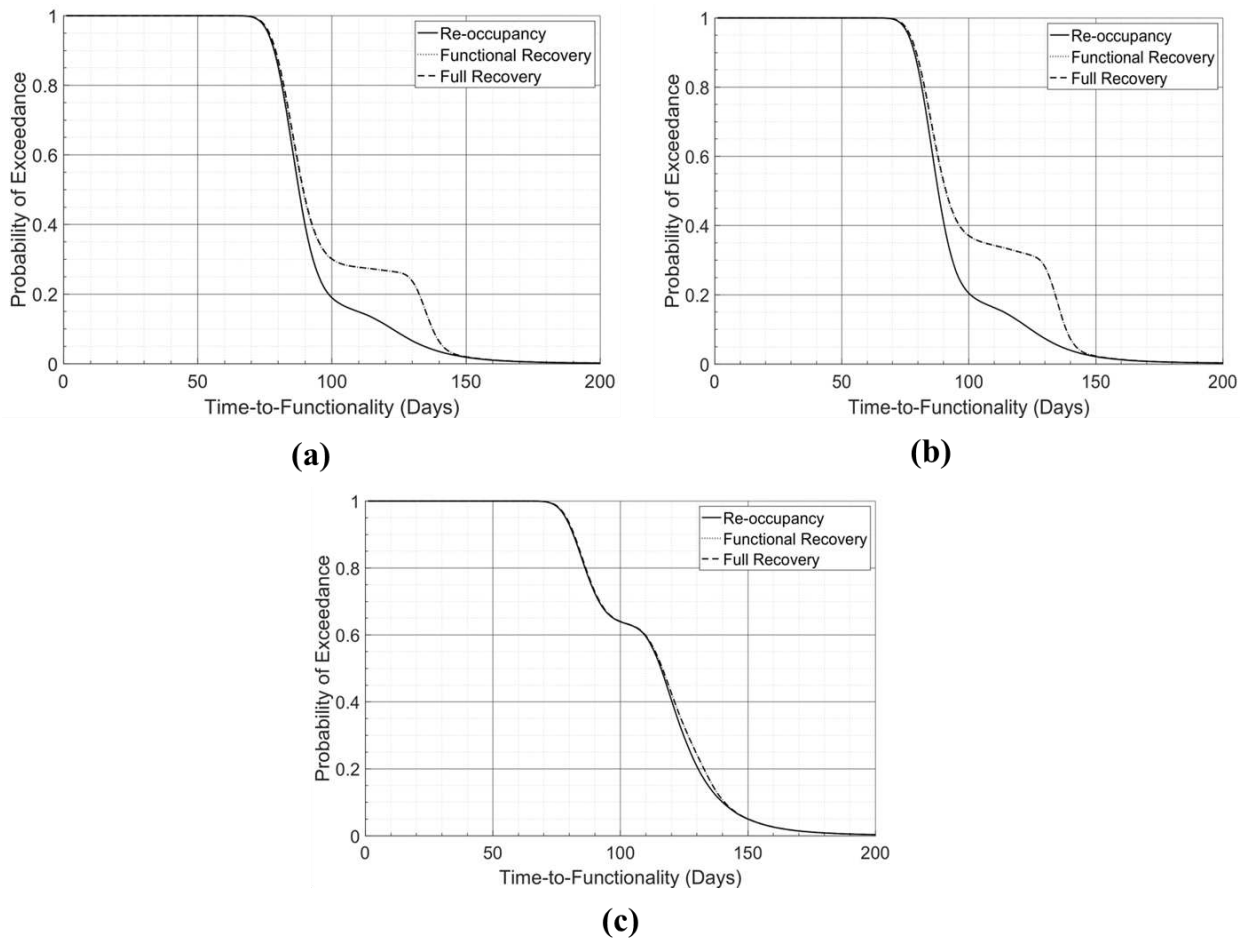

Figure 47: Two-story design with: (a) 2 UFPs, (b) 3 UFPs, (c) 4 UFPs

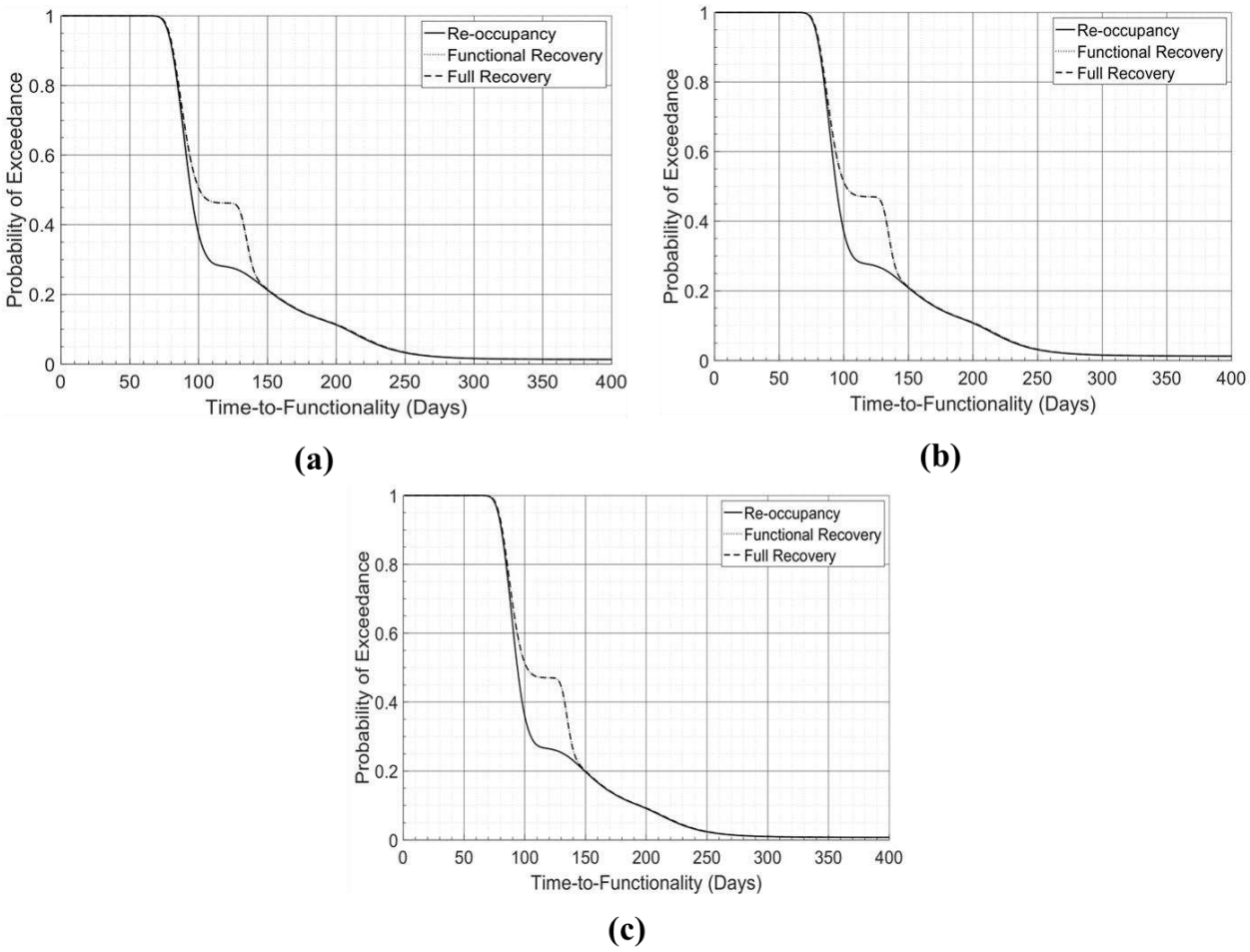

Figure 48: Six-story design with: (a) 2 UFPs, (b) 3 UFPs, (c) 4 UFPs

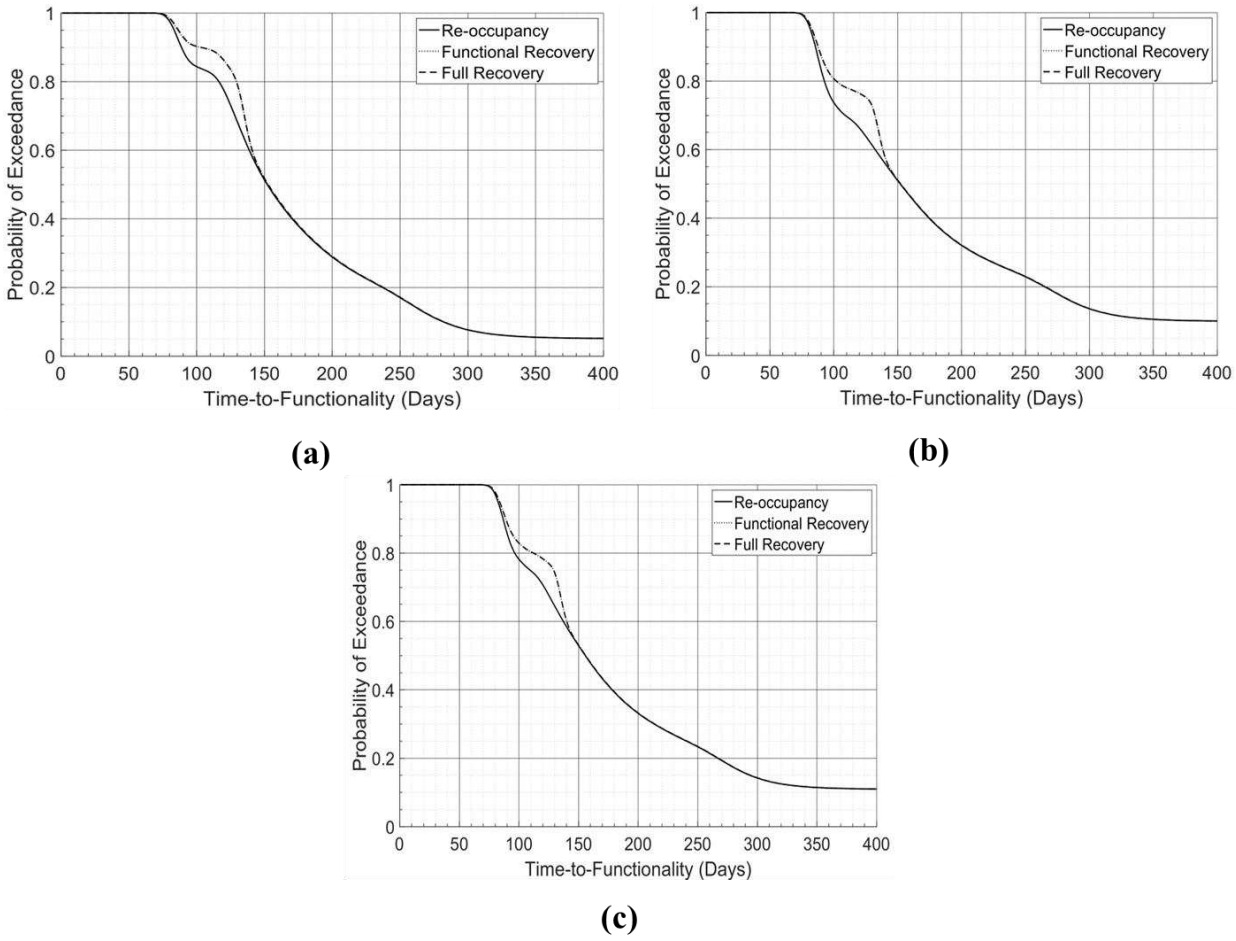

Figure 49: Ten-story design with: (a) 2 UFPs, (b) 3 UFPs, (c) 4 UFPs

Post-Tensioning Rod Diameter in Relation to TTF Performance

The relation of the diameter of the post-tensioning rods on TTF performance for the two-story archetype is relatively straightforward in comparison to the other components. Increasing the diameter decreases the Re-occupancy downtime, while increasing the Functional and Full Recovery downtime. The reason for this is straightforward, the increased diameter of the post tensioning rods increases the overturning moment capacity of the system and reduces the drift of the structure but will increase the floor accelerations. Since most of the Re-occupancy components (not all) are inter-story drift based, lowering the drift will decrease the Re-occupancy downtime. Conversely, there are many Full and Functional Recovery components (including long lead time

components) that are acceleration based, so increasing the floor acceleration will increase Full and Functional Recovery downtimes. The six-story and ten-story behavior is more complicated. Increasing the diameter of the post-tensioning worsened the TTF performance for both the six-story and ten-story archetypes, seemingly contrary to the proposed explanation for the two-story. However, there is an important consideration for the six-story and ten-story archetypes that are not applicable for the two-story. The seemingly better performance of the small diameter post-tensioning rod is most likely caused in combination by the drift limit for the component damage states and the inability of the model to predict collapse. Such small diameter post-tensioning rods would allow for large magnitude drifts in mid-rise buildings like the six-story and ten-story archetypes. In fact, the drifts may be high enough to induce collapse. The TTF methodology is not designed for such scenarios and will only consider the drift value, and while a high drift will cause damage to components, the amount of damage does not increase past the maximum damage state values for the components. So drifts above this point will not cause more damage to drift based components, but higher drifts (caused by less overturning moment, a greater period, and less stiffness) will most likely lower the floor accelerations and reduce the damage to acceleration-based components. So what is observed in the behavior of the six-story and ten-story is a case where all of the drift based components are damaged, but the acceleration based components are less so, leading to a scenario where increasing the overturning moment capacity (increasing the stiffness, and decreasing the period) by increasing the diameter of the post-tensioning rods does not reduce the drift enough (through the increased stiffness) to lower the damage to the drift components, but increases the acceleration (also from the increase stiffness) enough to cause more damage to the acceleration components; Thus causing “worse” TTF performance by increasing the overturning moment capacity of the post-tensioning rods, highlighting an important limitation

of the TTF methodology that will be further discussed in Chapter 7. Figures 50-52 show the post-tensioning rods behavior of the two-story, six-story, and ten-story respectively.

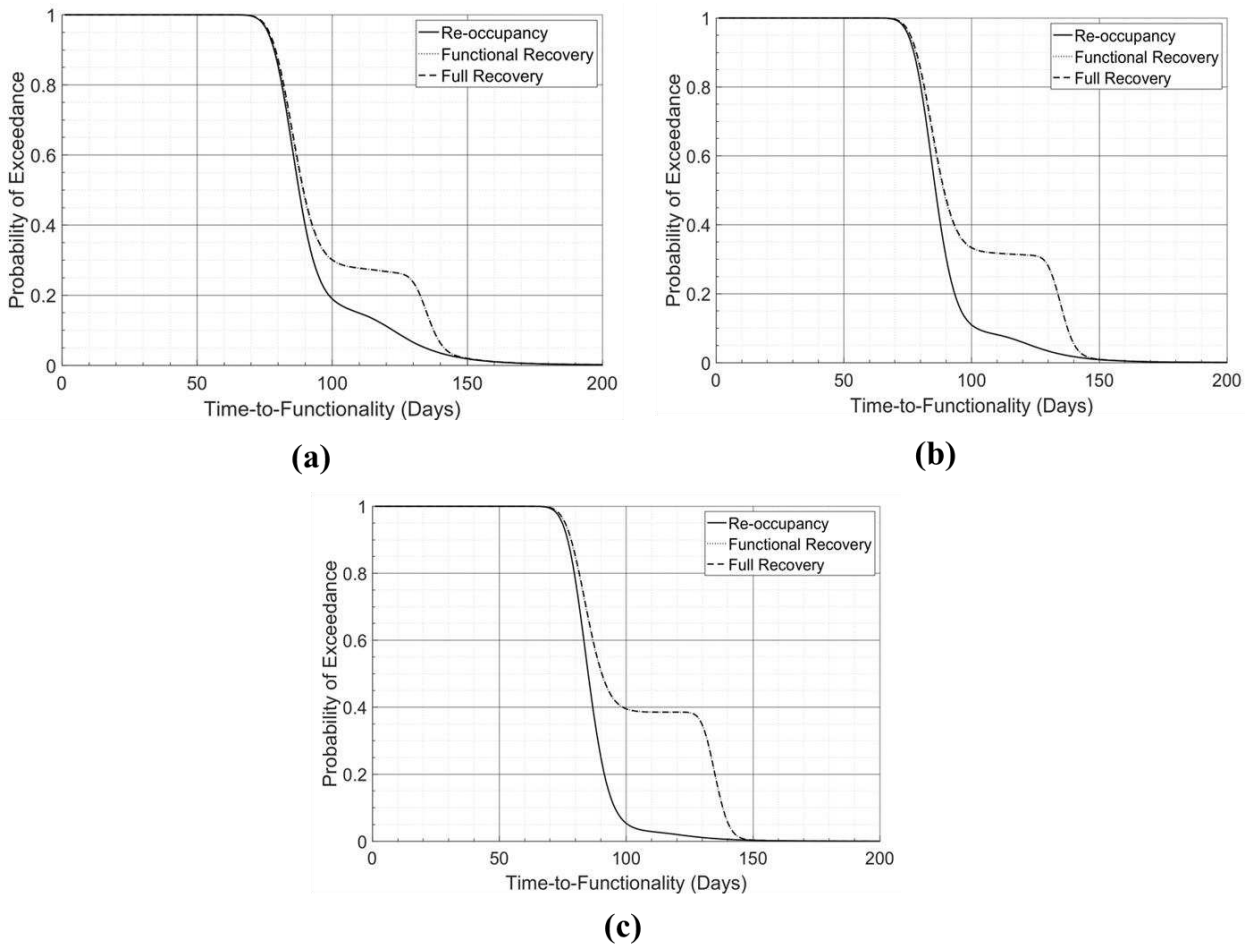

Figure 50: Two-story design with: (a) 15.8 mm (0.625”) dia. pt rods, (b) 254 mm (10”) dia. pt rods, (c) 508 mm (20”) dia. pt rods

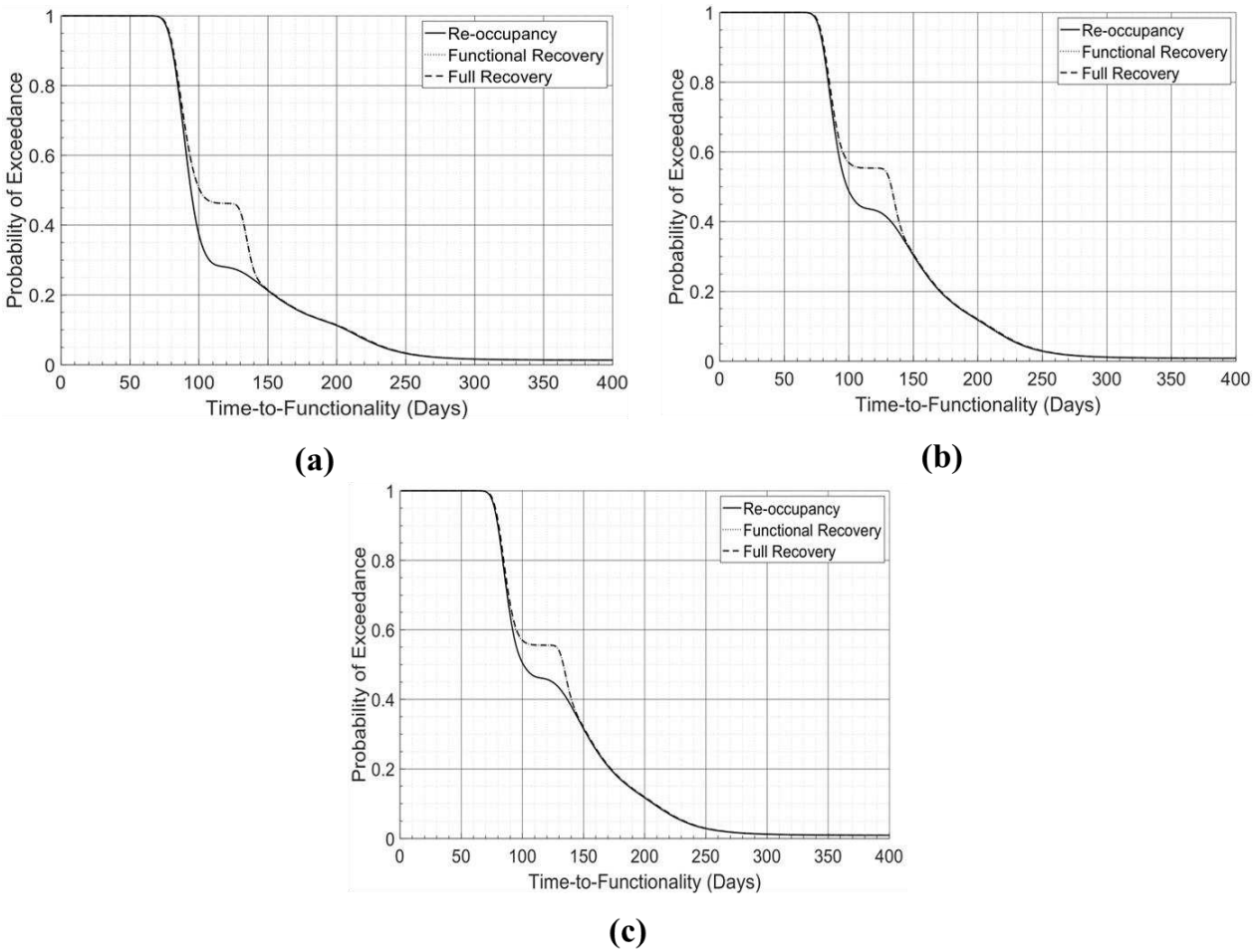

Figure 51: Six-story design with: (a) 15.8 mm (0.625”) dia. pt rods, (b) 254 mm (10”) dia. pt rods, (c) 508 mm (20”) dia. pt rods

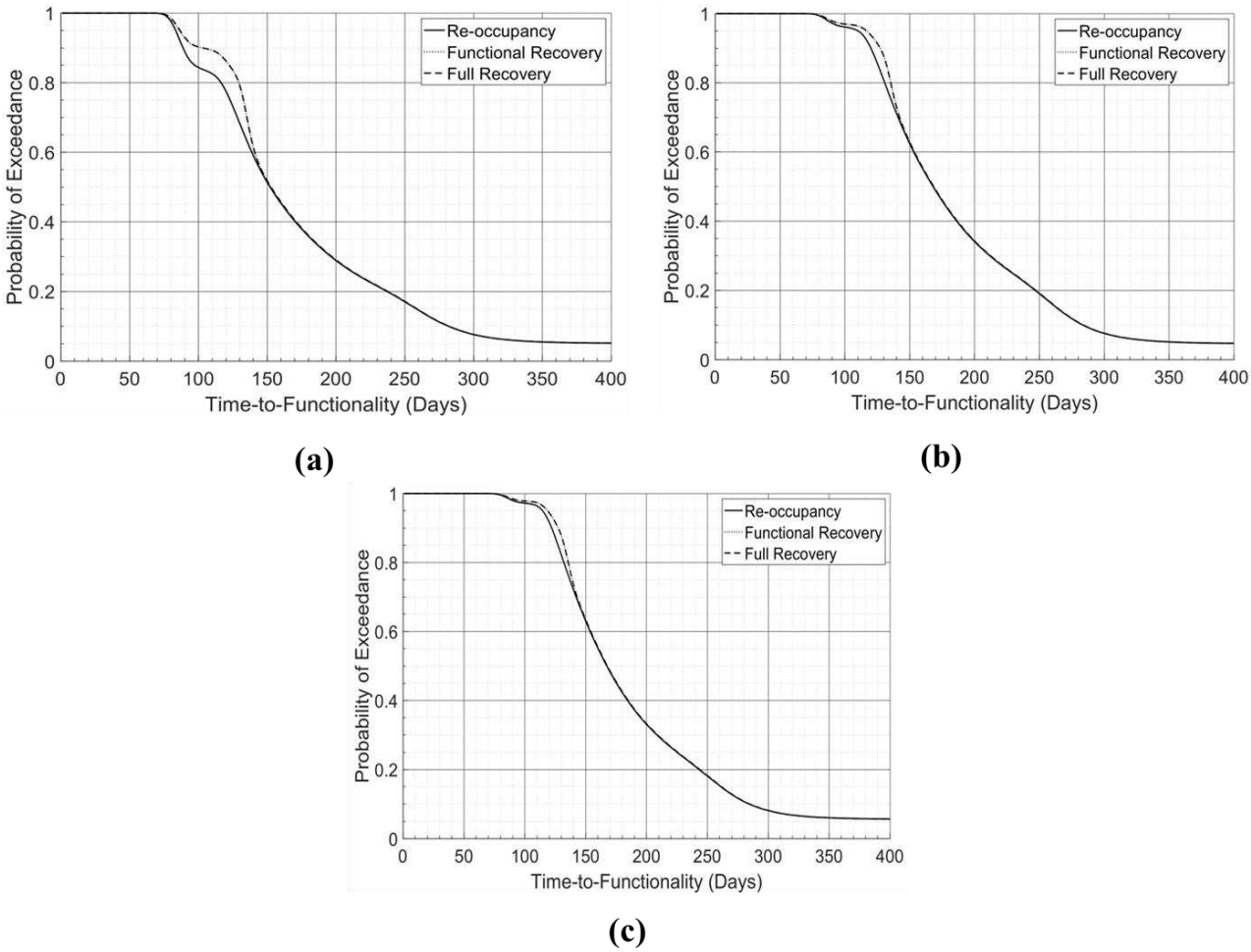

Figure 52: Ten-story design with: (a) 15.8 mm (0.625") dia. pt rods, (b) 254 mm (10") dia. pt rods, (c) 508 mm (20") dia. pt rods

Closing

The database of 243 designs detailed in this Chapter are capable of being used in a design guidance process based on downtime and TTF, further recommendations will be detailed in Chapter 7; however, several observations can still be made. Across all of the archetypes, increasing the stiffness and energy dissipation (through the rocking mechanism) by increasing wall width seems to be the most impactful in terms of increasing TTF performance for both the six-story and ten-story archetypes. However, the two-story sees diminishing returns, with even a negative impact on Full and Functional Recovery downtimes in some cases. Increasing the stiffness by increasing

the panel thickness through the number of plys can have a positive impact in certain scenarios on the TTF performance, but can also negatively impact the TTF performance in some scenarios, mostly depending on the height of the building. Increasing the stiffness and energy dissipation of the system by increasing the number of UFPs had a negative impact on the TTF performance of the two story, minimal impact on the six-story, and a positive impact on the ten-story archetype. Increasing overturning moment capacity and ultimately the stiffness of the building by increasing the post-tensing rod diameter positively impacted the Re-occupancy downtime of the two-story archetype while negatively impacting the other recovery levels. While the six-story and ten-story saw their performance impacted negatively by increasing the diameter of the post-tensioning rods, this is an artifact of the limitations of the method. In general, the results in the chapter highlights the complex nature of TTF performance, and the balancing act between the displacement and floor acceleration of the building which is primarily affected by the stiffness of the building. While this database is only relevant to buildings with a CLT rocking wall system, the process detailed here is applicable to any structural system and can be applied to create a similar database.

CHAPTER 7 – RESILIENCE-BASED SEISMIC DESIGN GUIDANCE USING THE TTF DATABASE

Introduction to Design Guidance

With the database constructed in Chapter 6, it is possible to develop seismic design guidance incorporating TTF considerations without the need to run complicated non-linear dynamic and functionality analyses. Instead, the database will be leveraged as a resource to suggest designs that meet certain criteria supplied by the designer, then designs that meet these criteria will form the basis for the further refinement of the design. The design guidance introduced herein will consider TTF performance, cost, footprint of the structure, and performance-based design. While not an explicit step by step guide, five general steps are suggested and details of what each step should include is expanded upon. Many of the steps follow procedures that should be familiar to most design engineers, but the incorporation of the rocking wall database is an exception, and several examples of how to properly leverage the database will be given later in this Chapter. The objective of this design guidance is to provide an outline for design engineers that are interested in incorporating downtime considerations as well as how to properly leverage the database of the CLT Rocking Wall designs into real design applications. The five steps included in this chapter are: Step 1: Select Location, Initial Design, and TTF Requirements; Step 2: Design selection based on TTF Requirements and Building Period Iteration; Step 3: Geometric and Viability Check; Step 4: Cost Analysis; and Step 5: Performance Evaluation using Alternative Means/Methods in Code. Figure 53 shows a flowchart for the design guidance and a brief description of the five steps.

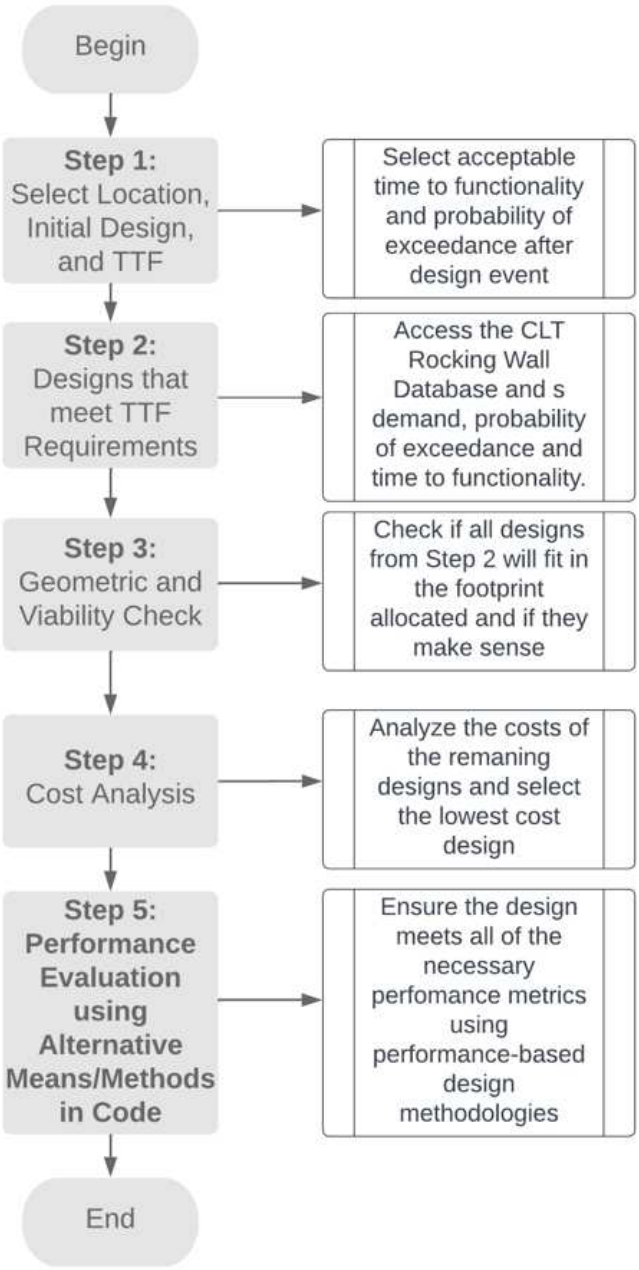

Figure 53: Design process incorporating TTF considerations

Step 1: Select Location, Initial Design, and TTF Requirements

The first step to any seismic design is to identify the site on which the structure will be built and to estimate the seismic demand for design. This is typically done using ASCE 7 and produces a design response spectrum that will later be used to select the designs from the database as well as

the later performance-based design. In addition, an estimate of the building period is required, the method used to obtain this estimate is up to the designer, but it should be noted that an initial design can be useful to inform decision making later (particularly in Step 3). A desired TTF for the design event and associated probability of exceedance also needs to be selected. For the TTF selection, it would be possible to select a design target for any of the recovery levels (Re-occupancy, Functional Recovery, Full Recovery), however in general the most interest is in the time until functional recovery; due to the fact this is the recovery level where the structure can return mostly to normal operation. Later in the Chapter two examples using the design method will be presented, one with a TTF target of Re-occupancy, and the other with Functional Recovery. The probability of exceedance target represents the acceptable level of risk for the design team and owner, in particular, in terms of meeting the functionality target; what percentage of potential outcomes not meeting the target TTF is acceptable? To select these measures there are a variety of options, it can be as simple as estimating the economic loss from non-functionality per day after an event and selecting an acceptable monetary target, followed by selecting a probability of exceedance based on how vital it is to achieve that target. Or it could involve a more complicated risk analysis that incorporates the stochastic nature of the TTF estimates and estimates both the downtime and probability of exceedance. The importance of the building in terms of the larger community can also be considered in the selection of the TTF and probability of exceedance targets. In terms of larger community resilience, selecting an appropriate target may be difficult and could require the incorporation of a larger community resilience model to inform and to select the TTF targets. There are many potential factors that can influence the TTF factors in terms of community resilience, such as occupancy type, location, economic impact, etc While there are a variety of methods (including estimations using something other than economic loss) to determine

the necessary inputs, a Sa demand for the design event, building period estimate, a TTF target for a recovery level, and a probability of exceedance target for that TTF target are required.

Step 2: Designs that meet TTF Requirements

This step in the design is where the database constructed in Chapter 6 is fully leveraged. With the Sa demand, building period, TTF target, and probability of exceedance target determined in Step 1, the database can provide designs that meet the requirements. The number of designs returned will be a direct result of how strict the targets are. A lower demand and more relaxed TTF and probability of exceedance targets will of course increase the number of applicable designs. Each of these designs has their own building period based on the design components selected. Therefore, it is necessary to iterate once with the selected design at their respective building periods to ensure that the designs still meet the requirements at their building period. This process will be demonstrated later in the Chapter, and each of the designs have their associated building period located in Tables 23-25 in the Appendix. A few limitations of the database should be noted; the seismic lateral resisting system is assumed to be the CLT Rocking Wall system detailed in Chapters 3 and 6, with the assumption of a mixed-use structure (first-floor retail and residential above that). In addition, all the models are non-simulated collapse models, and require additional performance-based design. These assumptions are reasonable in the context of resilient mass-timber tall structures, but it does limit the database's current applicability. However, as mentioned previously, the database can be expanded to include additional structural and non-structural systems. Eventually with enough data produced, a more prescriptive form estimation can be developed and replace this step in the design. For now, the database used here can be seen as a contribution to that knowledge base, and as time goes on more designs and structural and non-structural systems will be incorporated.

Step 3: Geometric and Viability Check

This step has two parts, each with the objective of eliminating designs that do not meet certain criteria. Each of the designs should be evaluated for obvious conflicts with the surrounding systems and architectural requirements, such as the lateral wall system being wider than the allocated footprint. In addition, engineering judgement should be used to eliminate any design that will obviously not meet performance requirements; this portion of the step is not strictly required, but eliminating any obviously inadequate designs will save the analyst time in Step 4 and Step 5 where designs are further evaluated for cost and performance. This is where knowledge gained about the behavior of the structure in the initial design can be levered to save time in later steps; as previously mentioned in Step 2, the models are non-simulated collapse models, so compliance to performance aspects such as drift limits will need to be done in a later step.

Step 4: Cost Analysis

After some of the designs have been filtered out, a cost analysis should be performed to select the most cost-effective designs. The complexity of this analysis as well as the number of designs to consider is up to the designer, it can be as simple as an estimate of materials, transport, and installation costs, or it can be a complete Life Cycle Cost Analysis. The objective of this step is to select the optimal design or designs that reduce cost while meeting all of the requirements from Steps 1:3.

Step 5: Performance Evaluation using Alternative Methods in ASCE-7

By this point, the various designs produced in Step 2 should have been narrowed down to several (or even a single) design(s) that meets the TTF, geometric, and cost requirements of the design. The purpose of this step is to ensure an acceptable level of performance in metrics such as life-

safety, drift, acceleration, etc. Since the rocking wall system used to develop this database is not currently explicitly included in design code, alternative methods are required to ensure that the design will achieve the desired structural response performance goals. This can be done in a variety of ways including non-linear time history analysis, direct displacement methodology, or some other peer reviewed design methodology. A prescriptive design method specific to the mass timber rocking walls was developed and is presented in Busch et al. (2022) [12]. The exact requirements for the methodology are laid out specifically in Chapter 16 of ASCE 7-16 (ASCE 2016 [7]), and later in this Chapter the illustrative examples will demonstrate the individual steps for these requirements.

Illustrative Design Guidance Examples

To better illustrate the use of the TTF database, two different examples are presented in this Chapter. The first example will select designs based on a Re-occupancy TTF target, while the second example will focus on Functional Recovery. The examples will focus primarily on Steps 1-3, demonstrating the use of the database. Steps 4 and 5 will be briefly discussed, but not expanded upon in detail. Both examples will consider the same example building at the Risk-Targeted Maximum Considered Earthquake MCE_R, the 10-story mass timber building tested as a part of the larger NHERI TallWood project, which has been mentioned previously in earlier chapters. Since the building will remain the same between the examples, the same MCE_R design response spectrum and initial building period estimate will be used for both examples. This MCE_R design response spectrum as well as the initial period estimate was developed primarily by the University of Washington with additional consultation with professional design engineers and more details about its development can be found in Wichman et. al (2022) [77]. An initial building period of 2.3 seconds was estimated using preliminary designs of the 10-story building, and the

MCE_R design response spectrum for the hypothetical building location in Seattle, Washington can be seen in Figure 54.

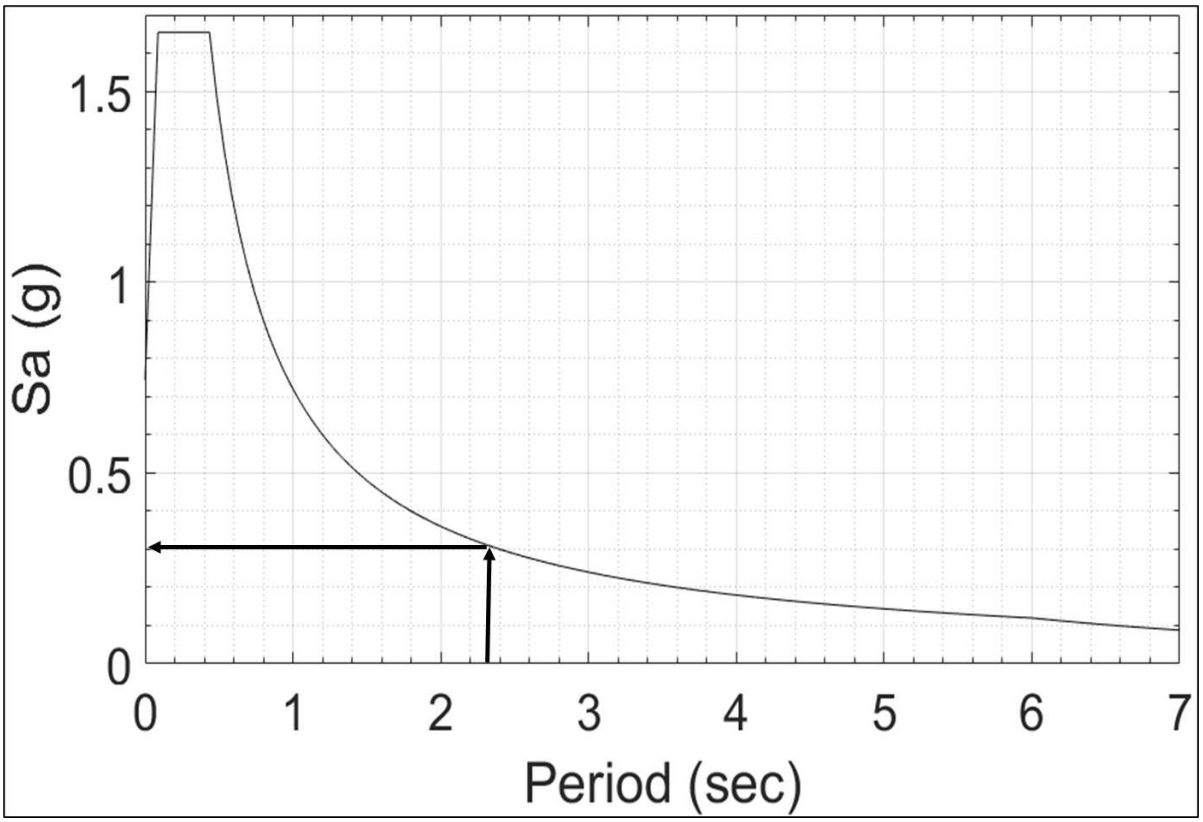

Figure 54: MCE_R Design Response Spectrum for 10-story building with an estimated period of 2.3 seconds Wichman et. al (2022) [77]

10-story Re-occupancy at MCE_R

Step 1 is to determine the various performance targets as well as develop a design spectrum for the building location. A target of Re-occupancy by 100 days after the event with a probability of exceedance of 10% were selected as the TTF targets for this example. These targets were selected to best represent the process, the targets are not overly strict, but are also not lax, so a good illustration of Step 2 can be performed. As mentioned previously, the NHERI TallWood ten-story experimental test design response spectrum and the initial building period estimate was used to determine the spectral acceleration demand used for the example. Using Figure 54 as well as the

estimated period of 2.3 seconds, a spectral acceleration demand of approximately 0.3 g can be determined.

Step 2 involves the leveraging of the TTF database and the selection of designs based on the established demands and targets in Step 1. To do this, one would use the TTF versus probability of exceedance plots for the spectral acceleration demand (0.3 g) and determine the probability of exceedance for the TTF functionality target (Re-occupancy by 100 days with 10% probability of exceedance). Figure 55 demonstrates how one would read the TTF versus probability of exceedance plots using the 0.3 g plot for Design 224, while Table 18 shows all the ten-story designs in the database that meet both the TTF downtime and probability of exceedance target at 0.3 g

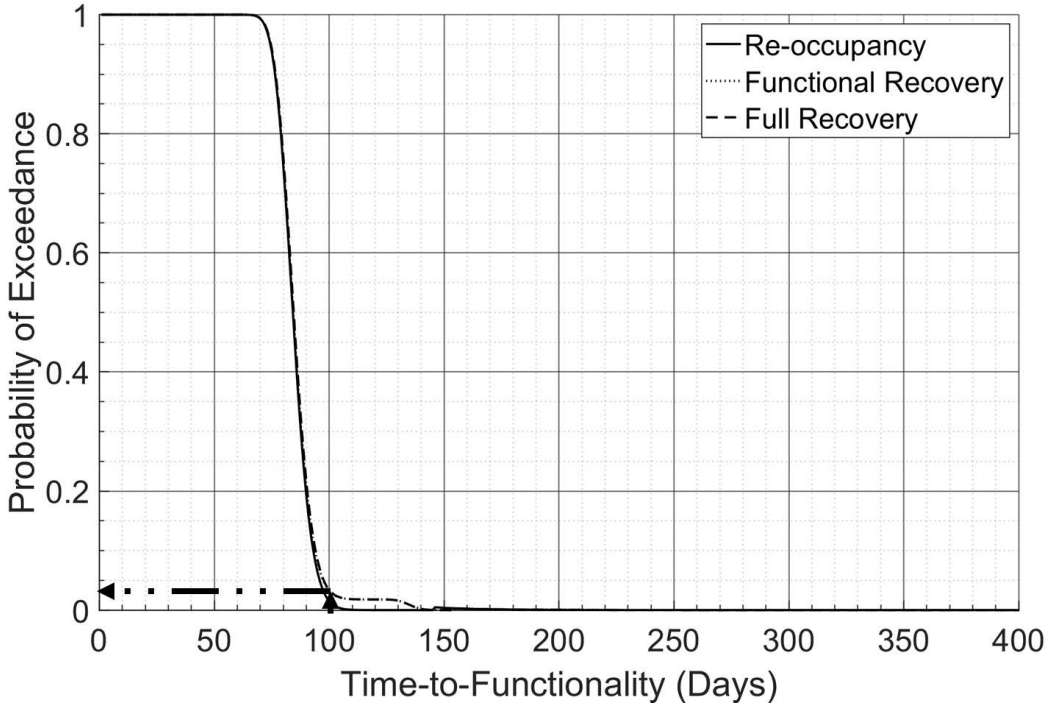

Figure 55: Design 224 TTF versus probability of exceedance at 0.3 g

Table 18: Example 1 Designs at Estimate Building Period that Meet Criteria

Design	Panel Width (mm)	Panel Width (ft)	Panel Plys	Number of UFPs	Dia. of PT rods (mm)	Dia. of PT rods (in)	1st Mode Period (sec)
Design 194	254	10	5	3	31.75	1.25	1.11
Design 195	254	10	5	4	31.75	1.25	1.11
Design 197	254	10	5	3	50.8	2	1.09
Design 198	254	10	5	4	50.8	2	1.09
Design 199	254	10	7	2	15.8	0.625	0.95
Design 201	254	10	7	4	15.8	0.625	0.95
Design 203	254	10	7	3	31.75	1.25	0.95
Design 204	254	10	7	4	31.75	1.25	0.95
Design 206	254	10	7	3	50.8	2	0.93
Design 207	254	10	7	4	50.8	2	0.93
Design 208	254	10	9	2	15.8	0.625	0.84
Design 209	254	10	9	3	15.8	0.625	0.84
Design 210	254	10	9	4	15.8	0.625	0.84
Design 212	254	10	9	3	31.75	1.25	0.84
Design 213	254	10	9	4	31.75	1.25	0.84
Design 215	254	10	9	3	50.8	2	0.83
Design 216	254	10	9	4	50.8	2	0.83
Design 218	508	20	5	3	15.8	0.625	0.44
Design 219	508	20	5	4	15.8	0.625	0.44
Design 220	508	20	5	2	31.75	1.25	0.44
Design 221	508	20	5	3	31.75	1.25	0.44
Design 222	508	20	5	4	31.75	1.25	0.44
Design 223	508	20	5	2	50.8	2	0.44
Design 224	508	20	5	3	50.8	2	0.44
Design 225	508	20	5	4	50.8	2	0.44
Design 226	508	20	7	2	15.8	0.625	0.38
Design 227	508	20	7	3	15.8	0.625	0.38
Design 228	508	20	7	4	15.8	0.625	0.38
Design 229	508	20	7	2	31.75	1.25	0.38
Design 230	508	20	7	3	31.75	1.25	0.38
Design 231	508	20	7	4	31.75	1.25	0.38
Design 232	508	20	7	2	50.8	2	0.38
Design 234	508	20	7	4	50.8	2	0.38
Design 235	508	20	9	2	15.8	0.625	0.34
Design 236	508	20	9	3	15.8	0.625	0.34
Design 237	508	20	9	4	15.8	0.625	0.34
Design 238	508	20	9	2	31.75	1.25	0.34
Design 239	508	20	9	3	31.75	1.25	0.34

Design 240	508	20	9	4	31.75	1.25	0.34
Design 241	508	20	9	2	50.8	2	0.34
Design 242	508	20	9	3	50.8	2	0.34
Design 243	508	20	9	4	50.8	2	0.34

From Figure 55 one can determine that at a spectral acceleration of 0.3 g the Re-occupancy downtime of 100 days has a probability of exceedance of approximately 4%, meeting the TTF target and is therefore included in the passing designs. However, it can be seen that many of the passing designs have drastically different periods than the initial estimates. This requires an additional check to ensure that the designs still pass the TTF targets at spectral acceleration demands determined by their period. For example, Design 224 has a first mode period of approximately 0.44 seconds, which using the demand response spectrum in Figure 54, results in a spectral acceleration demand of 1.7g. Figure 56 shows the TTF versus probability of exceedance for Design 224 at 1.6 g.

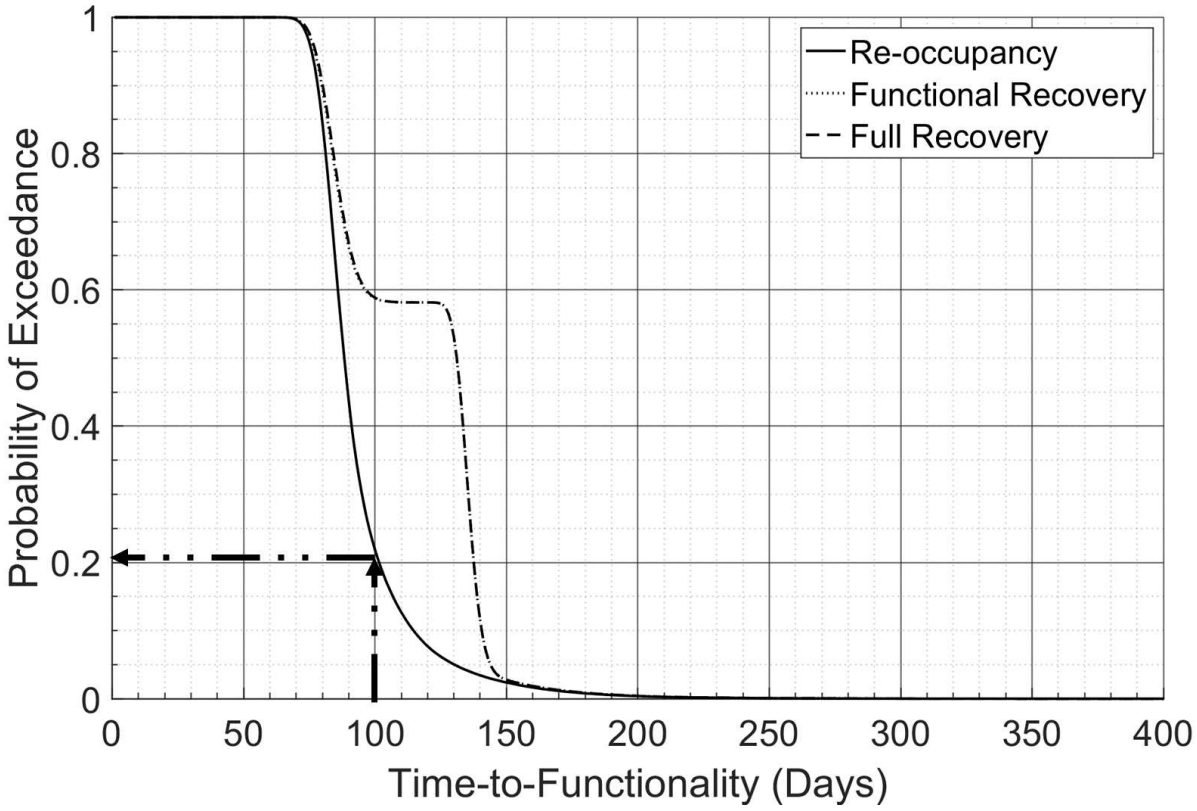

Figure 56: Design 224 TTF versus probability of exceedance at 1.6 g

From Figure 56 it is clear to see that at a spectral acceleration of 1.6 g, the probability of exceedance for 100 days of Re-occupancy is greater than the 10% target that was set in Step 1, thus disqualifying the design from consideration. Table 19 shows the designs that still meet the TTF requirements at the demands determined by the response spectrum and their respective 1st mode periods.

Table 19: Example 1 Designs at Actual Building Period that Meet Criteria

Design	Panel Width (mm)	Panel Width (ft)	Panel Plys	Number of UFPs	Dia. of PT rods (mm)	Dia. of PT rods (in)	1st Mode Period (sec)
Design 194	254	10	5	3	31.75	1.25	1.11
Design 195	254	10	5	4	31.75	1.25	1.11
Design 197	254	10	5	3	50.8	2	1.09
Design 198	254	10	5	4	50.8	2	1.09
Design 199	254	10	7	2	15.8	0.625	0.95
Design 201	254	10	7	4	15.8	0.625	0.95
Design 203	254	10	7	3	31.75	1.25	0.95
Design 204	254	10	7	4	31.75	1.25	0.95
Design 206	254	10	7	3	50.8	2	0.93
Design 207	254	10	7	4	50.8	2	0.93
Design 208	254	10	9	2	15.8	0.625	0.84
Design 209	254	10	9	3	15.8	0.625	0.84
Design 210	254	10	9	4	15.8	0.625	0.84
Design 212	254	10	9	3	31.75	1.25	0.84
Design 213	254	10	9	4	31.75	1.25	0.84
Design 215	254	10	9	3	50.8	2	0.83
Design 216	254	10	9	4	50.8	2	0.83

Step 3 consists of the geometric and viability check of the designs. For the geometric check, it will be assumed that there is a maximum wall width of 508 mm (20') for the lateral system. With the rocking wall design assumption, this would mean a panel width limited to 254 mm (10'). All of the currently considered designs meet this panel requirement, so no designs will be disqualified for geometric compatibility. In regard to the viability check, one could use the initial design to identify any designs that will obviously not meet performance requirements. In the case of this example, no designs will be disqualified by this method as there are no obviously inadequate designs.

Step 4 consists of the cost analysis and while Step 4 is not mandatory, it can be used as a tool to reduce the number of designs that will be considered during Step 5 while also optimizing for cost.

As can be seen from Table 19, there are still 17 designs that meet all of the requirements from Steps 1-3, so eliminating designs based on cost can be useful to limit the number of analyses in Step 5.

Step 5 is critical to the design; as mentioned multiple times previously, the TTF database utilizes non-simulated collapse models and therefore their results cannot be used to demonstrate requirements such as life-safety. If the selected design does not pass this step, then the TTF targets need to be readjusted and new designs selected. As an example of a performance based seismic design, the required steps for a non-linear time history analysis (NLTHA) in Chapter 16 of ASCE 7-16 (ASCE 2016 [7]) are outlined below as they pertain to the remaining rocking wall designs in Table 19:

- 16.1 General Requirements
    - 16.1.2 Linear Analysis
        - In addition to the NLTHA, a linear analysis is required using a method (such as equivalent lateral force [ELF]) present in Chapter 12 of ASCE 7-16 (ASCE 2016 [7]).
    - 16.1.3 Vertical Response Analysis
        - The vertical elements of the gravity force-resisting system are continuous, and therefore vertical response analysis is not required for the designs in this example.
    - 16.2.1 Target Response Spectrum
        - The design response spectrum in Figure 54 is consistent with a Method 1, 5%-damped MCE_R response spectrum, and can be used as a basis for the

NLTHA.

- 16.2.2 Ground Motion Selection
    - A suite of a minimum of 11 ground motions with two components in orthogonal horizontal directions are required. The FEMA P695 far-field ground motions that have been used extensively throughout this research meet this criteria and would be suitable for the NLTHA.
- 16.2.3 Ground Motion Modification
    - A period range is needed for the building consisting of a lower bound selected to incorporate the minimum number of elastic modes required to achieve 90% mass participation and an upper bound corresponding to at least twice the first mode period of the building.
    - The selected ground motions shall be scaled to create a maximum-direction spectrum such that the average of the maximum-direction spectrum either exceeds or does not fall below 90% of the design response spectrum in the determined period range.
    - The scaled suite will then be applied to the building at orthogonal orientations, ensuring the average of the component response spectrum is within 10% of the mean of the component response spectra in the developed period range.
- 16.3 Modeling and Analysis
    - For the CLT rocking wall building design, a 3-dimensional model accounting for P-Delta effects, torsion, and the direct modeling of hysteretic energy dissipation of structural members (CLT panels, UFPs, etc.) is required.
    - Gravity loading in the model will consider two scenarios; the first in which the

gravity load and live load are both considered using *1.0D +0.5L* where *D* is the gravity load of the structure, and *L* is the sum of 80% of the unreduced live load greater than 4.79 kN/m^2 (100 lb./ft^2) and 40% of the remaining unreduced live load, and the second in which only gravity load is considered and will be taken as *1.0D*.

- 16.4 Analysis Results and Acceptance Criteria
    - 16.4.1.1 Unacceptable Response. Any of the following are an unacceptable response to a ground motion:
        - Convergence failure of the analytical solution
        - Predicted demands on deformation-controlled elements exceed the valid modeling range.
        - The predicted demands on force-controlled elements exceed the element capacity.
        - Predicted deformation demands on elements not explicitly modeled exceed the deformation limits at which the elements can support their gravity loads.
    - 16.4.1.2 Story Drift
        - The mean story drift of the CLT rocking wall design will not exceed two times *0.015h* where *h* is the story height below the considered level.
    - 16.4.2 Element-Level Acceptance Criteria.
        - Elements actions will be evaluated and sorted into either force-controlled actions or deformation-controlled actions. For the CLT rocking wall system, both the CLT panels and the UFPs are deformation-controlled actions while the post-tensioning rods are force controlled actions.
        - For the post-tensioning rods, the design must satisfy:

$$(2.0)(1.25)(Q_u - Q_{ns}) + Q_{ns} \leq Q_e \quad (7)$$

Where Q_u is the mean value of the of the induced force on the post-tensioning rods obtained during the ground motion suite analysis, Q_{ns} is the demand caused by all other loads other than seismic, and Q_e is the expected component strength.

- For UFPs and CLT panels, the design must satisfy:

$$Q_u \leq (0.24)Q_{ne} \quad (8)$$

Where Q_u is the mean value of the of the induced deformation on either the CLT panels or UFPs for the ground motion suite analysis and Q_{ne} is the mean value of inelastic deformation at which loss of gravity-load-carrying capacity is expected to occur.

- For the remaining gravity force-resisting system, they shall be demonstrated to be capable of supporting the gravity loads from the NLTHA.

- 16.5 Design Review
  - A review by qualified reviewers as described in 16.5.1 will present a letter to the Authority Having Jurisdiction attesting.
    - The scope of the review performed
    - The agreement or disagreement with the analysis and its applicability to the design
    - Conformance of the design to applicable requirements of the standard
    - Any items requiring further resolution by the Authority Having Jurisdiction.

10-story Functional Recovery at MCE_R

The second example utilizing the database will focus on Functional Recovery of the same ten-story NHERI TallWood building used in example one. This means that the design response spectrum in Figure 54 will be used as well as the initial period estimation of 2.3 seconds and MCE_R demand of 0.3 g at the estimated period. Step 1 of this example is similar to the previous example except that the TTF target will be set for Functional Recovery by 100 days with a probability of exceedance of 20%.

Step 2 used the same method demonstrated in Figure 55; using the TTF versus probability of exceedance plots at the spectral acceleration demand determined by the estimated building period (0.3 g) to determine ten-story designs meeting the TTF targets. However, unlike Figure 55, Functional Recovery was the target, not Re-occupancy. An example using Design 195 can be seen in Figure 57, showing a probability of exceedance for Functional Recovery by 100 days of approximately 5%, while Table 20 compiles all of the ten-story designs that meet the TTF targets.

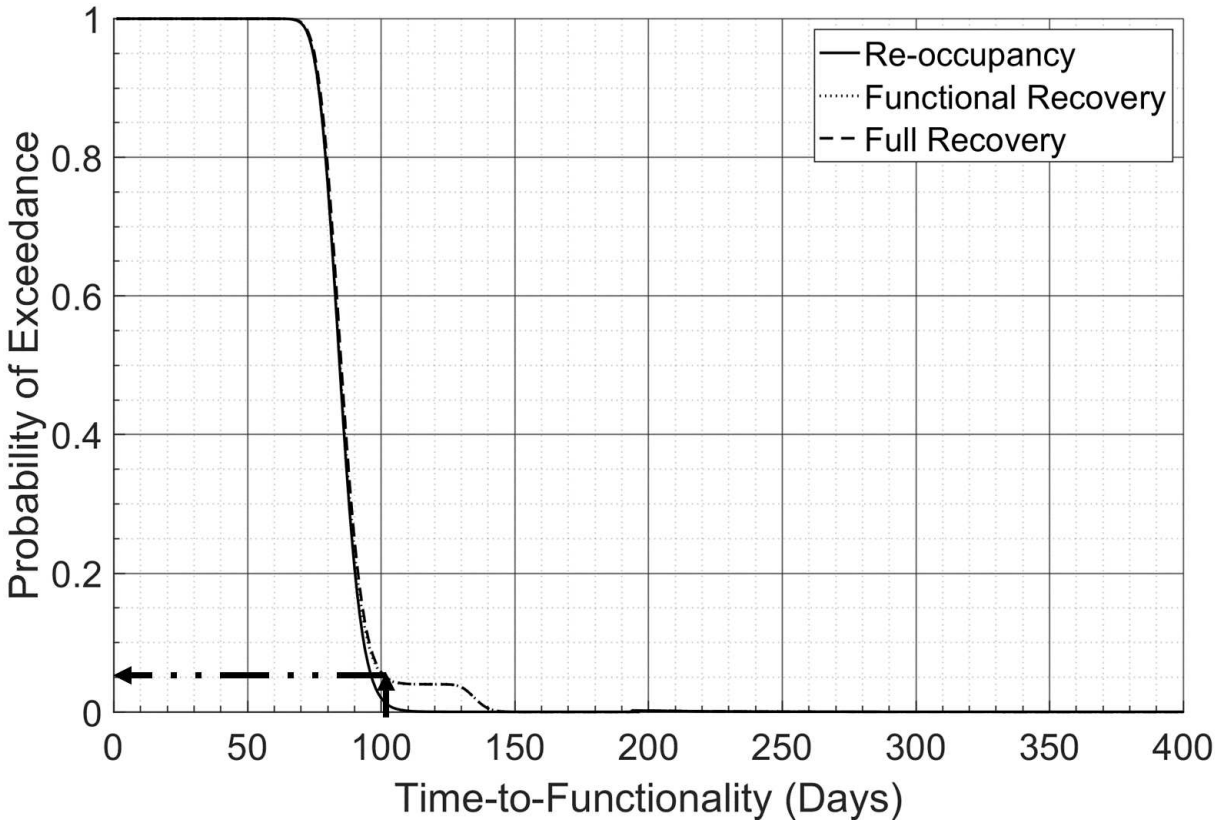

Figure 57: Design 195 TTF versus probability of exceedance at 0.3 g

Table 20: Example 2 Designs at Estimate Building Period that Meet Criteria

Design	Panel Width (mm)	Panel Width (ft)	Panel Plys	Number of UFPs	Dia. of PT rods (mm)	Dia. of PT rods (in)	1st Mode Period (sec)
Design 173	127	5	7	3	15.8	0.625	2.64
Design 179	127	5	7	3	50.8	2	2.31
Design 182	127	5	9	3	15.8	0.625	2.36
Design 185	127	5	9	3	31.75	1.25	2.31
Design 189	127	5	9	4	50.8	2	2.11
Design 195	254	10	5	4	31.75	1.25	1.11
Design 195	254	10	5	4	31.75	1.25	1.11

Design 196	254	10	5	2	50.8	2	1.09
Design 197	254	10	5	3	50.8	2	1.09
Design 198	254	10	5	4	50.8	2	1.09
Design 200	254	10	7	3	15.8	0.625	0.95
Design 202	254	10	7	2	31.75	1.25	0.95
Design 203	254	10	7	3	31.75	1.25	0.95
Design 204	254	10	7	4	31.75	1.25	0.95
Design 206	254	10	7	3	50.8	2	0.93
Design 207	254	10	7	4	50.8	2	0.93
Design 208	254	10	9	2	15.8	0.625	0.84
Design 209	254	10	9	3	15.8	0.625	0.84
Design 210	254	10	9	4	15.8	0.625	0.84
Design 211	254	10	9	2	31.75	1.25	0.84
Design 212	254	10	9	3	31.75	1.25	0.84
Design 213	254	10	9	4	31.75	1.25	0.84
Design 215	254	10	9	3	50.8	2	0.83
Design 216	254	10	9	4	50.8	2	0.83
Design 218	508	20	5	3	15.8	0.625	0.44
Design 219	508	20	5	4	15.8	0.625	0.44
Design 220	508	20	5	2	31.75	1.25	0.44
Design 221	508	20	5	3	31.75	1.25	0.44
Design 222	508	20	5	4	31.75	1.25	0.44
Design 223	508	20	5	2	50.8	2	0.44
Design 224	508	20	5	3	50.8	2	0.44

Design 225	508	20	5	4	50.8	2	0.44
Design 226	508	20	7	2	15.8	0.625	0.38
Design 227	508	20	7	3	15.8	0.625	0.38
Design 228	508	20	7	4	15.8	0.625	0.38
Design 229	508	20	7	2	31.75	1.25	0.38
Design 230	508	20	7	3	31.75	1.25	0.38
Design 231	508	20	7	4	31.75	1.25	0.38
Design 232	508	20	7	2	50.8	2	0.38
Design 234	508	20	7	4	50.8	2	0.38
Design 235	508	20	9	2	15.8	0.625	0.34
Design 236	508	20	9	3	15.8	0.625	0.34
Design 237	508	20	9	4	15.8	0.625	0.34
Design 238	508	20	9	2	31.75	1.25	0.34
Design 239	508	20	9	3	31.75	1.25	0.34
Design 240	508	20	9	4	31.75	1.25	0.34
Design 241	508	20	9	2	50.8	2	0.34
Design 242	508	20	9	3	50.8	2	0.34
Design 243	508	20	9	4	50.8	2	0.34

Like in the previous example, many of the designs that passed the initial selection process at the estimated building demand, have significantly different 1st mode periods than the original estimate, requiring a check at spectral acceleration demands determined by each of their respective periods. Design 195 has a 1st mode period of 1.11 seconds, which corresponds to a spectral acceleration demand of approximately 0.6 g. Figure 58 shows the TTF versus probability of exceedance plot

for Design 195 at 0.6 g, demonstrating it still meet the TTF targets, while Table 21 shows all of the designs that met the TTF targets at their respective 1st mode period demands.

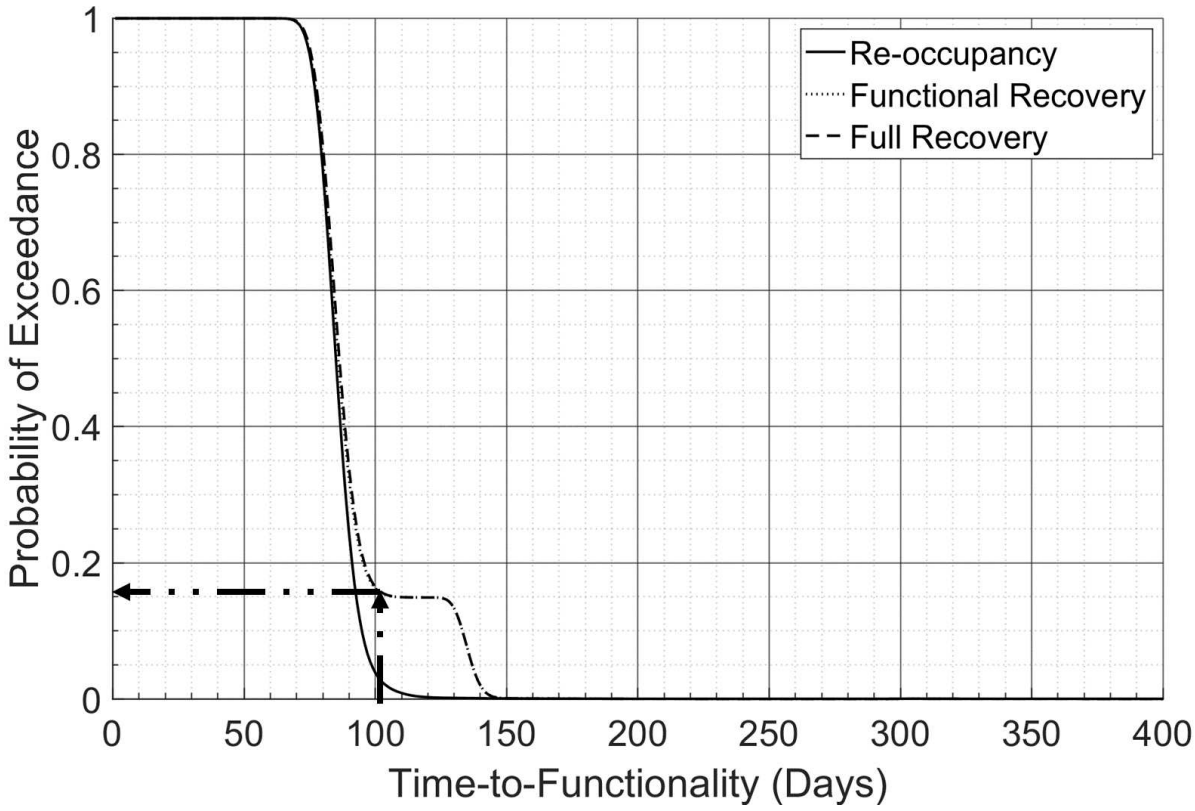

Figure 58: Design 195 TTF versus probability of exceedance at 0.6 g

Table 21: Example 2 Designs at Actual Building Period that Meet Criteria

Design	Panel Width (mm)	Panel Width (ft)	Panel Plys	Number of UFPs	Dia. of PT rods (mm)	Dia. of PT rods (in)	1st Mode Period (sec)
Design 173	127	5	7	3	15.8	0.625	2.64
Design 179	127	5	7	3	50.8	2	2.31
Design 182	127	5	9	3	15.8	0.625	2.36
Design 185	127	5	9	3	31.75	1.25	2.31
Design 189	127	5	9	4	50.8	2	2.11

Design 195	254	10	5	4	31.75	1.25	1.11
Design 195	254	10	5	4	31.75	1.25	1.11
Design 196	254	10	5	2	50.8	2	1.09
Design 197	254	10	5	3	50.8	2	1.09
Design 198	254	10	5	4	50.8	2	1.09
Design 200	254	10	7	3	15.8	0.625	0.95
Design 202	254	10	7	2	31.75	1.25	0.95
Design 203	254	10	7	3	31.75	1.25	0.95
Design 204	254	10	7	4	31.75	1.25	0.95
Design 206	254	10	7	3	50.8	2	0.93
Design 207	254	10	7	4	50.8	2	0.93

For Step 3 of this example, the geometric restrictions of the actual NHERI TallWood ten-story building were used, limiting the width of the lateral wall system to approximately 254 mm (10'), meaning a maximum panel width of 127 mm (5'). This limitation is due to the width of the shake table itself. Table 22 shows the designs remaining after the application of this restriction.

Table 22: Example 2 Designs that meet TTF and Geometric Criteria

Design	Panel Width (mm)	Panel Width (ft)	Panel Plys	Number of UFPs	Dia. of PT rods (mm)	Dia. of PT rods (in)	1st Mode Period (sec)
Design 173	127	5	7	3	15.8	0.625	2.64
Design 179	127	5	7	3	50.8	2	2.31
Design 182	127	5	9	3	15.8	0.625	2.36
Design 185	127	5	9	3	31.75	1.25	2.31

Design							
189	127	5	9	4	50.8	2	2.11

With five designs remaining, Step 4 can be used to narrow down designs based on a chosen cost analysis; however, like the first example, it is an optional step. Step 5 is also similar to the first example, and it can be referenced.

Closing

The design guidance presented in this Chapter is a general guideline of a procedure for approximate seismic design for a structure incorporating TTF considerations as well as more traditional considerations such as cost, geometric constraints, and performance-based design. Five general steps were established in this Chapter, with freedom given to the designer to in each step to fit the needs of various different designs. While the database leveraged in this guidance is limited in its applications currently, the framework to expand the database to other structural systems is in place and eventually a more prescriptive estimation of TTF can be introduced and used for design. In addition to establishing general design guidance utilizing the TTF database, two examples demonstrating two different situations were given to demonstrate how the database would be leveraged within this framework. The same building was used in both examples, but different TTF targets were selected and different geometric constraints were applied.

CHAPTER 8– CONCLUSIONS, CONTRIBUTIONS, AND RECOMMENDATIONS FOR FUTURE WORK

Mass timber and resilient design have both recently enjoyed increasing popularity in North America and across the world. The purpose of this dissertation was to investigate the feasibility of incorporating resilience design considerations into mass timber design, specifically the seismic design of tall mass timber buildings. The conclusions of this research are multi-faceted and incorporate both mass timber and resilience-based seismic design. The development of the Time-to-Functionality methodology incorporated existing downtime and resilience design considerations into a new stochastic method specifically designed to be included in a larger decision framework, which was then applied to state-of-the-art seismic mass timber design to evaluate its resilience performance. In general, the CLT rocking wall system evaluated using the TTF methodology performed well in the context of TTF downtime. The structural system itself remains undamaged or minimally damaged for a wide variety of seismic hazards, particularly in terms of residual drift; however, the non-structural components that accompany this rocking wall system need to be selected carefully, as the ability of the structural system to rock to dissipate energy can induce damage in drift sensitive non-structural components. A well-executed design incorporating these considerations can overcome this challenge, and in general the CLT rocking wall system proved a capable system for resilience-based mass timber seismic design.

During the development of the TTF methodology, many data gaps in the seismic or downtime performance of various mass timber products were identified. To address some of the research gaps identified in this research as well as in previous research, mass timber NLT/DLT diaphragms

were tested using quasi-static monotonic loading to assess their lateral capacity. Fragility curves were also developed for the NLT/DLT diaphragms using damage states identified during the testing. The conclusions of this testing were that the tested mass timber diaphragms are suitable for lateral systems in mid-rise mass timber structures, with capacities well above any standard light frame wood diaphragm, and in line of what one would expect for a mass timber diaphragm. In addition, it was demonstrated that nail pullout, shearing, and sheathing failure were the primary modes of failure for the diaphragms. Similarly, the identified damage states and resulting damage fragility curves primarily involved the nails and sheathing.

With the TTF method developed, and some of the knowledge for the lateral and downtime performance of mass timber (specifically NLT/DLT diaphragms) filled, design guidance for the design of tall mass timber structures with resilience considerations were developed. To develop this method, a TTF database leveraging the TTF methodology was constructed, and evaluated over 200 different mass timber designs across three archetypes (two-story, six-story, ten-story). These designs used the CLT rocking wall system, and the major components of this system (CLT panel width, CLT panel thickness, number of UFPs per wall, and diameter of post-tensioning rods) were varied over the archetypes to produces the different considered designs. The conclusions of these efforts were that TTF performance is directly affected by the stiffness and ductility of the structure, with a delicate balance between energy dissipation, lateral, and overturning moment capacity needed to manage the inter-story drift and floor accelerations that control the TTF performance. This can be adjusted by altering components such as the width of the panel, the thickness of the panel, the number of UFPs per wall, and the diameter of the post-tensioning walls, with differing effects between each of the archetypes. In general, higher stiffness benefits the taller archetypes

more than the two-story archetypes; reducing the drift for the two-story archetype via more energy dissipation, lateral capacity, or overturning moment does not necessarily ensure better TTF performance. With this database as the core, design guidance was developed around it, incorporating more traditional considerations such as cost, geometric constraints, and performance-based design. Incorporating the database, the resulting guidelines, and the included examples, it was demonstrated that it is indeed possible to incorporate resilience considerations directly into the design process of a tall mass timber structure.

The focus of this research was primarily to incorporate research from the fields of resilient seismic engineering in progress and mass timber to produce design guidance and database useful in designing tall mass timber buildings with resilience considerations. In the pursuit of this objective many direct contributions to the field of both mass timber and resilience-based seismic design were made. A robust stochastic methodology incorporating components from both FEMA P-58 and REDi was developed to estimate various recovery level downtimes of buildings subjected to seismic hazards. During this process, fragility curves and downtime considerations were developed for the state-of-the-art CLT rocking wall system, and it was evaluated in terms of recovery downtime for the first time. Lateral capacity testing for NLT/DLT diaphragms were also conducted to inform decision making and design of these diaphragms as lateral systems in NHERI TallWood project. Initial damage fragility curves were also established for these systems, addressing a gap in research identified during the earlier TTF methodology development. While this effort was successful, the contribution of this research does not end there in that this research sets the foundation for future expansion of resilience considerations using the TTF methodology beyond mass timber, as well as identifying and addressing some clear areas of research interest in

mass timber. Eventually with some expansion and enough considered archetypes, general TTF behavior can be determined, and a more prescriptive method can be developed to incorporate TTF considerations into design.

The TTF methodology and damage fragility curves herein were applied to an array of archetypes to construct a database of TTF performance for CLT rocking system buildings. This database was then evaluated and trends affecting the TTF performance of the various designs were identified and can be used to inform the design of CLT rocking systems for TTF performance considerations. In fulfillment of the original objective, design guidance leveraging the TTF database was then developed, to allow for the design of tall mass timber buildings for seismic resilience considerations. This research sets the foundation for future expansion of resilience considerations using the TTF methodology beyond mass timber, as well as identifies and addresses some clear areas of research interest in mass timber. Eventually with some expansion and enough considered archetypes, general TTF behavior can be determined, and a more prescriptive method can be developed to incorporate TTF considerations into design.

There are clear gaps in the damage fragility curves and time consequence functions of mass timber products that were acutely demonstrated in this research. While a few of the gaps were partially closed in the course of this research, many more are still apparent, demonstrating the need for experimental testing of various mass timber components with the explicit goal of developing damage fragility curves. In addition, studies are needed to leverage the expertise of the mass timber industry to develop repair actions, repair time estimates, and time consequence functions for mass timber products. Specifically, almost no data exists in terms of fragility and repair

information on mass timber products typically used for lateral systems such as laminated veneer lumber (LVL), CLT and MPP shear walls, and CLT and other mass timber diaphragms. Additionally, mass timber gravity frame materials (such as Glulam) as well as connections used for mass timber suffer from a similar lack of fragility and repair time consequence information. Beyond the gaps in the damage fragility curve research for mass timber, the TTF methodology and the development of the CLT rocking wall TTF database represent the first steps in much larger goals.

In terms of mass timber, increasing its applicability into both the resilience seismic design space and the mid-rise to tall building segment has a variety of potential implications. Mass timber's potential upside in terms of things such as erection time, carbon capture, cost, etc. provides engineers with additional options to meet their various performance objectives or other needs. For the CLT rocking wall specifically, the demonstrated resilience performance in this dissertation shows that it is possible to design mid-rise to tall mass timber structures to sustain minimal structural damage and along with the other benefits of mass timber, can make it a compelling design option for some projects. As there is no one material or design that can meet the design of every project, increasing the number of options and technologies is vital in the grand scheme of structural engineering and society as a whole, as buildings are expected to do more and more while being more efficient, environmentally friendly, etc.

In terms of resilience, while the design of tall mass timber buildings with TTF downtime considerations is now possible utilizing the research and design guidelines presented here, the applicability of the current database beyond this niche is limited. However, it acts as a proof of

concept for design with resilience considerations, and the TTF methodology, the database, and the design guidance are tools that can be used to expand beyond the niche presented here. More archetypes with different structural systems and non-structural components can be added to the database expanding its applicability in the short term. In addition, it should be noted that selected the TTF performance targets could prove challenging, especially in terms of larger community resilience. There are many potential factors and determining TTF target for a singular structure to help achieve a certain level of community resilience is a difficult task. Developing a method that can help a designer to choose these targets while incorporating larger community resilience metrics would prove valuable, and is a potential area of expansion for this method. In the long term, with enough archetypes and designs, general conclusions can be drawn on the TTF performance of various buildings, and a more prescriptive solution applicable to a wide variety of buildings can be developed. In the context of the wider research area of resilience, this is valuable; there is a concentrated push to move resilience metrics, specifically functionality, codified within the next decade or so. This research, as well as the research that will be based upon the foundation presented here will contribute to this codification effort and ultimately contribute to the incorporation of resilience considerations into normal seismic design practices. The implications of this are significant, not every design has the budget, expertise, or desire to incorporate PBSD into the design process, much less any resilience considerations. Prescriptive solutions can assist the incorporation considerations from both PBSD and resilient design into projects that otherwise would consider neither. Looking at the building stock of almost any community, one would see the vast majority of buildings fall under the category that would not normally do a PBSD or a resilient design, so accessing this segment of design with prescriptive methods could prove essential to meeting larger community resilience and performance targets.

REFERENCES

[1] Sotayo A., Bradley D., Bather M., Sareh P., Oudjene M., El-Houjeyri I., Harte A. M., Mehra S., O'Ceallaigh C., Haller P., Namari S., Makradi A., Belouettar S., Bouhala L., Deneufbourg F., and Guan Z., 2020. "Review of state of the art of dowel laminated timber members and densified wood materials as sustainable engineered wood products for construction and building applications." *Developments in the Built Environment*, 1. SSN 2666-1659, https://doi.org/10.1016/j.dibe.2019.100004.

[2] Adhesive-Free Timber Buildings. 2016. "Towards adhesive-free timber buildings (AFTB) -Interreg North-West Europe." Available at: https://www.nweurope.eu/projects/proje ct-search/towards-adhesive-free-timber-buildings-aftb/. Accessed: 2nd August 2022.

[3] Akbas, T., Richard, S., Ricles, J., Ganey, R., Berman, J., Loftus, S., Dolan, J.D., Pei, S., van de Lindt, J.W., and Blomgren, H. 2017. "Analytical and Experimental Lateral-Load Response of Self-Centering Posttensioned CLT Walls." *J. Struct. Eng.*, 143 (6).

[4] Almufti, I. and Willford, M. 2013. "REDi™ Rating System" *Arup*. https://www.arup.com/perspectives/publications/research/section/redi-rating-system

[5] Amini, O., van de Lindt, J. W., Pei, S., Rammer, D., Line, P., and Popovski, M. 2014 "Overview of a Project to Quantify Seismic Performance Factors for Cross Laminated Timber Structures in the United States." *RILEM Bookseries*. 9, 531-541.

[6] Amini, M. O., J. W. van de Lindt, D. Rammer, S. Pei, P. Line, and M. Popovski. 2018. "Systematic experimental investigation to support the development of seismic performance factors for cross laminated timber shear wall systems." *Eng. Struct.* 172 (Oct): 392–404. https://doi .org/10.1016/j.engstruct.2018.06.021.

[7] ASCE. 2016. "Minimum design loads and associated criteria for buildings and other structures." *ASCE 7-16*. Reston, VA: ASCE

[8] Baker, J. W. 2015. "Efficient analytical fragility function fitting using dynamic structural analysis." *Earthquake Spectra*, 31(1): 579-599.

[9] Blomgren, H., Pei, S., Powers, J., Dolan, J., Wilson, A., Morrel, I., and Jin, Z. 2018. "Cross-Laminated Timber Rocking Wall with Replaceable Fuses: Validation Through Full-Scale Shake Table Testing." *In World Conference on Timber Engineering (WCTE 2018)*, Seoul, Korea.

[10] Buchanan, A., Deam, B., Fragiacomo, M., Pampanin, S., and Palermo, A. 2008.

"Multi-storey prestressed timber buildings in New Zealand." *Structural Engineering International,* 18 (2): 166-173.

[11] BS EN 1995-1-1. 2004. “Eurocode 5: Design of Timber Structures.” *British Standards Institution*, London.

[12] Busch A., Zimmerman R. B., Pei S., McDonnell E., Line P., and Huang D. 2022. “Prescriptive Seismic Design Procedure for Post-Tensioned Mass Timber Rocking Walls.” *J. Struct. Eng.*, 148 (3). https://ascelibrary.org/doi/abs/10.1061/%28ASCE%29ST.1943-541X.0003240

[13] Canadian Wood Council (CWC). 2017. “Wood Design Manual.” *Canadian Wood Council*.

[14] Ceccotti, A. (2008). “New technologies for construction of mediumrise buildings in seismic regions: The XLAM case.” *Struct. Eng. Int.,* 18 (2): 156–165.

[15] Ceccotti, A., Sandhaas, C., Okabe, M., Yasumura, M., Minowa, C., and Kawai, N. 2013. “SOFIE project—3D shaking table test on a sevenstorey full-scale cross-laminated building.” *Earthquake Eng. Struct. Dyn.*, 42 (13): 2003–2021.

[16] Cimellaro, G. P., A. M. Reinhorn, and M. Bruneau. 2010. “Framework for analytical quantification of disaster resilience.” *Eng. Struct.,* 32 (11): 3639–3649. https://doi.org/10.1016/j.engstruct.2010.08.008.

[17] Cutfield, M., K. Ryan, and Q. Ma. 2016. “Comparative life cycle analysis of conventional and base-isolated buildings.” Earthquake Spectra 32 (1): 323–343. https://doi.org/10.1193/032414EQS040M.

[18] Derikvand, M. Jiao, H. Kotlarewski, N. Lee, M. Chan, A. and Nolan, G. 2019. “Bending performance of nail-laminated timber constructed of fast-grown plantation eucalypt.” *Eur. J. Wood Prod.* 77: 421–437. https://doi.org/10.1007/s00107-019-01408-9

[19] Dujic, B., Aicher, S., and Zarnic, R. 2006. “Testing of wooden wall panels applying realistic boundary conditions.” *9th World Conf. on Timber Engineering*, Oregon State Univ., Corvallis, OR.

[20] Dujic, B., Pucelj, J., and Zarnic, R. 2004. “Testing of racking behavior of massive wooden wall panels.” *Proc., 37th CIB-W18 Meeting, International Council for Building Research and Innovation*, Rotterdam, Netherlands.

[21] Dujic, B., and Zarnic, R. 2006. “Study of lateral resistance of massive X-Lam wooden wall system subjected to horizontal loads.” *COST E29 Int. Workshop on Earthquake Engineering on Timber Structures*, *European Cooperation in Science and Technology*, Brussels, Belgium, 97–104.

[22] Ellingwood, B.R., H. Cutler, P. Gardoni, W.G. Peacock, J.W. van de Lindt, and N. Wang. 2016. "The Centerville Virtual Community: A Fully Integrated Decision Model of Interacting Physical and Social Infrastructure Systems." *Journal of Sustainable and Resilient Infrastructure*, 1:3-4, 95-107.

[23] FEMA. 2018. "Seismic performance assessment of buildings. Volume 1- Methodology." *FEMA P-58-1.*

[24] FEMA. 2009. "Quantification of building seismic performance factors." *FEMA P695*

[25] FEMA. 2011. "National Disaster Recovery Framework." *FEMA National Disaster Recovery Framework.*

[26] FEMA. 2012. "The Performance Assessment Calculation Tool (PACT)." *FEMA P-58-1.*

[27] Ganey, R. S. 2015. "Seismic design and testing of rocking cross laminated timber walls." *M.S. thesis*, University of Washington, Seattle, WA.

[28] Ganey, R., Berman, J., Akbas, T., Loftus, S., Dolan, J. D., Sause, R., Ricles, J., Pei, S., van de Lindt, J. W., and Blomgren, H. 2017. "Experimental Investigation of Self-Centering Cross-Laminated Timber Walls." *J. Struct. Eng.*, 143 (10).

[29] Gavric I., Ceccotti A., Fragiacomo M. (2011). "Experimental cyclic tests on cross-laminated timber panels and typical connections." *Proceedings of the 14th ANIDIS Conference*, Bari, Italy.

[30] Gavric, I., Fragiacomo, M., and Ceccotti, A. (2012). "Strength and deformation characteristics of typical XLam connections." *World Conf. on Timber Engineering 2012*, *New Zealand Timber Design Society*, Auckland, New Zealand.

[31] Hasani, H., Ryan, K., Amer, A., Ricles, J. M., and Sause, R. "Pre-Test Seismic Evaluation of Drywall Partition Walls Integrated with a Timber Rocking Wall." In Eleventh U.S. National Conference on Earthquake Engineering, Los Angeles, California, 2018; 11.

[32] Holden, A., Devereux, C., Haydon, S., Buchanan, A. and Pampanin, S. "Innovative structural design of a three storey post-tensioned timber building." *Auckland, New Zealand: World Conference on Timber Engineering (WCTE)*, 15-19 Jul 2012. In Architecture and Engineering Case Studies, 323-330 (2012).

[33] Hong, K. E. M. (2017). "Structural performance of nail-laminated timber-concrete composite floors (T)." *University of British Columbia*. Retrieved from https://open.library.ubc.ca/collections/ubctheses/24/items/1.035448

[34] Karacabeyli, E., and Douglas, B. 2013. "CLT handbook." *FPInnovations*, Pointe-

Claire, QC, Canada.

[35] Kratzig W.B., Meyer I.F., and Meskouris K. 1989. "Damage evolution in reinforced concrete members under cyclic loading." *Proceedings of the 5th Int. Conf. on Structural Safety and Reliability*, 2: 795-802. San Francisco, CA.

[36] Krawinkler, H., Parisi, F., Ibarra, L., Ayoub, A., and Medina, R. 2001. "Development of a testing protocol for wood frame structures." *Technical Report W-02*, CUREE-Caltech Woodframe Project, Richmond, CA.

[37] Krawinkler H., Gupta A., Median R., and Luco N. 2000. "Loading histories for seismic performance testing of SMRF components and assemblies." *SAC Joint Venture*, Report No. SAC/BD-00/10.

[38] Lauriola, M. P., and Sandhaas, C. 2006. "Quasi-static and pseudodynamic tests on XLAM walls and buildings." *COST E29 Int. Workshop on Earthquake Engineering on Timber Structures, European Cooperation in Science and Technology*, Brussels, Belgium.

[39] Lin, P., and Wang, N., 2017. "Stochastic post-disaster functionality recovery of community building portfolios I: Modeling." *Structural Safety,* 69: 96-105.

[40] Lin, P., and Wang, N., 2017. "Stochastic post-disaster functionality recovery of community building portfolios II: Application." *Structural Safety,* 69: 106-117.

[41] Mayes, R., Wetzel, N., Tam, K., Weaver, B., Brown, A., and Pietra, D. 2013. "Performance based design of buildings to assess damage and downtime and implement a rating system." *New Zealand Society of Earthquake Engineering (NZSEE).*

[42] Mazzoni, S., McKenna, F., Scott, M., and Fenves, G. 2009. "Open Systems for Earthquake Engineering Simulation User Command-Language Manual – OpenSees version-2.0." *Pacific Earthquake Engineering Research Center*, University of California, Berkeley, Berkeley, CA .

[43] Mitrani-Reiser, J. 2008. "Risk Management Products Team Downtime Model." *Background Document FEMA P-58/BD-3.7.7*.

[44] Mosqueda, G. 2016. "Interior cold-formed steel framed gypsum partition walls." *Background Document FEMA P-58/BD-3.9.32*.

[45] American Wood Council (AWC). 2018. "National Design Specification® (NDS®)."

[46] Ozcelik, O., Luco, J. E., Conte, J. P., Trombetti, T. L., and Restrepo, J. I. 2008. "Experimental characterization, modeling and identification of the NEES-UCSD shake table mechanical system." *Earthquake Eng. Struct. Dyn.,* 37(2): 243-264.

[47] Palermo, A., Pampanin, S., Fragiacomo, M., Buchanan, A. H., and Deam, B. L. 2006. "Innovative seismic solutions for multi-storey LVL timber buildings." *9th World Conference on Timber Engineering (WCTE 2006),* Portland (U.S.A.).

[48] Pei, S., Popovski, M., and van de Lindt, J. W. 2013. "Analytical study on seismic force modification factors for cross-laminated timber buildings." *Can. J. Civ. Eng.,* 40(9): 887–896.

[49] Pei, S., Popovski, M., and van de Lindt, J. W. 2013. "Analytical study on seismic force modification factors for cross-laminated timber buildings." *Can. J. Civ. Eng.,* 40(9): 887–896.

[50] Pei, S., Rammer, D., Popovski, M., Williamson, T., Line, P., and van de Lindt, J. 2016. "An Overview of CLT Research and Implementation in North America." *In World Conference on Timber Engineering (WCTE 2016)*, Vienna, Austria.

[51] Pei, S. and van de Lindt, J.W., 2007. "User's Manual for SAPWood for Windows: Seismic Analysis Package for Woodframe Structures." *Colorado State University*, Fort Collins, CO.

[52] Pei, S., J. W. van de Lindt, A. Barbosa, J. Berman, E. McDonnell, J. D. Dolan, H. Blomgren, R. Zimmerman, D. Huang, and S. Wichman. 2019. "Experimental seismic response of a resilient two-story mass timber building with post-tensioned rocking walls." *J. Struct. Eng.* 145 (11): 04019120. https://doi.org/10.1061/(ASCE)ST.1943-541X .0002382.

[53] Pei, S., van de Lindt, J., Popovski, M., Beman, J., Dolan, J., Ricles, J., Sause, R., Blomgren, and H., Rammer, D. 2016. "Cross-Laminated Timber for Seismic Regions: Progress and Challenges for Research and Implementation." *Journal of Structural Engineering*, 142 (4).

[54] Popovski, M., and Gavric, I. 2016. "Performance of a 2-Story CLT House Subjected to Lateral Loads." *Journal of Structural Engineering,* 142 (4).

[55] Popovski, M., and Karacabeyli, E. 2012. "Seismic behaviour of crosslaminated timber structures." *World Conf. on Timber Engineering 2012, New Zealand Timber Design Society*, Auckland, New Zealand.

[56] Popovski, M., Karacabeyli, E., and Ceccotti, A. 2011. "Seismic performance of cross-laminated timber buildings." *Chapter 4, Canadian design handbook on cross-laminated timber*, FPInnovations Special Publication SP-528E.

[57] Popovski, M., Schneider, J., and Schweinsteiger, M. 2010. "Lateral load resistance of cross-laminated wood panels." *World Conf. on Timber Engineering, Italian National Research Council*, Rome, Italy, 20–24.

[58] Porter, K. 2009. “Fragility of Air Compressors.” *Background Document FEMA P-58/BD-3.9.20*.

[59] Porter, K. 2009. “Fragility of Chillers.” *Background Document FEMA P-58/BD-3.9.15*.

[60] Porter, K. 2009. “Fragility of Cooling Tower.” *Background Document FEMA P-58/BD-3.9.28.*

[61] Rombach. 2018. “Rombach Nur Holz.” Available at: http://www.nur-holz.com/startseite/
6/de/home.html.

[62] Sahabi, A., Reis, E., and Khorram, D. 2018. “The Case for Earthquake Resilience: Why Safer Structures Protect and Promote Social and Economic Vitality.” *U.S. Resiliency Council*.

[63] Sandhaas, C., and Schädle, P. 2017. “Joint properties and earthquake behaviour of buildings made from dowel-laminated timber.” *16th World Conference of Earthquake Engineering (WCEE)*, Santiago, Chile.

[64] Sarti, F., Palermo, A., Pampanin, S., and Berman, J. 2017. “Determination of the seismic performance factors for post-tensioned rocking timber wall systems.” *Earthquake Engng. Struct. Dyn.,* 46: 181– 200. doi: 10.1002/eqe.2784.

[65] Schneider, J., Stiemer, S. F., Tesfamariam, S., Karacabeyli, E., and Popovski, M. 2012. “Damage assessment of cross laminated timber connections subjected to simulated earthquake loads.” *World Conf. on Timber Engineering 2012, New Zealand Timber Design Society*, Auckland, New Zealand.

[66] Simpson Strong-Tie. 2016. “Strong-Rod™ Systems for Multi-Storey Overturing Restraint.” *Canadian Edtion*, Simpson Strong-Tie.

[67] Spieth, H. A., Carr, A. J., Pampanin, S., Murahidy, A. G., and Mander, J. 2004. “Modeling of precast prestressed concrete gram structures with rocking beam-column connections.” *Report No. 2004-01*, University of Canterbury. Christchurch, New Zealand.

[68] StructureCraft. 2018. “Dowel laminated timber - the all wood panel - mass timber design
guide.” Available at: https://structurecraft.com/blog/dowel-laminated-timber-design-guide-and-profile-handbook. Accessed: 2nd August ,2022

[69] Terzic, V., S. Mahin, and M. Comerio. 2014. “Comparative life-cycle cost and performance analysis of structural systems for buildings.” *In Proc., 10th US National Conf. on Earthquake Engineering: Frontiers of Earthquake Engineering*, Oakland, CA: Earthquake Engineering Research Institute.

[70] Terzic, V., Merrifield, S. K., and Mahin, S. 2012. “Lifecycle Cost Comparisons of Different Structural Systems.” *Berkeley: Structural Engineers Association of California*.

[71] Terzic, V., D. Yoo, and A. H. Aryan. 2016. “Repair time model for buildings considering the earthquake hazard.” *In Proc., Implementation Manual USRC Building Rating System for Earthquake Hazards*. Sacramento, CA: Structural Engineers Association of California.

[72] USRC. 2015. “Implementation Manual USRC Building Rating System for Earthquake Hazards.” *U.S. Resiliency Council Implementation Manual*.

[73] Vamvatsikos, D., and Cornell, C. 2002. “Incremental Dynamic Analysis” *Earthquake Engng. Struc. Dyn.*

[74] van de Lindt, J., Amini, M., Rammer, D., and Popovski, M., 2022. “Determination of seismic performance factors for cross-laminated timber shear walls based on FEMA P695 methodology.” *Report No FPL-GTR-281,* US Forest Service.

[75] van de Lindt, J., Pei, S., Pryor, S., Shimizu, H., and Isoda, H. 2010. “Experimental Seismic Response of a Full-Scale Six-Story Light-Frame Wood Building” *J. Struct. Eng.,* 136 (10): 1262-1272. DOI:10.1061/(ASCE)ST.1943-541X.0000222.

[76] Wichman, S., Berman, J., and Pei, S. 2022. “Experimental investigation and numerical modeling of rocking cross laminated timber walls on a flexible foundation.” *Earthquake Engng Struct Dyn*. 51: 1697– 1717. https://doi.org/10.1002/eqe.3634.

[77] Wichman, S., Berman, J., Zimmerman R., and Pei, S. 2022. “Lateral Design of a 10-story Building Specimen with Mass Timber Rocking Walls.” *12th NCEE, Earthquake Engineering Research Institute*, Salt Lake City, UT.

[78] Yamin, L., A. Hurtado, R. Rincon Garcia, J. Dorado, and J. Reyes. 2017. “Probabilistic seismic vulnerability assessment of buildings in terms of economic losses.” *Eng. Struct.* 138 (2): 308–323. https://doi.org/10.1016 /j.engstruct.2017.02.013.

[79] Yang, T., J. Moehle, B. Stojadinovic, and A. Kiureghian. 2009. “Seismic performance evaluation of facilities: Methodology and implementation.” *J. Struct. Eng.* 135 (10): 1146–1154. https://doi.org/10.1061/(ASCE)0733 -9445(2009) 135:10(1146).

[80] Zeng, X., Lu, X., Yang, T. Y., and Xu, Z. 2016 “Application of the FEMA-P58 methodology for regional earthquake loss prediction.” *Natural Hazards 2016*, 83(1): 177–192. DOI: 10.1007/s11069-016-230.

APPENDIX

Table 23: Two-story building archetype designs

Design	Panel Width (mm)	Panel Width (ft)	Panel Plys	Number of UFPs	Dia. of PT rods (mm)	Dia. of PT rods (in)	1st Mode Period (sec)
Design 1	127	5	5	2	15.8	0.625	1.00
Design 2	127	5	5	3	15.8	0.625	1.00
Design 3	127	5	5	4	15.8	0.625	1.00
Design 4	127	5	5	2	31.75	1.25	0.86
Design 5	127	5	5	3	31.75	1.25	0.86
Design 6	127	5	5	4	31.75	1.25	0.86
Design 7	127	5	5	2	50.8	2	0.55
Design 8	127	5	5	3	50.8	2	0.55
Design 9	127	5	5	4	50.8	2	0.55
Design 10	127	5	7	2	15.8	0.625	1.00
Design 11	127	5	7	3	15.8	0.625	1.00
Design 12	127	5	7	4	15.8	0.625	1.00
Design 13	127	5	7	2	31.75	1.25	0.86
Design 14	127	5	7	3	31.75	1.25	0.86
Design 15	127	5	7	4	31.75	1.25	0.86
Design 16	127	5	7	2	50.8	2	0.55
Design 17	127	5	7	3	50.8	2	0.55
Design 18	127	5	7	4	50.8	2	0.55
Design 19	127	5	9	2	15.8	0.625	0.99
Design 20	127	5	9	3	15.8	0.625	0.99
Design 21	127	5	9	4	15.8	0.625	0.99
Design 22	127	5	9	2	31.75	1.25	0.86
Design 23	127	5	9	3	31.75	1.25	0.86
Design 24	127	5	9	4	31.75	1.25	0.86
Design 25	127	5	9	2	50.8	2	0.55
Design 26	127	5	9	3	50.8	2	0.55
Design 27	127	5	9	4	50.8	2	0.55

Design 28	254	10	5	2	15.8	0.625	0.99
Design 29	254	10	5	3	15.8	0.625	0.99
Design 30	254	10	5	4	15.8	0.625	0.99
Design 31	254	10	5	2	31.75	1.25	0.86
Design 32	254	10	5	3	31.75	1.25	0.86
Design 33	254	10	5	4	31.75	1.25	0.86
Design 34	254	10	5	2	50.8	2	0.55
Design 35	254	10	5	3	50.8	2	0.55
Design 36	254	10	5	4	50.8	2	0.55
Design 37	254	10	7	2	15.8	0.625	0.99
Design 38	254	10	7	3	15.8	0.625	0.99
Design 39	254	10	7	4	15.8	0.625	0.99
Design 40	254	10	7	2	31.75	1.25	0.86
Design 41	254	10	7	3	31.75	1.25	0.86
Design 42	254	10	7	4	31.75	1.25	0.86
Design 43	254	10	7	2	50.8	2	0.56
Design 44	254	10	7	3	50.8	2	0.56
Design 45	254	10	7	4	50.8	2	0.56
Design 46	254	10	9	2	15.8	0.625	0.99
Design 47	254	10	9	3	15.8	0.625	0.99
Design 48	254	10	9	4	15.8	0.625	0.99
Design 49	254	10	9	2	31.75	1.25	0.86
Design 50	254	10	9	3	31.75	1.25	0.86
Design 51	254	10	9	4	31.75	1.25	0.86
Design 52	254	10	9	2	50.8	2	0.56
Design 53	254	10	9	3	50.8	2	0.56
Design 54	254	10	9	4	50.8	2	0.56
Design 55	508	20	5	2	15.8	0.625	0.99
Design 56	508	20	5	3	15.8	0.625	0.99
Design 57	508	20	5	4	15.8	0.625	0.99
Design 58	508	20	5	2	31.75	1.25	0.86
Design 59	508	20	5	3	31.75	1.25	0.86
Design 60	508	20	5	4	31.75	1.25	0.86
Design 61	508	20	5	2	50.8	2	0.56
Design 62	508	20	5	3	50.8	2	0.56
Design 63	508	20	5	4	50.8	2	0.56
Design 64	508	20	7	2	15.8	0.625	0.99
Design 65	508	20	7	3	15.8	0.625	0.99
Design 66	508	20	7	4	15.8	0.625	0.99
Design 67	508	20	7	2	31.75	1.25	0.86
Design 68	508	20	7	3	31.75	1.25	0.86
Design 69	508	20	7	4	31.75	1.25	0.86
Design 70	508	20	7	2	50.8	2	0.56

Design 71	508	20	7	3	50.8	2	0.56
Design 72	508	20	7	4	50.8	2	0.56
Design 73	508	20	9	2	15.8	0.625	0.99
Design 74	508	20	9	3	15.8	0.625	0.99
Design 75	508	20	9	4	15.8	0.625	0.99
Design 76	508	20	9	2	31.75	1.25	0.86
Design 77	508	20	9	3	31.75	1.25	0.86
Design 78	508	20	9	4	31.75	1.25	0.86
Design 79	508	20	9	2	50.8	2	0.56
Design 80	508	20	9	3	50.8	2	0.56
Design 81	508	20	9	4	50.8	2	0.56

Table 24: Six-story building archetype designs

Design	Panel Width (mm)	Panel Width (ft)	Panel Plys	Number of UFPs	Dia. of PT rods (mm)	Dia. of PT rods (in)	1st Mode Period (sec)
Design 82	127	5	5	2	15.8	0.625	1.86
Design 83	127	5	5	3	15.8	0.625	1.86
Design 84	127	5	5	4	15.8	0.625	1.86
Design 85	127	5	5	2	31.75	1.25	1.82
Design 86	127	5	5	3	31.75	1.25	1.82
Design 87	127	5	5	4	31.75	1.25	1.82
Design 88	127	5	5	2	50.8	2	1.63
Design 89	127	5	5	3	50.8	2	1.63
Design 90	127	5	5	4	50.8	2	1.63
Design 91	127	5	7	2	15.8	0.625	1.66
Design 92	127	5	7	3	15.8	0.625	1.66
Design 93	127	5	7	4	15.8	0.625	1.66
Design 94	127	5	7	2	31.75	1.25	1.64
Design 95	127	5	7	3	31.75	1.25	1.64
Design 96	127	5	7	4	31.75	1.25	1.64
Design 97	127	5	7	2	50.8	2	1.50
Design 98	127	5	7	3	50.8	2	1.50
Design 99	127	5	7	4	50.8	2	1.50
Design 100	127	5	9	2	15.8	0.625	1.53
Design 101	127	5	9	3	15.8	0.625	1.53
Design 102	127	5	9	4	15.8	0.625	1.53
Design 103	127	5	9	2	31.75	1.25	1.51
Design 104	127	5	9	3	31.75	1.25	1.51
Design 105	127	5	9	4	31.75	1.25	1.51
Design 106	127	5	9	2	50.8	2	1.40

Design 107	127	5	9	3	50.8	2	1.40
Design 108	127	5	9	4	50.8	2	1.40
Design 109	254	10	5	2	15.8	0.625	0.80
Design 110	254	10	5	3	15.8	0.625	0.80
Design 111	254	10	5	4	15.8	0.625	0.80
Design 112	254	10	5	2	31.75	1.25	0.79
Design 113	254	10	5	3	31.75	1.25	0.79
Design 114	254	10	5	4	31.75	1.25	0.79
Design 115	254	10	5	2	50.8	2	0.78
Design 116	254	10	5	3	50.8	2	0.78
Design 117	254	10	5	4	50.8	2	0.78
Design 118	254	10	7	2	15.8	0.625	0.68
Design 119	254	10	7	3	15.8	0.625	0.68
Design 120	254	10	7	4	15.8	0.625	0.68
Design 121	254	10	7	2	31.75	1.25	0.68
Design 122	254	10	7	3	31.75	1.25	0.68
Design 123	254	10	7	4	31.75	1.25	0.68
Design 124	254	10	7	2	50.8	2	0.67
Design 125	254	10	7	3	50.8	2	0.67
Design 126	254	10	7	4	50.8	2	0.67
Design 127	254	10	9	2	15.8	0.625	0.61
Design 128	254	10	9	3	15.8	0.625	0.61
Design 129	254	10	9	4	15.8	0.625	0.61
Design 130	254	10	9	2	31.75	1.25	0.61
Design 131	254	10	9	3	31.75	1.25	0.61
Design 132	254	10	9	4	31.75	1.25	0.61
Design 133	254	10	9	2	50.8	2	0.60
Design 134	254	10	9	3	50.8	2	0.60
Design 135	254	10	9	4	50.8	2	0.60
Design 136	508	20	5	2	15.8	0.625	0.33
Design 137	508	20	5	3	15.8	0.625	0.33
Design 138	508	20	5	4	15.8	0.625	0.33
Design 139	508	20	5	2	31.75	1.25	0.33
Design 140	508	20	5	3	31.75	1.25	0.33
Design 141	508	20	5	4	31.75	1.25	0.33
Design 142	508	20	5	2	50.8	2	0.33
Design 143	508	20	5	3	50.8	2	0.33
Design 144	508	20	5	4	50.8	2	0.33
Design 145	508	20	7	2	15.8	0.625	0.29
Design 146	508	20	7	3	15.8	0.625	0.29
Design 147	508	20	7	4	15.8	0.625	0.29
Design 148	508	20	7	2	31.75	1.25	0.29
Design 149	508	20	7	3	31.75	1.25	0.29

Design 150	508	20	7	4	31.75	1.25	0.29
Design 151	508	20	7	2	50.8	2	0.29
Design 152	508	20	7	3	50.8	2	0.29
Design 153	508	20	7	4	50.8	2	0.29
Design 154	508	20	9	2	15.8	0.625	0.26
Design 155	508	20	9	3	15.8	0.625	0.26
Design 156	508	20	9	4	15.8	0.625	0.26
Design 157	508	20	9	2	31.75	1.25	0.26
Design 158	508	20	9	3	31.75	1.25	0.26
Design 159	508	20	9	4	31.75	1.25	0.26
Design 160	508	20	9	2	50.8	2	0.26
Design 161	508	20	9	3	50.8	2	0.26
Design 162	508	20	9	4	50.8	2	0.26

Table 25: Ten-story building archetype designs

Design	Panel Width (mm)	Panel Width (ft)	Panel Plys	Number of UFPs	Dia. of PT rods (mm)	Dia. of PT rods (in)	1st Mode Period (sec)
Design 163	127	5	5	2	15.8	0.625	3.09
Design 164	127	5	5	3	15.8	0.625	3.09
Design 165	127	5	5	4	15.8	0.625	3.09
Design 166	127	5	5	2	31.75	1.25	2.99
Design 167	127	5	5	3	31.75	1.25	2.99
Design 168	127	5	5	4	31.75	1.25	2.99
Design 169	127	5	5	2	50.8	2	2.57
Design 170	127	5	5	3	50.8	2	2.57
Design 171	127	5	5	4	50.8	2	2.57
Design 172	127	5	7	2	15.8	0.625	2.64
Design 173	127	5	7	3	15.8	0.625	2.64
Design 174	127	5	7	4	15.8	0.625	2.64
Design 175	127	5	7	2	31.75	1.25	2.58
Design 176	127	5	7	3	31.75	1.25	2.58
Design 177	127	5	7	4	31.75	1.25	2.58
Design 178	127	5	7	2	50.8	2	2.31
Design 179	127	5	7	3	50.8	2	2.31
Design 180	127	5	7	4	50.8	2	2.31
Design 181	127	5	9	2	15.8	0.625	2.36
Design 182	127	5	9	3	15.8	0.625	2.36
Design 183	127	5	9	4	15.8	0.625	2.36
Design 184	127	5	9	2	31.75	1.25	2.31
Design 185	127	5	9	3	31.75	1.25	2.31

Design 186	127	5	9	4	31.75	1.25	2.31
Design 187	127	5	9	2	50.8	2	2.11
Design 188	127	5	9	3	50.8	2	2.11
Design 189	127	5	9	4	50.8	2	2.11
Design 190	254	10	5	2	15.8	0.625	1.11
Design 191	254	10	5	3	15.8	0.625	1.11
Design 192	254	10	5	4	15.8	0.625	1.11
Design 193	254	10	5	2	31.75	1.25	1.11
Design 194	254	10	5	3	31.75	1.25	1.11
Design 195	254	10	5	4	31.75	1.25	1.11
Design 196	254	10	5	2	50.8	2	1.09
Design 197	254	10	5	3	50.8	2	1.09
Design 198	254	10	5	4	50.8	2	1.09
Design 199	254	10	7	2	15.8	0.625	0.95
Design 200	254	10	7	3	15.8	0.625	0.95
Design 201	254	10	7	4	15.8	0.625	0.95
Design 202	254	10	7	2	31.75	1.25	0.95
Design 203	254	10	7	3	31.75	1.25	0.95
Design 204	254	10	7	4	31.75	1.25	0.95
Design 205	254	10	7	2	50.8	2	0.93
Design 206	254	10	7	3	50.8	2	0.93
Design 207	254	10	7	4	50.8	2	0.93
Design 208	254	10	9	2	15.8	0.625	0.84
Design 209	254	10	9	3	15.8	0.625	0.84
Design 210	254	10	9	4	15.8	0.625	0.84
Design 211	254	10	9	2	31.75	1.25	0.84
Design 212	254	10	9	3	31.75	1.25	0.84
Design 213	254	10	9	4	31.75	1.25	0.84
Design 214	254	10	9	2	50.8	2	0.83
Design 215	254	10	9	3	50.8	2	0.83
Design 216	254	10	9	4	50.8	2	0.83
Design 217	508	20	5	2	15.8	0.625	0.44
Design 218	508	20	5	3	15.8	0.625	0.44
Design 219	508	20	5	4	15.8	0.625	0.44
Design 220	508	20	5	2	31.75	1.25	0.44
Design 221	508	20	5	3	31.75	1.25	0.44
Design 222	508	20	5	4	31.75	1.25	0.44
Design 223	508	20	5	2	50.8	2	0.44
Design 224	508	20	5	3	50.8	2	0.44
Design 225	508	20	5	4	50.8	2	0.44
Design 226	508	20	7	2	15.8	0.625	0.38
Design 227	508	20	7	3	15.8	0.625	0.38
Design 228	508	20	7	4	15.8	0.625	0.38

Design 229	508	20	7	2	31.75	1.25	0.38
Design 230	508	20	7	3	31.75	1.25	0.38
Design 231	508	20	7	4	31.75	1.25	0.38
Design 232	508	20	7	2	50.8	2	0.38
Design 233	508	20	7	3	50.8	2	0.38
Design 234	508	20	7	4	50.8	2	0.38
Design 235	508	20	9	2	15.8	0.625	0.34
Design 236	508	20	9	3	15.8	0.625	0.34
Design 237	508	20	9	4	15.8	0.625	0.34
Design 238	508	20	9	2	31.75	1.25	0.34
Design 239	508	20	9	3	31.75	1.25	0.34
Design 240	508	20	9	4	31.75	1.25	0.34
Design 241	508	20	9	2	50.8	2	0.34
Design 242	508	20	9	3	50.8	2	0.34
Design 243	508	20	9	4	50.8	2	0.34